

**Modelling the EM properties of dipole reflections
with application to uniform chaff clouds**

by

Neil Kruger

Thesis presented in partial fulfilment of the requirements
for the degree of

Master of Science in Engineering

at the

University of Stellenbosch

Department of Electrical and Electronic Engineering,
University of Stellenbosch
Private Bag X1, 7602 Matieland, South Africa

Supervisor: Prof KD Palmer

December 2009

Declaration

By submitting this dissertation electronically, I declare that the entirety of the work contained therein is my own, original work, that I am the owner of the copyright thereof (unless to the extent explicitly otherwise stated) and that I have not previously in its entirety or in part submitted it for any qualification.

December 2009

Copyright © 2009 Stellenbosch University

All rights reserved

Abstract

The origin of chaff dates as far back as WWII, acting as a passive EM countermeasure it was used to confuse enemy radar systems and is still in use today. The purpose of this study is, firstly, to build up a knowledge base for determining chaff parameters and secondly, to calculate the theoretical Radar Cross Section (RCS) of a chaff cloud.

Initially dipole resonant properties are investigated relative to dipole physical dimensions. This is extended to the wideband spatial average RCS of a dipole with application to chaff clouds. A model is developed for calculating the theoretical RCS of a cloud typically produced by a single, multiband chaff cartridge.

This model is developed on the principles of sparse clouds with negligible coupling; the dipole density for which the model is valid is determined through the statistical simulation of chaff clouds.

To determine the effectiveness of chaff clouds, the E-field behaviour through a chaff cloud is investigated numerically. From simulation results a model is developed for estimating the position and drop in E-field strength. It is concluded that though it would be possible to hide a target behind a chaff cloud given ideal circumstances, it is not practical in reality. Given the presented results, recommendations are made for future work.

Opsomming

Die oorsprong van kaf dateer so ver terug as WOII. Dit was gebruik as 'n passiewe EM teenmaatreël teen vyandelike radar stelsels en is steeds vandag in gebruik. Die doel van hierdie studie is eerstens, om 'n kennisbasis op te bou vir die bepaling van kaf parameters en tweedens, om die teoretiese RDS van kafwolke te bereken.

Aanvanklik word die dipool resonante eienskappe ondersoek relatief tot die dipool dimensies. Die studie word uitgebrei tot die wyeband ruimte gemiddelde RDS van 'n dipool met toepassing op kafwolke. 'n Model word ontwikkel om die teoretiese RDS te bereken vir 'n tipiese kafwolk geproduseer deur 'n enkele, multi-band kafpakkie.

Die model is gegrond op die beginsels van lae digte kafwolke met weglaatbare koppeling; die dipool digtheid waarvoor die model geldig is, is bepaal deur statistiese simulاسie van kafwolke.

Om die effektiwiteit van kafwolke te bepaal, word die E-veld gedrag deur kafwolke numeries ondersoek. Vanaf simulاسie resultate word 'n model ontwikkel om die ligging van, en daling in E-veld sterkte af te skat. Daar word tot die gevolgtrekking gekom dat, alhoewel dit moontlik is om 'n teiken agter 'n kafwolk te versteek in ideale omstandighede, dit nie prakties is nie. Na aanleiding van die resultate verkry, is aanbevelings vir verdere werk gedoen.

Acknowledgements

A special word of thanks to:

- The CSIR and Christo Cloete for providing both the idea for the project and the financing
- Professor KD Palmer for his guidance and advice
- Professor JH Cloete for his interest and support
- My family for their encouragement and faith
- EC Lemmer & CH Booysen
- A Maritz
- JG Hoole

Table of Contents

Declaration.....	i
Abstract.....	ii
Opsomming.....	iii
Acknowledgements.....	iv
Table of Contents.....	v
List of Figures.....	vii
List of Tables.....	x
Nomenclature.....	xi
Abbreviations.....	xi
Chapter 1.....	1
Introduction.....	1
1.1 History of Chaff.....	1
1.2 Thesis Goals.....	2
1.3 Literature study & Modelling Parameters.....	4
1.4 Thesis Outline.....	8
Chapter 2.....	10
Resonant & Physical Properties of a Dipole.....	10
2.1 Introduction.....	10
2.2 Principles of Dipole Reflections.....	10
2.3 Chaff Material.....	11
2.4 Simulation & Results.....	12
2.5 Conclusion.....	14
Chapter 3.....	15
Single dipole RCS over a wide frequency band.....	15
3.1 Introduction.....	15
3.2 Using FEKO.....	15
3.3 Analytical Model of Dipole RCS.....	17
3.3.1 Monostatic / Bistatic RCS of a Dipole.....	17
3.3.2 Monostatic/bistatic average RCS of a dipole.....	20
3.3.3 Analytical Results vs. FEKO.....	22
3.4 Computational Model of Dipole RCS.....	27
3.4.1 Resonant length of a dipole.....	27
3.4.2 Convergence of RCS results.....	30
3.4.3 Modelling spatial average RCS.....	34
3.4.4 Validation of the modelling approach.....	39
3.4.5 Determining parameters for wideband modelling.....	43
3.4.6 Wideband spatial average RCS simulation.....	49
3.5 Wideband Dipole RCS Results.....	51
3.6 Verifying results with the literature.....	53
3.7 Verifying wideband results with a chaff cloud simulation.....	54
3.8 Conclusion.....	55

Chapter 4.....	56
Chaff cloud RCS & dipole density	56
4.1 Introduction.....	56
4.2 Backscatter RCS for N dipoles.....	57
4.3 Hypothesis of Forward Scatter RCS.....	57
4.4 Chaff Cloud Simulation – Approach & Parameters	59
4.4.1 Simulation Using Matlab and FEKO.....	59
4.4.2 Chaff Cloud Shape and Dipole Distribution.....	59
4.4.3 Simulation Results	60
4.5 Results for Sparse Cloud Simulation.....	61
4.5.1 Back Scatter RCS results	61
4.5.2 Forward Scatter RCS Results.....	62
4.5.3 Back Scatter & Forward Scatter RCS Results on dB scale	63
4.6 Results for Dense Cloud Simulation.....	64
4.7 Conclusion	67
Chapter 5.....	68
Screening Effect of Sparse Clouds	68
5.1 Introduction.....	68
5.2 Screening Hypothesis	69
5.3 Chaff Cloud Simulation investigating Hypothesis	72
5.4 Near field Results	74
5.5 Conclusion	80
Chapter 6.....	82
Conclusion	82
6.1 Conclusion.....	82
6.2 Recommendations.....	83
Bibliography	85
Appendix A.....	89
Deriving equations for equal spherical division	89
Appendix B.....	92
Graphical User Interface.....	92
B.1 Introduction.....	92
B.2 Chaff Cloud Wideband RCS Tool	94
B.3 E-field characteristics Tool	98
Appendix C	103
Matlab Simulation Functions.....	103

List of Figures

Figure 1 Thesis Layout	3
Figure 2 Dipole Resonant Length as a Function of the Diameter.....	12
Figure 3 Dipole Aspect Ratio from Literature [8, figure 1].....	13
Figure 4 Dipole Aspect Ratio from Simulation Results	13
Figure 5 Illustration of Bistatic Radar setup for the derivation of dipole RCS [10, fig 2.6]	18
Figure 6 RCS of a single dipole for varying ϕ and $\theta = 90^\circ$	22
Figure 7 RCS of a single dipole for varying θ and $\phi = 0^\circ$	23
Figure 8 Mathematical calculations vs. FEKO simulation values.....	23
Figure 9 Difference plot between calculated and simulated plot values over θ	24
Figure 10 Error function approximations	25
Figure 11 Mathematical calculations vs. FEKO simulation values with error correction applied.....	26
Figure 12 Dipole RCS over a 0.5GHz to 8GHz band.....	29
Figure 13 Bistatic radiation pattern of a single dipole at resonance.	29
Figure 14 Resonant frequencies for different segment lengths	31
Figure 15 Convolved RCS of a resonant dipole at 3GHz.....	33
Figure 16 Geometry of dipole in space, defined by length, theta and phi angle	35
Figure 17 Uniform dipole distributed over a disc. Figure 18 Uniform dipole distributed over a sphere	35
Figure 19 Integration in spherical coordinates [Advanced Engineering Mathematics, Z. Cullen].....	37
Figure 20 Triangular segmentation of a sphere in FEKO.....	38
Figure 21 Triangular segments of a half sphere (a) and far field points for a half sphere in FEKO (b)	39
Figure 22 Bistatic spatial average RCS of a dipole (a) 3D plot, (b) front view,.....	41
Figure 23 Bistatic spatial average RCS of a dipole at TG = 90° around Y axis.....	42
Figure 24 Bistatic spatial average RCS of a dipole at TG = 90° around Z axis	42
Figure 25 Average RCS as a function of the number of dipoles in as set, data plot for bistatic angle $\theta = 30^\circ$	44
Figure 26 Average RCS as a function of the number of dipoles in as set, data plot for bistatic angle $\theta = 60^\circ$	45
Figure 27 Average RCS as a function of the number of dipoles in as set, data plot for bistatic angle $\theta = 90^\circ$	45
Figure 28 RCS for an upright dipole over a wideband.....	47
Figure 29 RCS of a 150mm half wave dipole sampled over a 0.05 to 1 GHz frequency band.....	48
Figure 30 RCS of a 150mm half wave dipole, zoomed in view,	48
Figure 31 RCS of a 150mm half wave dipole, sampled over a 10 to 20 GHz frequency band.....	49

Figure 32 Illustration of frequency and dimension scaling	50
Figure 33 Monostatic spatial average RCS (m^2) of a dipole.....	51
Figure 34 Monostatic spatial average RCS of a dipole, normalized to wavelength (m^2/λ^2)	51
Figure 35 Normalized spatial average RCS on dB scale	52
Figure 36 Zoomed in view between 0 and -20dB over the frequency band	52
Figure 37 Spatial Average SCS [after Van Vleck <i>et al</i>]	53
Figure 38 Spatial Average SCS simulated.....	53
Figure 39 Dipole spatial average RCS Model vs. FEKO Simulation of a Chaff Cloud (see Figure 60).....	54
Figure 40 Generating a Spherical Chaff Cloud from a Cube.....	60
Figure 41 Back scatter RCS plot for a $1m^3$ chaff cloud with up to 1000 dipoles resonant at 3GHz	61
Figure 42 Average RCS plot along with the 50 simulations over which average RCS was calculated	62
Figure 43 Forward scatter RCS plot for a $1m^3$ chaff cloud with up to 1000 dipoles.....	63
Figure 44 Back scatter and Forward scatter RCS results on dB scale	64
Figure 45 RCS back and forward scatter results averaged over 50 simulations for a cloud of	65
Figure 46 E-field magnitude on a plane A-A for a plane wave incident on (a) a plane A-A	71
Figure 47 Near field points for calculating E-fields in $1m^3$ a chaff cloud	72
Figure 48 E-fields through a chaff cloud of $1m^3$ radiated at 3GHz	73
Figure 49 Near field points for calculating E-fields in a $1m^3$ chaff cloud,	74
Figure 50 E-field magnitude behind a chaff cloud for an increasing number of dipoles and increasing spherical volume, (constant density)	75
Figure 51 Drop in E-field behind a $1m^3$ spherical chaff cloud for an increasing number of dipoles	77
Figure 52 Drop in E-field behind a $1m^3$ spherical chaff cloud for an increasing number of dipoles	78
Figure 53 Validating the accuracy of derived hypothetical parameters for approximating the E-field minimum	79
Figure 54 Validating the accuracy of derived hypothetical parameters for approximating the distance to the E-field minimum	79
Figure 55 The accuracy of approximating the distance to the E-field minimum expressed as a percentage.	80
Figure 56 Integration in spherical coordinates, from [Advanced Engineering Mathematics, Z. Cullen]	90
Figure 57 Change in theta angle and sum of theta angles.....	91
Figure 58 GUI tool for Investigating Chaff Cloud RCS and E-field Properties.....	93
Figure 59 Default Wideband RCS Tool.....	94
Figure 60 Plotting Multiple Chaff Cuts over a wide frequency band.....	96
Figure 61 Plotting the Total RCS only, for the specifications set in the previous figure.	96
Figure 62 Plot total RCS on dB scale	97
Figure 63 GUI estimation vs. FEKO simulation	97
Figure 64 Default E-field characteristics Tool.....	98

Figure 65 E-field behaviour display for specified settings at reasonable dipole density	100
Figure 66 E-field behaviour display for specified settings at 1dB compression point density	100
Figure 67 Error display for specified settings beyond model limitations	101
Figure 68 Deterioration of Estimated results as dipole density increases for (a) 56 dipoles/m ³ , (b) 154 dipoles/m ³ , (c) 350 dipoles/m ³ , (d) 556 dipoles/m ³ ,	102

List of Tables

Table 1 Simulation parameters	27
Table 2 Simulation Results	28
Table 3 Simulation parameters	30
Table 4 Resonant frequencies for various segmentation lengths	31
Table 5 Resonant lengths	32
Table 6 Results for various Geometry orientations	40
Table 7 Average angle spacing between dipole orientations	44
Table 8 Simulation specifications	50
Table 9 Coupling results expressed as density	67
Table 10 Spherical dimensions for screening simulations	75
Table 11 Scattered E-field minimum and distance relationship behind cloud	76

Nomenclature

Abbreviations

BS	=	Back Scatter
CSA	=	Cross Sectional Area
DO	=	Dipole Orientation
DOs	=	Dipole Orientations
EM	=	Electromagnetic
FF	=	Far Field
FS	=	Forward Scatter
GUI	=	Graphical User Interface
RCS	=	Radar Cross Section
RF	=	Radio Frequency
SCS	=	Scattering Cross Section, total RCS
TG	=	Turn Geometry

Chapter 1

Introduction

Chaff, applied as a radar countermeasure, is designed to reduce the overall effectiveness of radar systems. Further applications have also been found in communications and weather monitoring [1] – [4]. The primary function of chaff is to disperse the energy which has been radiated in the direction of the target, so as to create a false target return signal.

Chaff consists of thin dipole elements cut to resonate at radar frequencies. Chaff dispensers usually contain several different lengths of chaff, in order to increase the bandwidth over which the chaff is effective. It is dispensed into the atmosphere to form “a cloud of dipole scatters” [5], by firing it from aircraft, naval vessels or land vehicles [6]. The purpose of the mission (deception, distraction confusion or screening) determines the method of dispensing the chaff.

1.1 History of Chaff

Chaff was used for the first time during WWII, [7]. Known to all the major combatants fighting in the war, it was used as a passive countermeasure to disrupt the effectiveness of enemy radar systems. The British called it *Window*, an unrelated code word. The Germans referred to it as *Düppel*, named after the test site near Berlin and the Japanese called it *Giman-shi*, which means “deceiving paper”.

On the night of 24 July 1943, the British were the first to use chaff in the night bombings of Hamburg, Germany [8]. More than 90 million foil strips, 1.5cm wide by 30 cm long, were dropped from the bombers, rendering the Wurzburg (570MHz) and Lichtenstein (490MHz) radars practically ineffective, and bomber loss rate dropped from 6.1% to 1.5%, proving the effectiveness of the chaff clouds.

By the time the Allies used chaff in a major deception operation in the build up to D-day, the Germans had learned that the Doppler-shift could be used to counter the effectiveness of chaff clouds. An aircraft could be distinguished from the chaff's backscatter by using the amplitude modulation resulting from the return signal from the propellers.

The Japanese and American also used chaff during attacks on each other. Japanese radars had a very low and wide (70 -200MHz) frequency range and the Americans had to use "rope". (Rope refers to untuned elements in the lower radar frequency spectrum, below 2GHz, was determined empirically.)

At the time of the war, purpose built dispensers had not yet been developed and chaff was dropped from aircraft by releasing it manually.

Though chaff was limited to airborne use for many years after WWII, it soon developed a use in naval applications. Chaff material did not lag behind either, with new chaff materials being developed in the 1950s. The two materials most commonly used were aluminium-coated glass filaments and silver-coated nylon monofilaments, both of which are still in use today.

1.2 Thesis Goals

The purpose of this thesis is to develop a tool for designing chaff parameters and to calculate the theoretical RCS of a single, multiband chaff cartridge as deployed by a typical fighter aircraft self protection launcher.

In the process of modelling chaff cloud RCS, however, two further research questions are raised:

- In what dipole density region is the model applicable and
- is it possible, or practical, to hide a target behind a chaff cloud?

The answers to these three questions are the goals which will form the basis of the research as illustrated in Figure 1. The following sections will discuss the factors influencing chaff RCS and the modelling approach as illustrated.

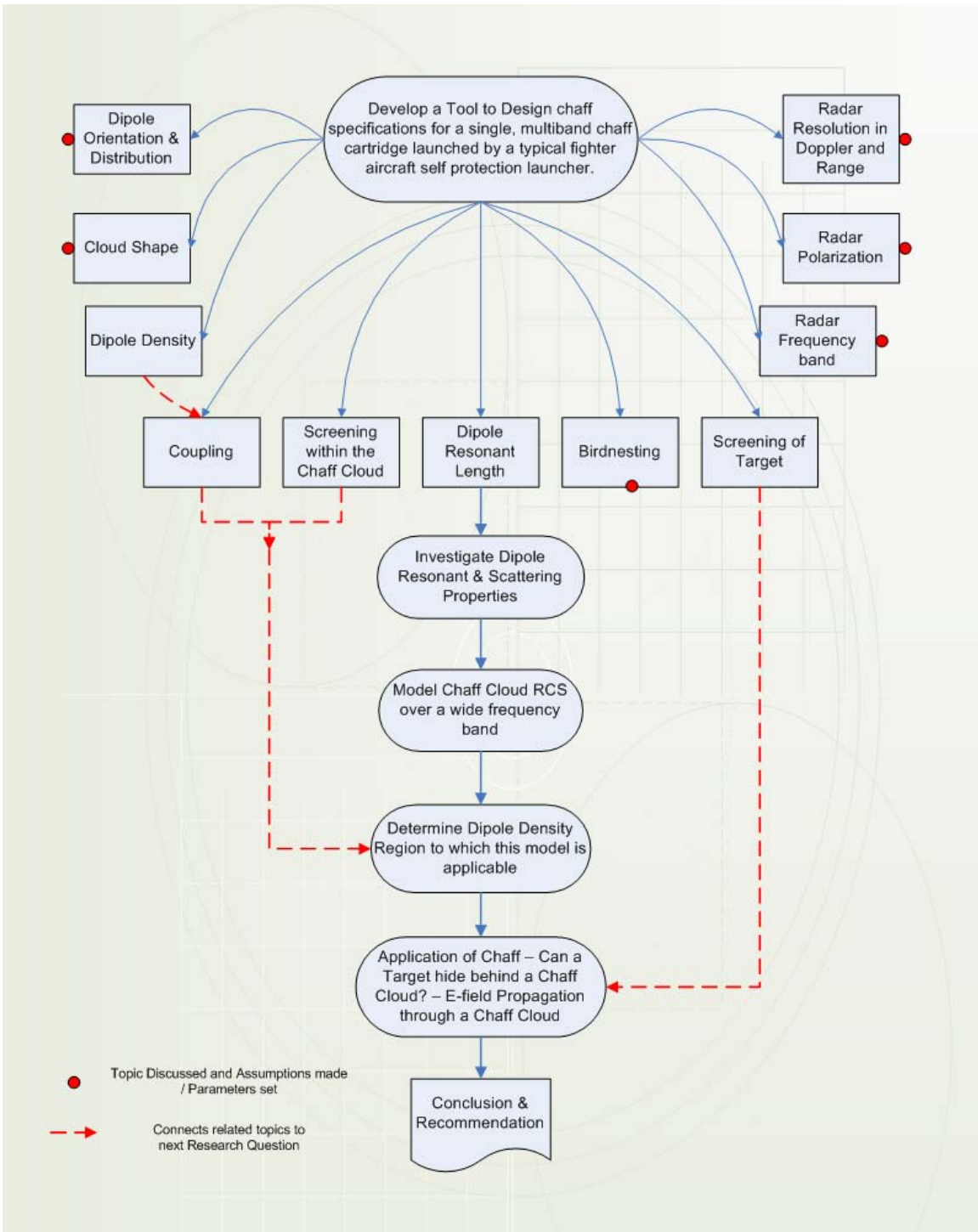


Figure 1 Thesis Layout

1.3 Literature study & Modelling Parameters

The factors influencing chaff cloud RCS are numerous and an attempt will be made to discuss the most important of these. Assumptions will be made regarding factors that either are not part of the modelling or cannot be incorporated. The purpose is to develop a general chaff model for air and naval application. The factors influencing the RCS of a chaff cloud can be divided in three groups:

Chaff Aerodynamic Factors:

- Initial atmospheric conditions (wind, rain, etc.)
- Platform of dispensing (aircraft, helicopter, ship)

The aerodynamic factors will be discussed under the headings of Dipole Orientation-and-Distribution and Cloud Shape

Chaff Electromagnetic Factors:

- Dipole Resonant Length, Diameter and Losses (energy)
- Birdnesting
- Dipole Density
- Coupling
- Screening within the chaff cloud

Radar Factors:

- Radar Polarization
- Radar Resolution in Doppler and Range
- Radar Frequency band

Dipole Orientation and Distribution

The dipole orientations and distribution are important factors determining the RCS of a chaff cloud. Dipole orientations affect the RCS of a chaff cloud in terms of either a more vertical, more horizontal (for a general naval case) or a spatial average orientation, relative to the radar polarization.

Assuming that all the dipoles are within the radar resolution cell, the distribution of dipoles in the chaff cloud will not affect the RCS for a low dipole density due to negligible coupling [6], [9], [10]. If, however, there is coupling within the chaff cloud,

the dipole distribution will have an effect on the RCS. Compare, for example, a uniform dipole distribution with that of a Gaussian distribution.

In practice, the dipole orientation and distribution of the chaff cloud differ for every scenario and measurement. This is due to the large number of factors influencing the behaviour of dipoles in the atmosphere. These factors range from the method of dispensing the chaff (whether this is perpendicular or parallel to the plane of movement and whether it is from an aircraft, naval vessel or helicopter) to the prevailing atmospheric conditions. In the case of aircraft, for example, each type of aircraft and chaff dispenser will have its own “aerodynamic signature” behind the aircraft, depending on the shape, fuel load and weapon load of the aircraft. The aerodynamic behaviour of chaff is, therefore, in every case dependent on the specific scenario and it is necessary to make assumptions for the modelling of chaff clouds with general application.

In the literature, analytical approximations are available for calculating the RCS of a dipole for any orientation [5], [10]. Regarding the dipole distribution within the cloud, a uniform or Gaussian distribution is usually assumed [6], [9], [11]. For the purpose of this study, the analytical RCS approximations will be investigated for any orientation.

Since it is not possible to determine the exact dipole distribution of a chaff cloud by means of analytical solutions or measurements, discussions were held with Radar, EM and EW engineers and specialists in the industry (Denel and CSIR), which led to a uniform dipole distribution being chosen for modelling purposes.

Cloud Shape

The cloud shape is dependent on the method of dispensing chaff, the platform from which it is dispensed and atmospheric conditions. In the case of all the dipoles falling within radar range and with negligible coupling, the cloud shape has little influence on the RCS. This is due to the linear relationship between RCS and the number of dipoles for sparse chaff clouds with negligible coupling [6], [9], [10].

For high density clouds with strong coupling between dipoles the shape does, however, affect the RCS as can be seen in the results presented in this document. Since the application of this chaff model is intended not for a single scenario, but for chaff application in general, two arbitrary chaff cloud shapes were considered: spherical and

elliptical. From academic discussions initiated by the literature [4], a hypothesis was formulated that, for a dense chaff cloud, the RCS of the cloud should approach that of a solid body with the same shape. For this purpose a spherical cloud shape was chosen for modelling, since the normalized RCS of a sphere is well known [12], [13]. If the RCS of the chaff cloud were to approach that of a solid sphere, it would give an indication of the accuracy of the modelling approach.

Dipole Resonant Length, Diameter and Loss

The half-wave dipole is known to resonate at a length a little shorter than 0.5λ and closer to $0.47\lambda - 0.48\lambda$, [8], [15], [16]. This is due to the EM wave travelling more slowly in the dipole medium than it does in free space. Investigating the ratio of resonant length to dipole diameter is part of this study and results will be presented. Since aluminium is the most widely used coating for chaff dipoles and has a high conductivity [5], [8], the energy losses are assumed to be negligible for the purposes of this study.

Birdnesting

Birdnesting, or clumping, is the result of dipoles clustering together and not spreading efficiently, thus rendering the chaff payload less effective [6], [8] [10].

Though birdnesting will not be investigated numerically, it will be incorporated in the chaff cloud RCS tool. For the purposes of this study it will be assumed that any specified percentage of birdnesting renders the same percentage of dipoles ineffective, thereby excluding them from the calculation.

Dipole Density

The dipole density is an important factor which determines the region of applicability of the linear relationship between chaff cloud RCS and the number of dipoles [4], [6], [9].

In this study the dipole density will be investigated relative to the linear relationship between RCS and the number of dipoles. Further investigation will be made into the region of non-linear RCS behaviour and into determining the limits of high dipole density.

Coupling

Inter-dipole coupling lowers the effective RCS of a chaff cloud. Losses of 3dB and 8.5dB respectively have been found in the literature for dipoles spaced 0.4λ and 0.25λ apart [5], [9]. This is due to dipole elements being spaced closely enough to influence the EM scattering properties of each other.

For the purpose of developing a chaff tool model it is assumed that the dipoles are far enough apart (2λ) to result in negligible coupling. The above mentioned figures serve as guidelines and will be compared with results investigating the dipole density regions.

Screening within the chaff cloud

Within a dense chaff cloud screening is a known problem. Like coupling, screening reduces the effective RCS of the chaff cloud [4], [6], [10]. This is a complex problem and will not be investigated formally, but is commented on along with the results of the investigation of dipole density regions. For the development of this chaff tool it is assumed that the dipole spacing is great enough (2λ) for the screening effect to be ignored.

Radar Polarization

Polarization has a big influence on RCS. The spatial average RCS of a dipole for linear and circular polarizations are given as $0.17\lambda^2$ and $0.11\lambda^2$ respectively [10], [17]. Since linear polarization is the case more generally found in the literature and as it can be extended to circular polarization [10], [17], chaff will be investigated for the case of linear polarization.

Radar Resolution in Range and Doppler

Radar resolution in range (along with the antenna beamwidth) determines the volume of the radar measurement into the chaff cloud. This determines the number of dipoles that influence the RCS measured. Radar resolution is, however, a radar capability which, though important, will not be incorporated in the scope of this study.

Another radar capability is radar resolution in Doppler. This is one of the measurements that make it possible to distinguish between the RCS of a target and that of a chaff cloud,

due to their differences in radial velocity. The Doppler measurement, for example, of an aircraft in flight is much higher than that of chaff a couple of seconds after deployment. Since this is a dynamic effect that will vary according to different dispensing platforms and methods over time, it will not be investigated. This study will focus on the steady-state RCS of a chaff cloud at a given time [12], [14].

Radar Frequency Band

The operating frequency of a chaff susceptible radar is usually in the X and Ku band and the frequency bandwidth is determined by the type of radar (search, tracking, missile-seeker head). To make this study as relevant as possible the RCS of a dipole will be modelled as widely as possible. In the results presented the dipole spatial average RCS is modelled from 0.05GHz to 20GHz. The frequency bandwidth is based on the limitations of simulation and the scaling accuracy of applied results.

The terms wideband and wide frequency band as used in this thesis can refer to either frequency bands greater than 1-2GHz or to the 0.05 to 20GHz band investigated in the RCS modelling.

1.4 Thesis Outline

In Chapter 2 an investigation is made into the physical properties of a dipole. Dipole dimensions and chaff material are discussed and simulation results of the resonant length as a function dipole diameter are presented.

Dipole scattering characteristics are investigated in Chapter 3. A single upright dipole is investigated analytically at resonance. Numerical software allows for investigation over a wide band and results are presented. Literature is also referenced for the RCS at resonance.

An analytical derivation for determining the dipole RCS at any orientation is presented along with that of the upright dipole. This result is verified by means of both a numerical investigation and the literature. The analytical derivation is applicable only to dipoles at resonance; for a wideband result the spatial average RCS is then modelled numerically.

In Chapter 4 the scattering properties of a chaff cloud are investigated. This is to determine the dipole density at which coupling starts affecting chaff cloud RCS. Simple equations are presented for calculating the back scatter RCS and a hypothesis is presented for calculating the forward scatter RCS. The forward and back scatter RCS are then investigated numerically. At the end of Chapter 4 results are presented and a conclusion is reached on the dipole density region for which the linear equations are valid.

The screening effect of chaff is investigated in Chapter 5. This is done by investigating the E-field scattering through the chaff cloud. No analytical derivations are currently available and a hypothesis is presented for empirical formulations. Numerical investigation is used to determine empirical parameters for sparse clouds, being limited to the number of dipoles in the spherical chaff cloud.

The findings are concluded in Chapter 6 and recommendations are made for future research.

Chapter 2

Resonant & Physical Properties of a Dipole

2.1 Introduction

In this literature an investigation is made into the resonant properties of a dipole at the hand of its physical dimensions. The purpose of this study is to investigate the range of dipole diameters for which the generally accepted resonant length formula $L_{res} = 0.47\lambda$ [8], [16] applies. Theory from the literature will be presented and results from both literature and simulation will be discussed.

2.2 Principles of Dipole Reflections

A chaff cloud consists of millions of wire elements. These wire elements are cut to form resonant dipoles that radiate at specific frequencies. A chaff cloud consisting of different dipole cut lengths can therefore absorb and reradiate or reflect energy from radar for a wide range of radar frequencies.

The physical length of a resonant dipole is less than half the free-space wavelength. This is due to the EM wave travelling more slowly in the dipole conductor than it does in free space. As the dipole diameter becomes less the dipole resonant length becomes greater [8]. This length to diameter ratio is called the aspect ratio and defined as:

$$A = \frac{l}{d} \tag{2.1}$$

where l is the dipole length and d is the diameter, see Figure 3 and Figure 4. As the diameter decreases the dipole length approaches a value of 0.5λ , as can be seen in Figure 2 from simulation results.

In practice the maximum RCS of a dipole is found to be lower than the theoretical, mainly because of losses due to the RF resistance. The free space resistance of a dipole is approximately 72Ω . The proportion of energy received that can be reradiated is given by [8] as:

$$\frac{72}{72 + R} \quad (2.2)$$

with R being the RF resistance. From the equation it is clear that RF resistance is required to be as low as possible. The materials that can therefore be used for dipoles are aluminium, silver, copper and zinc. Although of these silver has the highest conductivity, aluminium is more commonly used as it is cheaper, readily available, yet has a high conductivity.

2.3 Chaff Material

Chaff consists of a glass or fibre filaments which are coated with a conducting material. The most common used chaff material [15] is aluminium coated glass with a diameter of $25\mu\text{m}$. It is the cheapest chaff material and has the smallest diameter, making it possible to get more chaff elements into a cartridge.

Another chaff material is silver-coated nylon fibres with a diameter of $90\mu\text{m}$. This is a less popular chaff material due to two disadvantages: Greater diameter means less chaff in a cartridge and the silver coating makes it more expensive than other materials. There are also other materials which are used for chaff, but they have the disadvantages of higher RF resistance and susceptibility to corrosion [8].

2.4 Simulation & Results

A simulation was run in FEKO to investigate the dipole resonant length as a function of the diameter. The dipole diameters were simulated from 10 μm to 140 μm in 0.25 μm increments.

It can be seen in Figure 2 that the generally assumed resonant length of 0.47λ is 2.7% below the simulation result of 0.483λ for a dipole with a diameter of 25 μm , which is the diameter of aluminium coated glass filaments. For silver-coated nylon fibres with a diameter of 90 μm , the assumed resonant length of 0.47λ is 1.8% below the simulation result of 0.478λ .

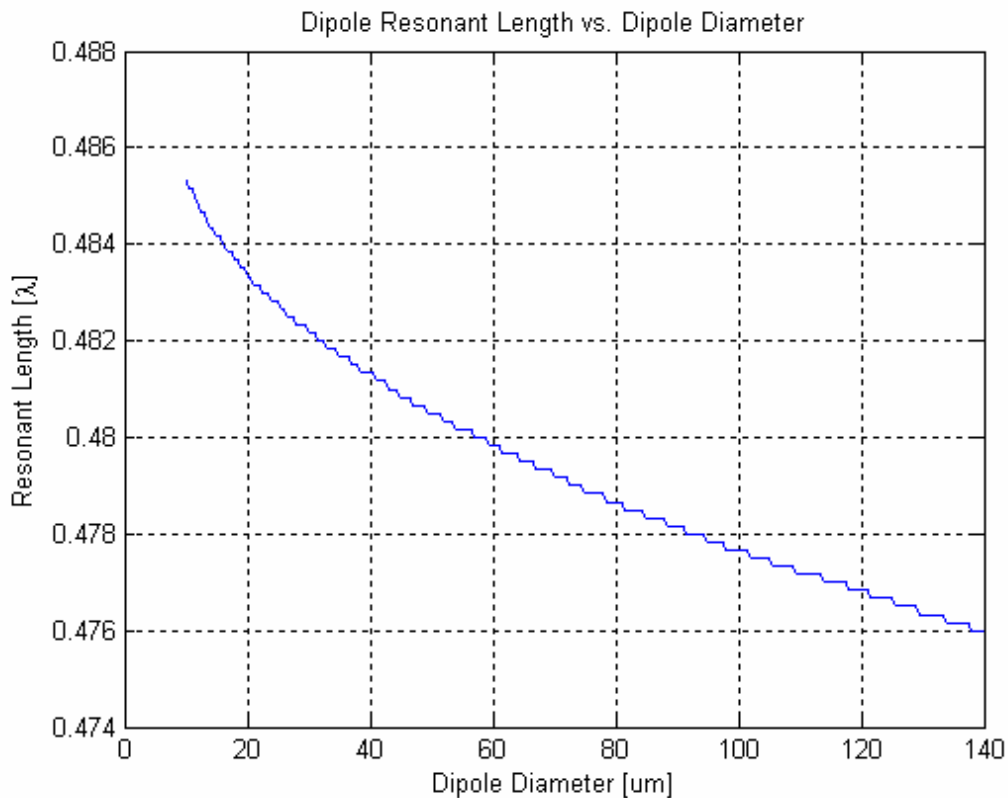


Figure 2 Dipole Resonant Length as a Function of the Diameter

The dipole aspect ratios from literature and simulation results are presented in Figure 3 and Figure 4. At $A = 1000$ the resonant length from literature and simulation differ by 0.15% and seem to be in good agreement.

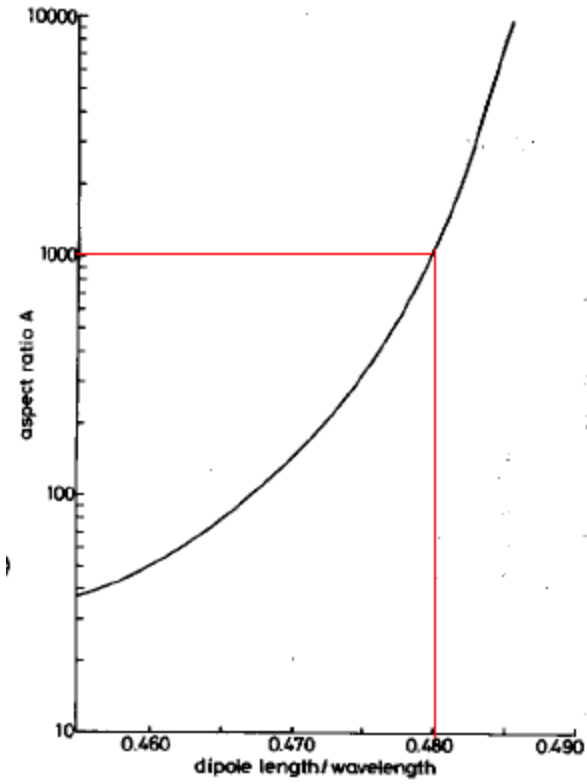


Figure 3 Dipole Aspect Ratio from Literature [8, figure 1]

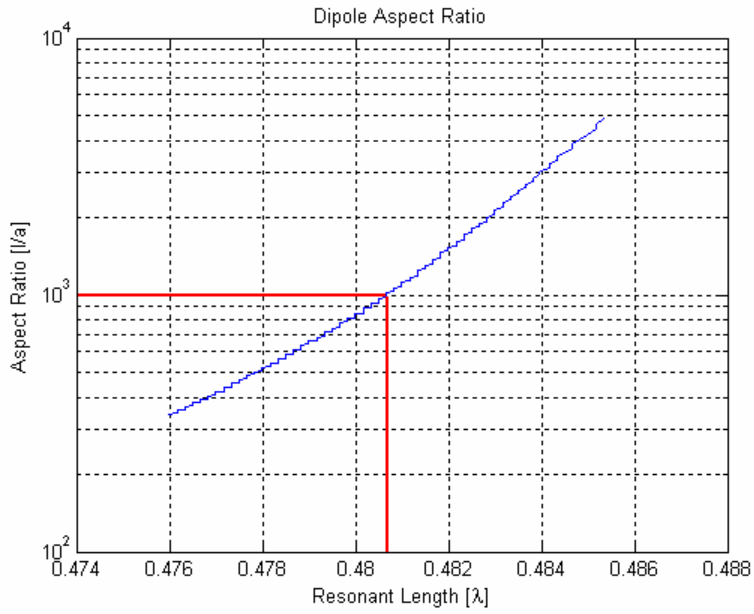


Figure 4 Dipole Aspect Ratio from Simulation Results

2.5 Conclusion

The reason for the difference between the general resonant length (as found in the literature) and the simulation results is not clear. One possibility is that the general resonant length of 0.47λ was first determined during the early years after WWII, in the developmental stage of chaff. Since then, technological improvement has enabled the development of thinner dipoles with an increase in the aspect ratio, while the general resonant length has never been altered to allow for / adapt to the narrower dipoles. It is concluded that the differences of 1.8% and 2.7% between the general length and that of the simulation results are still low enough to justify the general approximation of 0.47λ .

Chapter 3

Single dipole RCS over a wide frequency band

3.1 Introduction

One of the outcomes of this thesis is the calculation of the theoretical RCS of a chaff cloud for a typical chaff cartridge containing multiple cut-lengths of chaff. This entails calculating the RCS over a wide frequency band, due to different radar frequencies that are used for different types of radar.

Before the RCS of a chaff cloud can be determined, the EM scattering properties of a single dipole needs to be investigated and modelled over a wide frequency band.

In this chapter the monostatic and bistatic RCS of a single dipole are investigated and modelled by means of analysis and numerical simulation, as presented in sections 3.3 and 3.4. Using these results along with the linear relationship discussed in Chapter 4, it is possible to calculate the theoretical RCS of a chaff cloud. Results are compared with the literature in section 3.6 and with a chaff cloud simulation in section 3.7.

3.2 Using FEKO

For the purpose of calculating chaff cloud RCS numerically, two options are possible: Using an existing EM numerical code like FEKO or CST, or writing a numerical code capable of calculating the E-fields and RCS.

For the purpose of building up a chaff knowledge base, the existing EM numerical code has the advantage of an existing GUI for viewing results and allowing the immediate/instantaneous investigation of scattering properties. The disadvantage of

existing numerical codes against writing a numerical code is the limitation in the number of dipole elements that can be simulated. This is due to the large computer resource consumption (up to 70 Gigabytes of memory) and the limited computer resources available. Large simulations therefore have impractically long running times (up to 180 hours for 15000 dipole elements).

The GUI of existing codes assists in a better display of results and allows a better understanding of what is happening in the simulation environment. Due to the random nature of chaff it is possible to investigate and model chaff clouds statistically. This allows the simulation to be done with an existing EM numerical code, as opposed to developing one. Although developing a numerical code especially for the purpose of calculating chaff cloud RCS would allow a much more realistic number of dipole elements in the chaff cloud, this is not the purpose of this investigation.

The development of a numerical code for calculating chaff cloud RCS would have been a possibility, but since this study aims at building a general knowledge base of the EM properties of chaff, it was decided to use an existing EM numerical code with more useful features.

FEKO is the EM software program that was used for simulation. It is a numerical EM code that makes use of the Method of Moments to solve electromagnetic calculations. The FEKO EM simulation results will be determined by simulation settings as well as chaff and cloud parameters. Before the results can be validated, it must be determined whether results have converged (section 3.4.2), in order to ensure accuracy. The converged results can then be compared with data from theory, analytical and/or computational results for validation.

3.3 Analytical Model of Dipole RCS

In this section an analytical method is presented whereby the monostatic or bistatic RCS of the dipole can be found. Complete and approximate equations are given

3.3.1 Monostatic / Bistatic RCS of a Dipole

For a single dipole, the monostatic RCS is at a maximum when the polarization of the incident E-field, radiated by the transmitting antenna, is parallel to the dipole axis as well as to the polarization of the receiving antenna. According to literature [8], [10], [16], the maximum RCS can be calculated from the following approximation for dipoles cut to the half-wavelength resonance:

$$\sigma_m = \sigma_{\max} \approx 0.86\lambda^2 \quad (3.1)$$

The value of 0.86 is a normalized value of the average current distribution over a dipole. (If the average current is found over a wide bandwidth, analytically or computationally, it would be possible to calculate the maximum RCS over a wide bandwidth).

Since the dipole will not always be parallel to the polarization of the incident E-field, an equation needs to be derived for calculating RCS at various angles of cross polarization. In [10] simple approximations are derived allowing the calculation of monostatic as well as bistatic RCS of a single dipole.

For the purpose of the derivation, a transmitting antenna (T_x) is located at point A, a dipole at centre point O and a receiving antenna (R_x) at point B, as illustrated in Figure 5. A Cartesian coordinate system is used, as illustrated by X_1, Y_1, Z_1 . The X-axes all lie parallel to each other, while the Y-axes all lie in the same AOB plane (see Figure 5). The Z_1 -axis is in the direction of the incident field, from T_x to the dipole. The Z_2 -axis is in the direction opposite to that of the scattered field, from R_x to the dipole. The dipole is assumed to be illuminated by a plane wave from T_x . The polarization is linear and its direction is given by the unit vector \mathbf{e}_{in} , falling in the X_1Y_1 plane and making an angle α_1 with X_1 . The polarization of the receiving antenna is depicted by \mathbf{e}_r and makes an angle

α_2 with X_2 . As can be seen in the figure, the unit vector ρ indicates the dipole orientation as determined by θ and ϕ . The difference between Z_1 and Z_2 is given by the bistatic angle β .

The unit vectors can be written in terms of their projections on their X, Y and Z axes:

$$\mathbf{e}_{in} = (\cos\alpha_1, \sin\alpha_1, 0) \quad (3.2)$$

$$\mathbf{e}_r = (\cos\alpha_2, \sin\alpha_2, 0) \quad (3.3)$$

$$\rho = (\sin\theta \cdot \cos\phi, \sin\theta \cdot \sin\phi, \cos\theta) \quad (3.4)$$

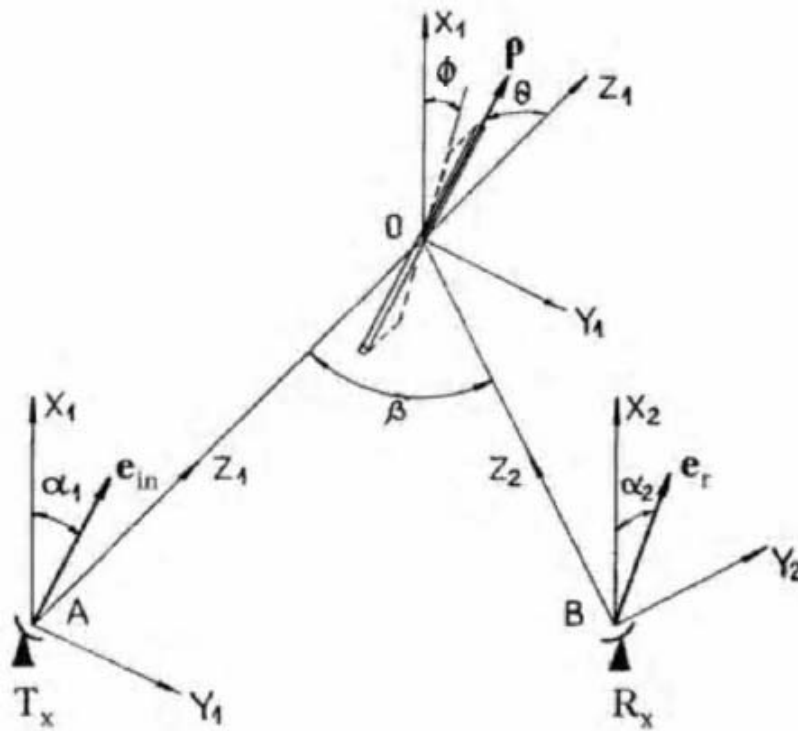


Figure 5 Illustration of Bistatic Radar setup for the derivation of dipole RCS [10, fig 2.6]

The radiation pattern of a half-wavelength dipole can be expressed as follows:

$$F_1 = \frac{\cos^2[(\pi/2)\sqrt{1-(\boldsymbol{\rho}\cdot\mathbf{e}_{in})^2}]}{(\boldsymbol{\rho}\cdot\mathbf{e}_{in})^2} \quad (3.5)$$

Or as a function of α_1 , ϕ and θ :

$$F_1(\alpha_1, \phi, \theta) = \frac{\cos^2[(\pi/2)\sqrt{1-\cos^2(\phi-\alpha_1)\sin^2\theta}]}{\cos^2(\phi-\alpha_1)\sin^2\theta} \quad (3.6)$$

The above equation accounts for the component of the incident E-field that is parallel to the dipole axial direction, from there the $\mathbf{e}_{in}\cdot\boldsymbol{\rho}$ product. The power directivity pattern for the receiving antenna can be written in the same manner as that of the radiation pattern:

$$F_2 = \frac{\cos^2[(\pi/2)\sqrt{1-(\boldsymbol{\rho}\cdot\mathbf{e}_r)^2}]}{(\boldsymbol{\rho}\cdot\mathbf{e}_r)^2} \quad (3.7)$$

To express the above equation in terms of orientation angles θ and ϕ , the vector \mathbf{e}_r needs to be rotated through the bistatic angle β . The transformation matrix to achieve this can be written as:

$$\mathbf{e}_r = \begin{pmatrix} 1 & 0 & 0 \\ 0 & \cos\beta & -\sin\beta \\ 0 & \sin\beta & \cos\beta \end{pmatrix} \begin{pmatrix} \cos\alpha_2 \\ \sin\alpha_2 \\ 0 \end{pmatrix} = \begin{pmatrix} \cos\alpha_2 \\ \cos\beta\sin\alpha_2 \\ \sin\beta\sin\alpha_2 \end{pmatrix} \quad (3.8)$$

The projection of \mathbf{e}_r onto the X_1 , Y_1 and Z_1 axes is given by the part of the above equation on the right. By substituting equation 3.8 into equation 3.7, the directivity pattern can be written as a function of β , α_1 , ϕ and θ :

$$F_2(\beta, \alpha_1, \phi, \theta) = \frac{\cos^2[(\pi/2)\sqrt{1-[\sin\theta(\cos\alpha_2\cos\phi + \cos\beta\sin\alpha_2\sin\phi) + \cos\theta\sin\beta\sin\alpha_2]^2}]}{[\sin\theta(\cos\alpha_2\cos\phi + \cos\beta\sin\alpha_2\sin\phi) + \cos\theta\sin\beta\sin\alpha_2]^2} \quad (3.9)$$

To evaluate the RCS for a single orientation the power patterns, along with the maximum value, need to be evaluated in conjunction with each other:

$$\sigma_b(\beta, \alpha_1, \alpha_2, \phi, \theta) = \sigma_{\max} F_1(\alpha_1, \phi, \theta) F_2(\beta, \alpha_2, \phi, \theta) \quad (3.10)$$

Approximate relationships exist for a more practical evaluation of the bistatic RCS for a single orientation:

$$F_1(\alpha_1, \phi, \theta) = \cos^2(\phi - \alpha_1) \sin^2 \theta \quad (3.11)$$

$$F_2(\beta, \alpha_1, \phi, \theta) = [\sin \theta (\cos \alpha_2 \cos \phi + \cos \beta \sin \alpha_2 \sin \phi) + \cos \theta \sin \beta \sin \alpha_2]^2 \quad (3.12)$$

For the monostatic case this reduces to

$$F_2(\alpha_2, \phi, \theta) = \cos^2(\phi - \alpha_2) \sin^2 \theta \quad (3.13)$$

Equations have been derived for evaluating the RCS of a dipole for a single orientation and approximations have been given for simpler calculations.

3.3.2 Monostatic/bistatic average RCS of a dipole

From the previous equations it would be possible to calculate the RCS of a chaff cloud if the orientation of each dipole was known. A simpler approach would be to assume the dipoles' orientations as randomly distributed over a sphere, and calculate the RCS of the chaff cloud from an average dipole RCS value. To calculate the average RCS of a dipole, equations 3.11 and 3.12 can be averaged over a sphere as shown below:

$$\overline{\sigma_b}(\beta, \alpha_1, \alpha_2) = \frac{\sigma_{\max}}{4\pi} \int_0^{2\pi} \int_0^\pi F_1(\alpha_1, \phi, \theta) F_2(\beta, \alpha_2, \phi, \theta) \sin \theta d\theta d\phi \quad (3.14)$$

From the equations above, simple equations can be derived for the calculation of the average RCS of a half-wavelength dipole for linear polarization. For the bistatic case we have:

$$\overline{\sigma}_b(\beta, \alpha_1, \alpha_2) \approx (0.86\lambda^2 / 15)[1 + 2(\cos \alpha_1 \cos \alpha_2 + \cos \beta \sin \alpha_1 \sin \alpha_2)^2] \quad (3.15)$$

and for the monostatic case with $\beta = 0^\circ$

$$\overline{\sigma}_m(\Delta\alpha) \approx (0.86\lambda^2 / 15)[2 + \cos 2\Delta\alpha^2] \quad (3.16)$$

where $\Delta\alpha = \alpha_1 - \alpha_2$. For co-polarization the monostatic RCS is at a maximum given by:

$$\overline{\sigma}_m(0^\circ) \approx 0.17\lambda^2 \quad (3.17)$$

and for cross-polarization at a minimum:

$$\overline{\sigma}_m(90^\circ) \approx 0.057\lambda^2 \quad (3.18)$$

The above value for co-polarization can also be found by averaging the maximum RCS

$$\sigma_{\max} = \frac{G^2 \lambda^2}{\pi} \quad (3.19)$$

over 4π sterad, assuming a random dipole orientation [8]. Both the theoretical values are from simple approximations and are slightly higher than the values given in other literature sources. Reference [5] gives $\overline{\sigma}_m(0^\circ) \approx 0.158\lambda^2$, based on a one of the earliest wire models for a dipole, using simple analyses and assuming infinite conductivity. A more practical value found in radar analysis [14] gives an even lower value of $\overline{\sigma}_m(0^\circ) \approx 0.15\lambda^2$, making general provision for the effectiveness of chaff in terms of losses and birdnesting. This last value is close to the values of $\overline{\sigma}_m(0^\circ) \approx 0.153\lambda^2$ mentioned in [18] and $\overline{\sigma}_m(0^\circ) \approx 0.155\lambda^2$ found in [15].

These approximations compare well, as they all lie within 1dB of one another. They do vary, however, from reference to reference due to the different modelling approaches

used and the spatial average RCS will therefore be determined numerically (section 3.4) in order to reach a conclusion.

3.3.3 Analytical Results vs. FEKO

From spatial average bistatic results (see Figure 22 to Figure 24), we know that the average RCS radiation pattern is a function of the polarization angle α and not of the bistatic angle β . Therefore only the monostatic RCS with vertical linear polarization (from there the θ component) is investigated and presented here.

The mathematical results were compared to the FEKO simulation results. The first figure, Figure 6, shows the RCS for $\theta = 90^\circ$ as ϕ changes. It is interesting to note that an exact sinusoidal relationship of \cos^2 exists for the normalized scattering cross section (SCS or total RCS). The normalized results presented in the following graphs are normalized to the maximum RCS of an upright dipole unless otherwise illustrated or stated.

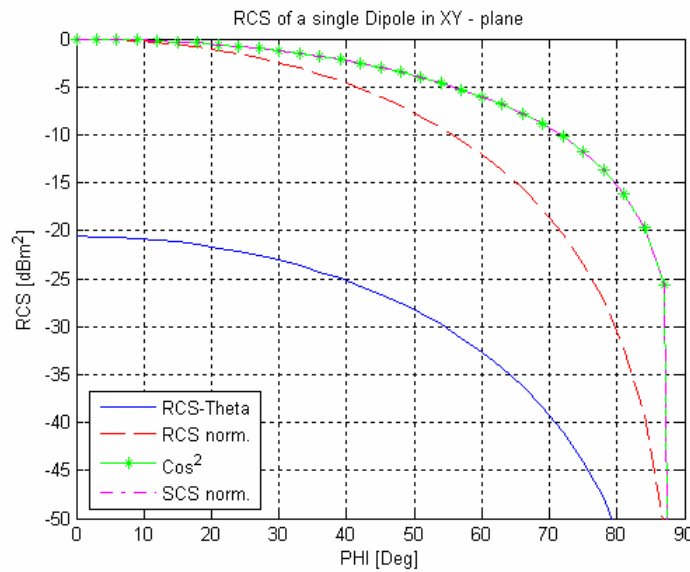


Figure 6 RCS of a single dipole for varying ϕ and $\theta = 90^\circ$

In Figure 7 the RCS plot is shown for $\phi = 0^\circ$ as θ varies. It can be seen that the normalized RCS theta-component agrees exactly with the SCS plot. This is because no RCS phi-component exists, due to the E-field polarization being in the same plane as the

dipole orientation. The \sin^2 plot illustrates that no sinusoidal relationship exists for either SCS or RCS in this plane of orientation.

In Figure 8 plots are shown for various values of ϕ . It is clear that as θ approaches 90° the calculated and simulated values coincide better. This shows that for dipole orientations off centre, the accuracy of the mathematical derivations decreases.

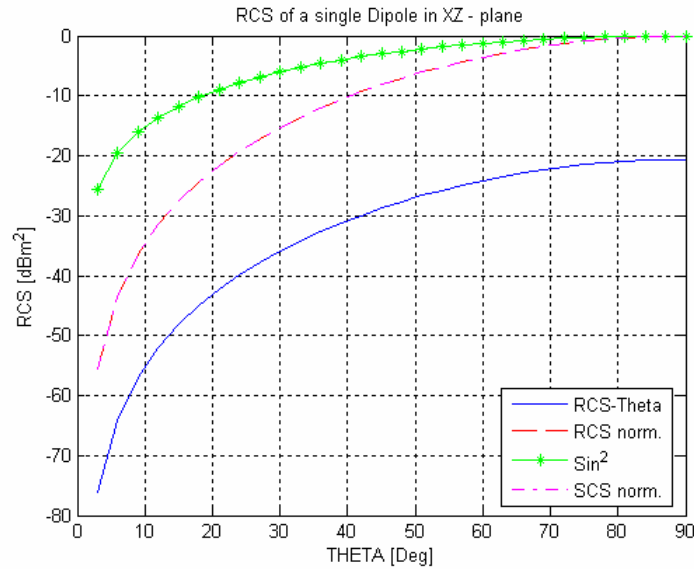


Figure 7 RCS of a single dipole for varying θ and $\phi = 0^\circ$

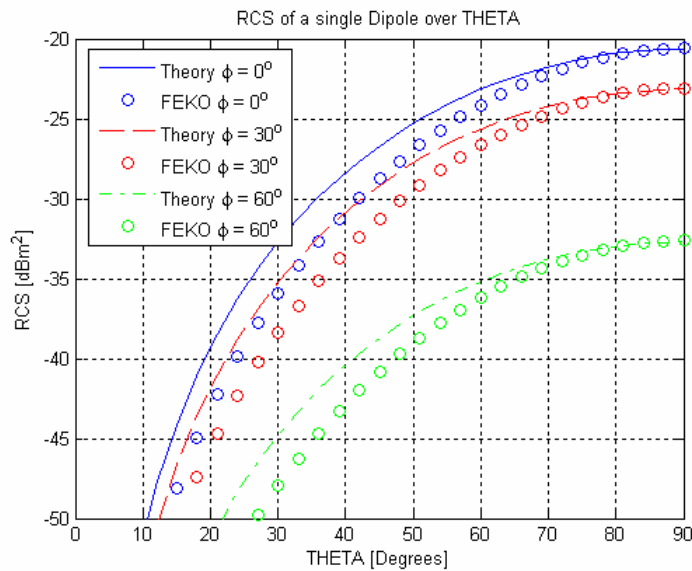


Figure 8 Mathematical calculations vs. FEKO simulation values

The difference between the calculated and simulated values is plotted in Figure 9. The difference is ascribed to the fact that in FEKO the finite diameter of the dipole is modelled, while the analytical solution is an approximation for an infinitely thin dipole with a linear current distribution [10].

It can be seen that the difference in analytical and computational values are independent of ϕ . The maximum error between theory and simulated results is slightly less than 4.5dB.

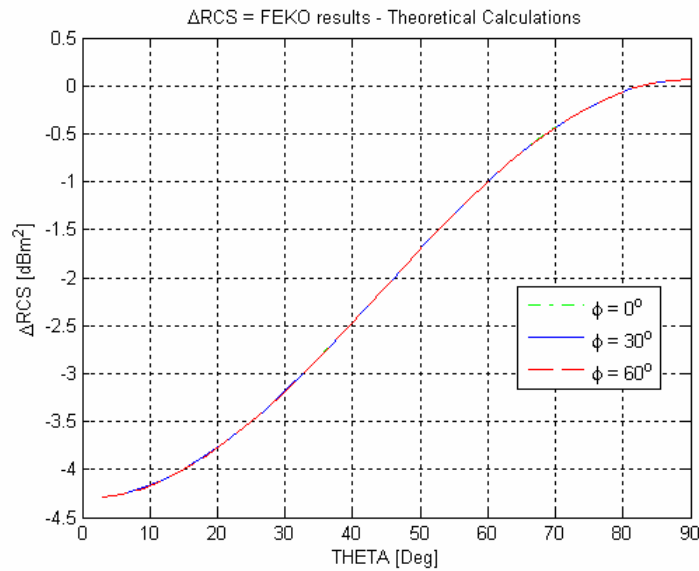


Figure 9 Difference plot between calculated and simulated plot values over θ

An error correction term may be added to the analytical results; in Figure 10 two such error functions are shown. The first is a cos function and the other is a polynomial fit to the error signal using Matlab.

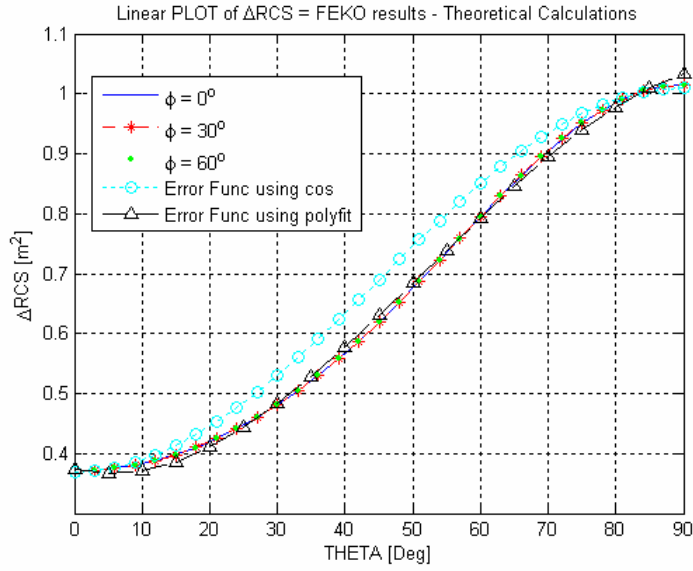


Figure 10 Error function approximations

The mathematical expressions for these two error functions are as follows: the cos relationship used is

$$\Delta\text{RCS}(\theta) = 0.37 + [(1.02 - 0.37)/2](1 - \cos(2\theta)) \quad (3.20)$$

and the polynomial approximation is

$$\Delta\text{RCS}(\theta) = -0.3149\theta^3 + 0.8597\theta^2 - 0.1530\theta + 0.3726 \quad (3.21)$$

where θ is given in radians.

With the error correction term added it is now possible to calculate the exact RCS for any orientation and angle distribution, as illustrated in Figure 11.

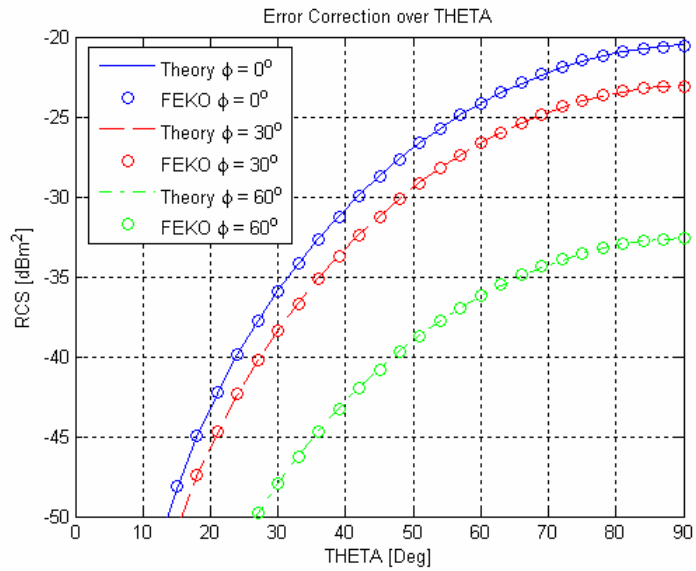


Figure 11 Mathematical calculations vs. FEKO simulation values with error correction applied

The RCS of a dipole can now be calculated for any orientation, though it is still limited to the resonant frequency. Older literature sources [19] – [21] addressing this problem are available. More recent papers on the topic do, however, most often refer to a derivation by O. Einarsson [23] and this is quoted by [22] as the most accurate and up to date derivation.

As the original Einarsson paper was obtainable while a revised version [24] was not, it was decided to direct the modelling approach from a more analytical to a more computational approach.

3.4 Computational Model of Dipole RCS

The previous section discussed the analytical model for calculating the RCS of a dipole. This section will investigate the RCS and modelling properties of a dipole using computation, the goal being to model the spatial average RCS of a single dipole over a wide frequency band.

The modelling approach is described in this section, starting with the resonance of a single upright dipole and ending with the data model of the spatial average RCS over a wideband (section 3.5).

3.4.1 Resonant length of a dipole

The first property to be investigated is the resonance of a dipole. Physically, the resonance is a property of dipole dimension, but in computational modelling it is influenced by meshing, as will be discussed in the next section.

3.4.1.1 Simulation setup

A FEKO simulation was set up for a single upright dipole. The dipole was excited with an incident plane wave. Simulation parameters are presented in Table 1.

Table 1 Simulation parameters

Parameter	Value
Frequency	3GHz
Dipole diameter	125 μ m
Dipole length	0.5 λ
Segment length	$\lambda/20$

A segment length of $\lambda/20$ is a good choice in general, but it can be varied to increase accuracy or shorten simulation time. Since this is a single dipole with a single orientation, simulation time is not of any concern. The actual dipole diameter is more in the order of

25 μ m. The use of a 5 times larger diameter in the simulation is due to the frequency scaling that will be applied, as explained in section 3.4.6

3.4.1.2 Single frequency monostatic results

Simulation results are presented in Table 2.

Table 2 Simulation Results

Parameter	FEKO Value	Analytical Value
Resonant Frequency	2.894GHz	3GHz
Resonant wavelength	0.10366m	0.1m
RCS Peak	0.0092m ²	0.0086m ²
RCS Peak / λ^2	0.856	0.86

The normalized RCS of $0.856\lambda^2$ agrees well with the analytical value of $0.86\lambda^2$ in section 2.2.1. Note that the resonant frequency and the frequency used for calculating the dipole length differ. This is because a dipole resonates at a length slightly less than half a wave length.

3.4.1.3 Wideband monostatic results

The previous FEKO simulation was run again, but this time for a wide frequency band, in order to determine the dipole behaviour. The results are compared with those obtained from another simulation package, CST Microwave studio. Results from both these simulations are shown in Figure 12. The results show the same fluctuating behaviour for a half wave dipole, but the RCS given by the two simulations differs by up to 4.5dB. The reason for the big difference in the RCS results is unclear. From discussion with academics a possible reason was identified as the fact that the time domain solution in CST is not well suited for RCS calculations. No licence was available for the CST frequency domain calculation.

It is not within the scope of this thesis to resolve the difference between these two numerical codes and the matter will therefore not be further investigated.

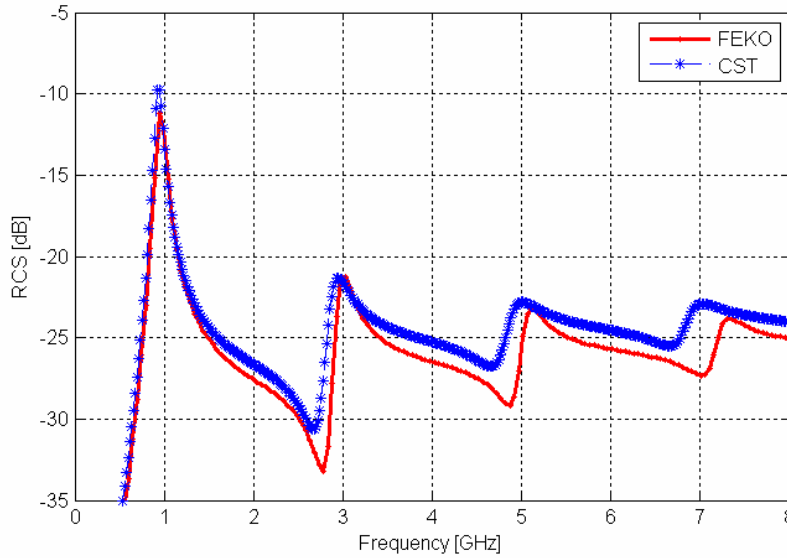


Figure 12 Dipole RCS over a 0.5GHz to 8GHz band

3.4.1.4 Bistatic results

The bistatic RCS of the dipole at resonant frequency is presented in Figure 13. The dipole absorbs energy from the plane wave and reradiates it in a symmetrical pattern. This agrees with the radiation pattern of a dipole as presented in [16] and, as one might expect, the symmetrical structure radiates a symmetrical pattern.

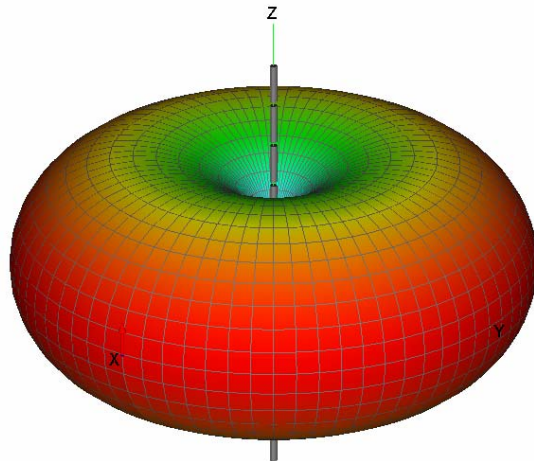


Figure 13 Bistatic radiation pattern of a single dipole at resonance.

3.4.2 Convergence of RCS results

The accuracy of the results of a simulation depends on the meshing (dividing the structure or space into segments). In general terms, the higher the meshing (resolution) of a simulation, the greater the accuracy will be. Before the result of a simulation can be accepted as accurate it must be determined whether the results have converged.

A higher segmentation also results in longer simulation time. This is not a significant factor for a single dipole simulation, but can become large factor for multiple orientations over multiple frequency points and for chaff cloud simulations. Ideally, one wants the lowest degree of segmentation that will produce a converged result that falls within a reasonable limit. An absolute value of 5% is chosen as being sufficient accuracy for RCS results, because in practice many parameters for chaff are not accurately known.

3.4.2.1 Resonant Frequency

The resonant frequency is the simplest to determine from simulation in FEKO and is investigated first. The simulation was for an upright dipole, radiated by a plane wave with linear polarization over a wide frequency band. The parameters are presented below.

Table 3 Simulation parameters

Parameter	Note	Value
Dipole Frequency		3GHz
Dipole diameter	$25\mu\text{m} * 5$	125 μm
Dipole length	0.5λ	50mm
Segment lengths	$\lambda/10$ to $\lambda/40$	5mm to 1.25mm

The results obtained for the above simulations are presented in Figure 14. From the figure it is clear that the RCS peak frequency shifts to a lower frequency and the RCS becomes larger as simulation results become more accurate with higher segmentation.

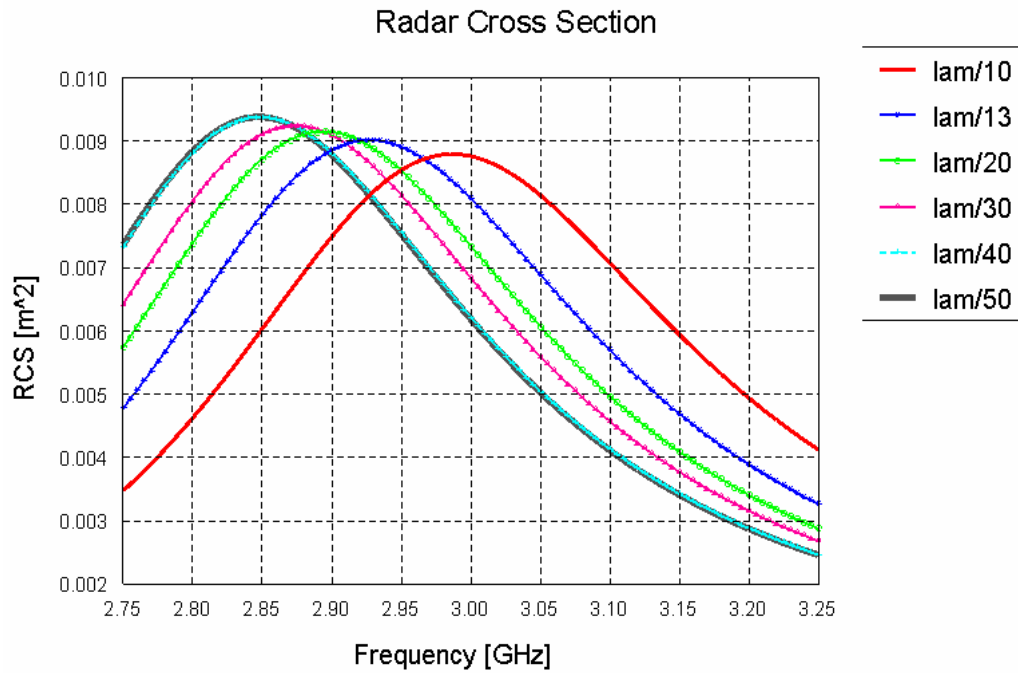


Figure 14 Resonant frequencies for different segment lengths

The resonant frequencies as determined from the Figure 14 are presented in Table 4.

Table 4 Resonant frequencies for various segmentation lengths

Segment length	Resonant frequency (GHz)	Wavelength (m)	Change (%)
$\lambda / 10$	2.987	0.10043	-
$\lambda / 13$	2.927	0.10249	2.05
$\lambda / 20$	2.894	0.10366	1.14
$\lambda / 30$	2.874	0.10438	0.69
$\lambda / 40$	2.849	0.10530	0.87
$\lambda / 50$	2.846	0.10541	0.10

This table gives the changing resonant frequencies for a half wavelength dipole as determined by the various meshing parameters.

3.4.2.2 Resonant Length

For simulations it is helpful to know what length the dipole should be to resonate at a desired frequency.

It is known from the literature [16] that a dipole resonates at a length a little less than half the wavelength, as shown in the previous section. A simple relationship exists between the intended resonant frequency and the simulated frequency used to calculate the length of the half wavelength dipole. This may be derived from Table 4 and is presented in Table 5. A dipole length of 0.47λ is a popular general choice, [16], [25].

Table 5 Resonant lengths

Segment length	Dipole length (λ)
$\lambda / 10$	0.4978
$\lambda / 13$	0.4878
$\lambda / 20$	0.4823
$\lambda / 30$	0.4790
$\lambda / 40$	0.4748
$\lambda / 50$	0.4743

3.4.2.3 Combined Results

The converged result can now be determined by repeatedly simulating the RCS of a single dipole with a higher segmentation each time, using Table 5 to keep the frequency of the result constant. The simulation converges when the variance between results becomes very small.

The results in Figure 15 show good convergence for segment lengths smaller than $\lambda/20$. Results for both $\lambda/20$ and $\lambda/30$ fall within 1% of the converged $\lambda/50$ plot, which is well within the specified 5% acceptability. Even the $\lambda/13$ and $\lambda/10$ curves are within a 2.4% and 1.2% variance respectively from the $\lambda/50$ curve.

The converged RCS peak value is approximately 0.0085m^2 which is slightly (1.2%) lower than the expected value of $0.86\lambda^2 = 0.0086\text{m}^2$ from [16]. This is possibly due to the finite diameter of the dipole.

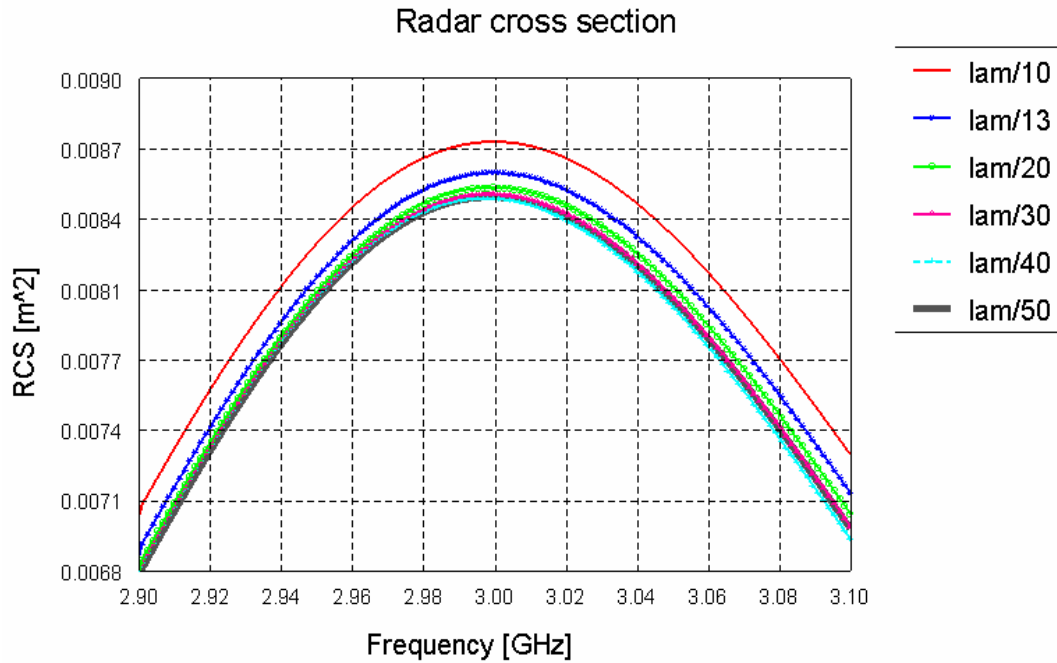


Figure 15 Convolved RCS of a resonant dipole at 3GHz

3.4.2.4 Summary

The RCS behaviour of a single upright dipole has been investigated. Results from theory and simulation were found to compare well for both monostatic and bistatic RCS. More importantly, the first of a series of parameters affecting the modelling has been determined, namely the dipole segmentation. Various segment lengths have been investigated and results compared to ensure that they fall within a reasonable limit of variance from the converged result. An appropriate segmentation length can be chosen that will result in accurate simulation with effective and practical simulation time for large simulations.

3.4.3 Modelling spatial average RCS

The term “spatial average” refers to the RCS found by averaging the RCS of a dipole over various orientation angles. When all orientations are assumed to be equally likely, the average is called the “uniform” spatial average. Simple relationships exist for calculating chaff cloud RCS if the spatial average RCS of a dipole at resonance is known. This will be discussed in Chapter 3.

From the literature [5], [10], [14] and [26] it was found that the monostatic average RCS for a dipole varied over the range $0.15\lambda^2 - 0.28\lambda^2$. Further literature study distinguished between the average RCS values below:

- $0.15\lambda^2 - 0.17\lambda^2$ for a dipole orientation uniformly distributed over a sphere and referred to as the spatial average.
- $0.20\lambda^2 - 0.22\lambda^2$ are the values derived for the Scattering Cross Section (SCS) when polarization is not taken into account.
- $0.27\lambda^2 - 0.28\lambda^2$ for a dipole orientation uniformly distributed over a disc.

To illustrate the difference between the two uniform distributions, the dipole geometry must first be defined. This is shown in Figure 16.

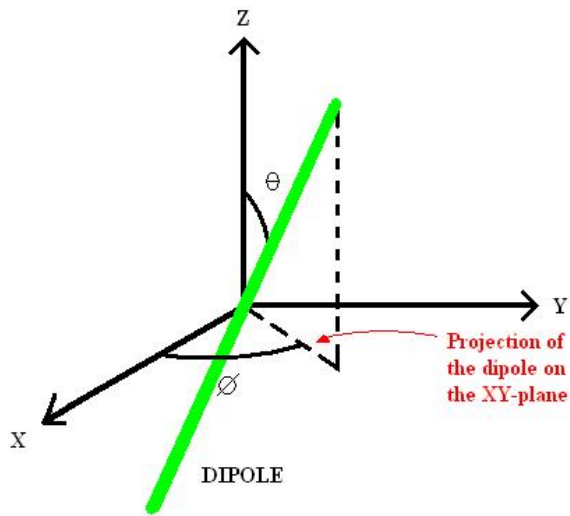


Figure 16 Geometry of dipole in space, defined by length, theta and phi angle

For the sake of clarity, the differences in the uniform dipole distributions are illustrated in Figure 17 and Figure 177.

For a uniform distribution over a disc, the step size in angle between the dipole orientations in θ and ϕ are kept the same.

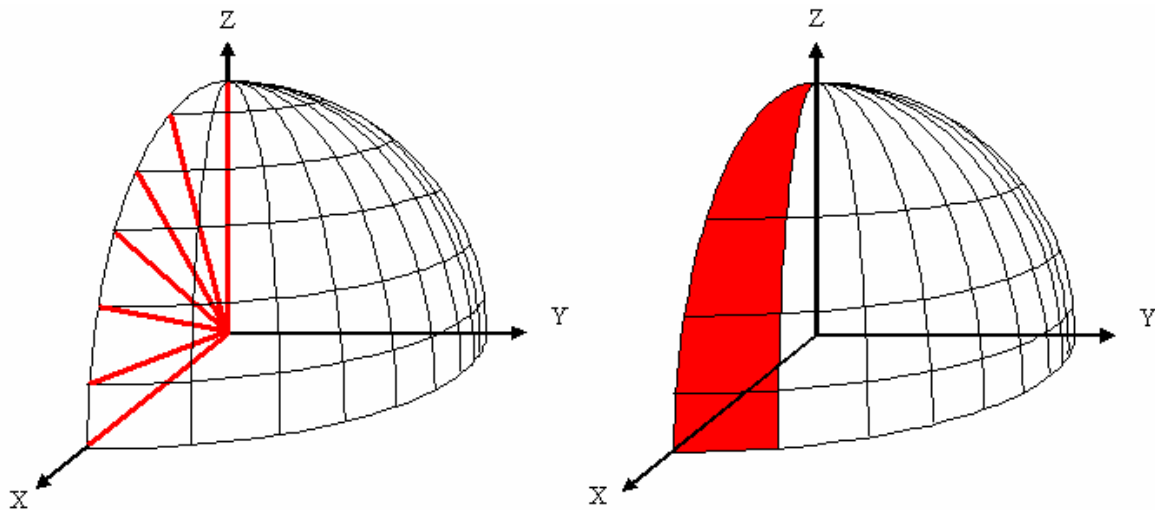


Figure 17 Uniform dipole distributed over a disc. Figure 18 Uniform dipole distributed over a sphere

For a uniform distribution over a sphere, ideally the sphere will be divided into areas of equal size and shape. The mathematical derivation to achieve such division is, however, complex. A simpler approach would possibly be to keep the ϕ division uniform while varying the θ division to achieve an equal area. See section 2.3.3.1.

From both the literature and simulation it is known that the monostatic spatial average RCS varies between $0.15\lambda^2$ and $0.17\lambda^2$. This value, however, is only for a single dipole at resonance and the spatial average value needs to be expanded over a wide frequency band.

Initially the modelling of the spatial average at resonance will be considered and will be expanded over a wide frequency band.

To find the spatial average RCS the set of dipole orientations must be such that all orientations are equally likely. Two methods to accomplish this are investigated:

3.4.3.1 Modelling by Calculating Dipole Orientation

The first method generated dipole orientations directly, using the cylindrical coordinate system. Here the spherical surface is broken into incremented areas. Where the incremented area is small ($dA = \rho \cdot \sin\theta \cdot d\phi \cdot d\theta$), few dipoles are included, with a proportionally larger number of dipoles being included as the area becomes larger (see Figure 19). This approach was implemented and investigated but found to be unsatisfactory for small numbers of dipoles due to the discontinuity of the incremental arc on the z-axis at $\theta = 0^\circ$. In this case the dipoles will have more of a horizontal than a vertical orientation, leading to an uneven dipole orientation distribution.

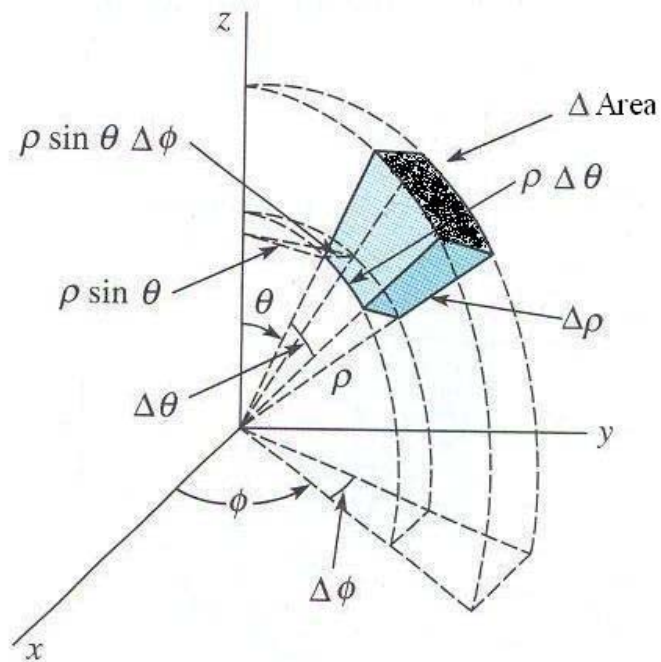


Figure 19 Integration in spherical coordinates [Advanced Engineering Mathematics, Z. Cullen]

3.4.3.2 Modelling by simulating dipole orientation

Although the previous method delivered reasonable results it is not ideal. If the dipole orientations could be more accurately and evenly distributed over the sphere, fewer orientations would be needed for accurate calculation of the spatial average RCS. A method was sought by which to divide a sphere into equal areas. When a spherical shape is simulated in FEKO (Figure 20), the sphere is divided into approximately equal triangular segments. If currents are to be calculated, FEKO outputs the centre coordinates of each triangular segment, which could then easily be used to calculate a set of θ and ϕ angles.

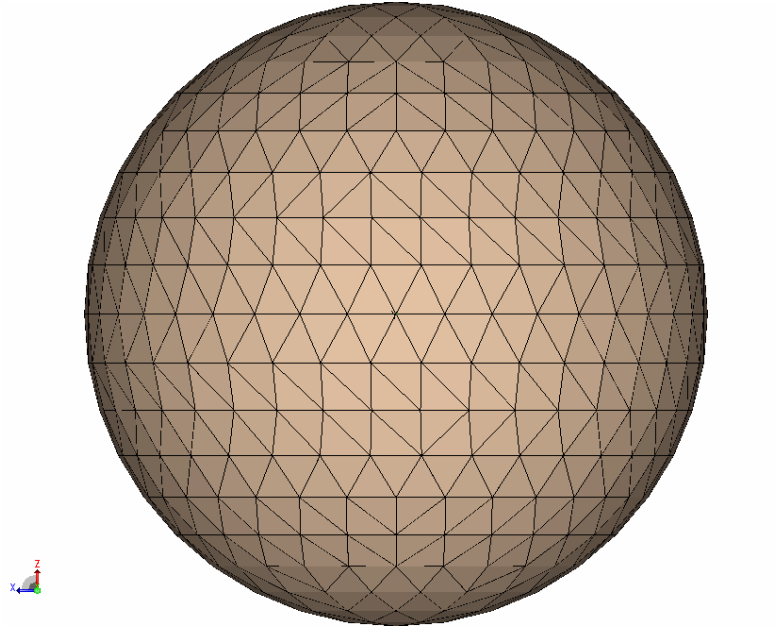


Figure 20 Triangular segmentation of a sphere in FEKO

3.4.3.3 Simulation using Matlab and FEKO

For simulation purposes, Matlab and FEKO were used in conjunction with each other as follows:

All the simulation modelling parameters are set in Matlab. When executed, Matlab calls FEKO to run the simulation and compute the preset parameters. FEKO then outputs a data file that is read into Matlab for data processing.

The first time FEKO is called up, the number of dipole orientations (DOs) specified in Matlab will be calculated from a sphere. On the second FEKO call the actual EM computation will be done.

3.4.4 Validation of the modelling approach

Before using this approach more extensively (over a wide frequency band), the validity of the model needs to be confirmed. To do this the dipole was orientated through the segmented coordinates of half a sphere. In effect the dipole turns through a full sphere, due to its symmetrical shape.

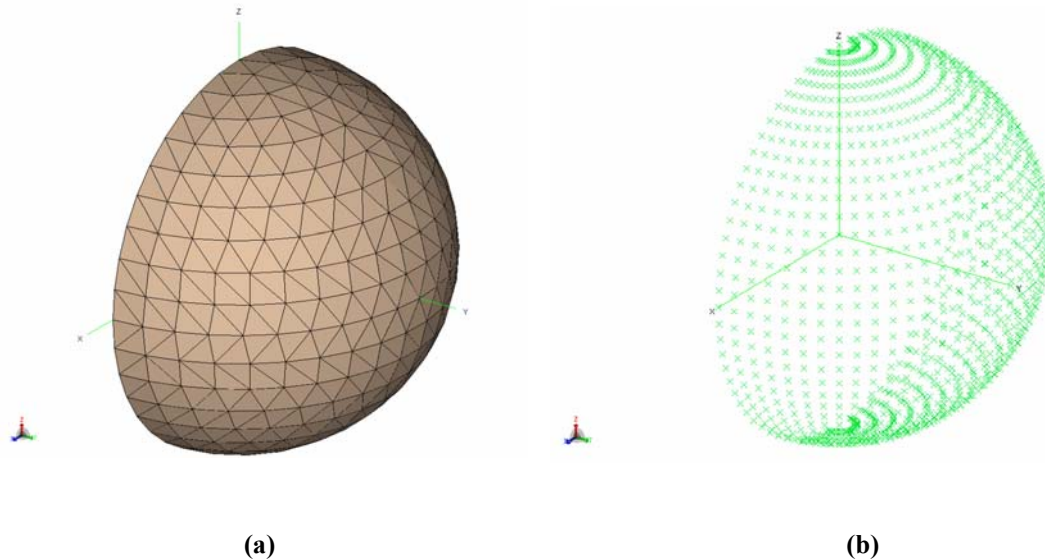


Figure 21 Triangular segments of a half sphere (a) and far field points for a half sphere in FEKO (b)

To check the accuracy of the dipole orientation approach, three different simulations were run. The same coordinates were used to calculate dipole orientation each time, but by using the TG (Turn Geometry) card in FEKO the geometry could be rotated for a new set of orientations and results with each simulation.

The three simulations comprised the original coordinate set with no rotation, a second set with rotation of 90° around the Z axis and a third with rotation of 90° around the Y axis. As a first indication of accuracy only the monostatic RCS was investigated. As discussed in section 3.4.3, the expected value was between $0.15\lambda^2$ and $0.17\lambda^2$.

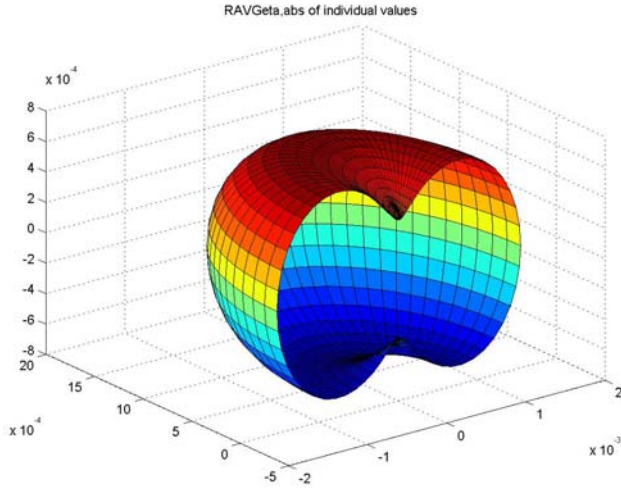
The simulation was run for 500 dipole orientations through half a sphere. This is equivalent to a step angle size of about 8° between far field (FF) points (which is used as the minimum step size).

The results were found to agree well with both the values from the literature and with each other and are presented in Table 6.

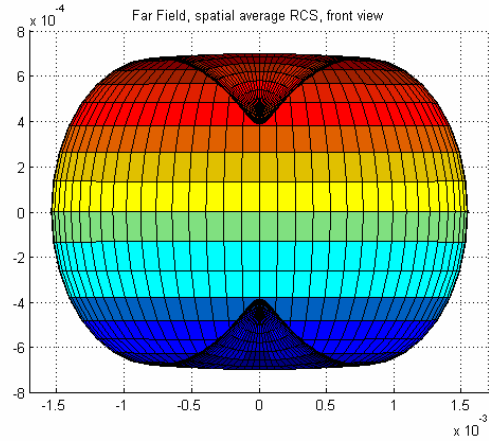
Table 6 Results for various Geometry orientations

	TG = 0°	TG = 90° around Z axis	TG = 90° around Y axis
Monostatic Spatial Average RCS normalized	0.15368 λ^2	0.15366 λ^2	0.15132 λ^2

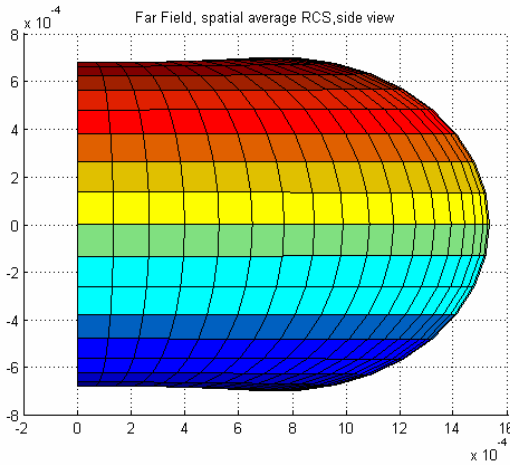
Simulations were done with $f = 3\text{GHz}$ thus $\lambda = 0.1\text{m}$. To further validate the model, simulations for the far fields were run and the 3D bistatic FF results compared, with results as presented in the following figures.



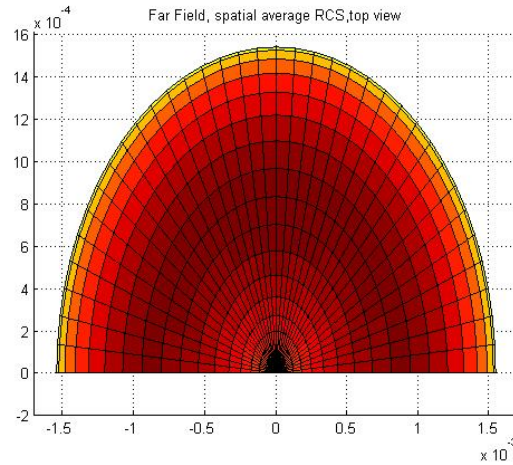
(a)



(b)



(c)



(d)

Figure 22 Bistatic spatial average RCS of a dipole (a) 3D plot, (b) front view, (c) side view, (d) top view. Only the plot shape is significant, axes and colour coding should be ignored.

It can be seen that the spatial average RCS agrees well with the radiation pattern of a dipole at resonant frequency, as illustrated in [9]. The expected RCS value of $0.15\lambda^2$ is also clearly visible on the edges of the “donut” shaped radiation pattern.

The 3D farfield plots for the turned geometries agreed well with that of the original set of orientations and these are presented in Figure 23 and Figure 24.

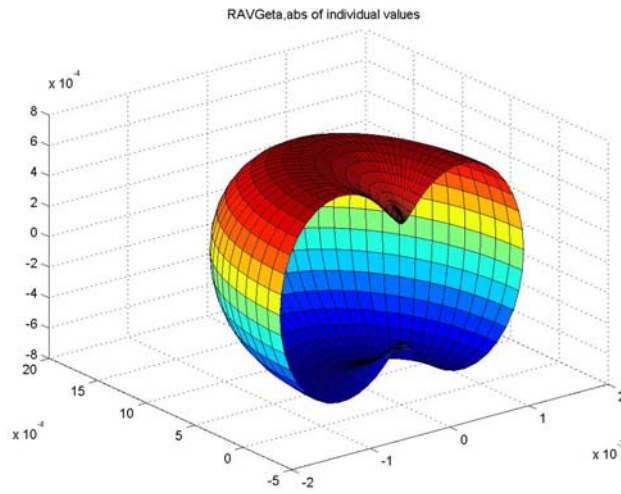


Figure 23 Bistatic spatial average RCS of a dipole at $TG = 90^\circ$ around Y axis

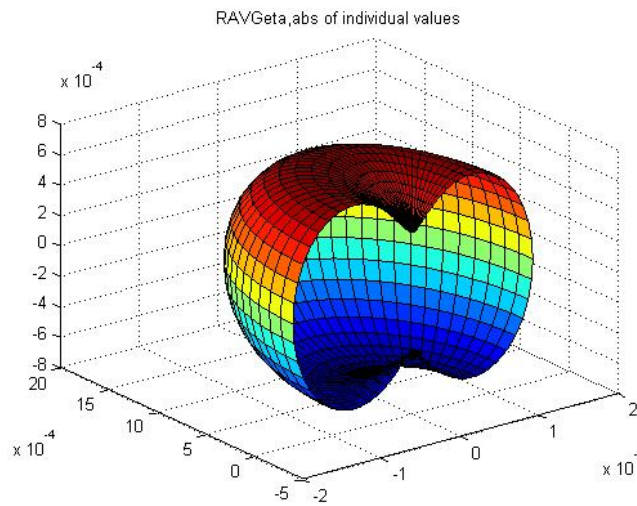


Figure 24 Bistatic spatial average RCS of a dipole at $TG = 90^\circ$ around Z axis

The RCS results are consistent with the literature and also over different geometry orientations; the orientation approach is therefore validated.

3.4.4.1 Summary

The spatial average RCS was computed for a dipole at resonant length and frequency and results were found to be in good agreement with the literature.

3.4.5 Determining parameters for wideband modelling

The model can now be further developed to investigate the RCS behaviour of a dipole over a wide frequency band. This is essential for the modelling of a practical chaff cloud comprising various dipole lengths.

Before effective wideband modelling can proceed a few other parameters need to be investigated. These parameters do not necessarily influence accuracy, but do affect simulation time and data storage size. These parameters were investigated and determined as follows.

3.4.5.1 Determining the number of dipole orientations

One of the factors that greatly influence simulation time is the number of dipole orientations (DOs). The number of orientations should be the minimum that will allow for the least possible total simulation time without compromising accuracy.

Since the dipole orientations are uniformly distributed in θ and ϕ due to FEKO's method of meshing a sphere, the number of DOs can be significantly reduced over the whole frequency band of interest. To confirm this, the bistatic spatial average RCS for a number of dipole orientations will be investigated.

Simulation Parameters

For each simulation the number of dipole orientations was determined so as to give a particular average angle spacing between orientations, which is presented in Table 7.

Table 7 Average angle spacing between dipole orientations

Number of orientations	Average angle spacing [Degrees]	Rounded angle value [Degrees]
500	8.0°	8°
1000	5.7°	6°
1500	4.6°	5°
2000	4.0°	4°
4000	2.8°	3°
8000	2.0°	2°

Results

The values are required to be within an arbitrarily set 5% of the values of the simulation with the highest number of dipoles. Results are presented in Figure 25 to Figure 27.

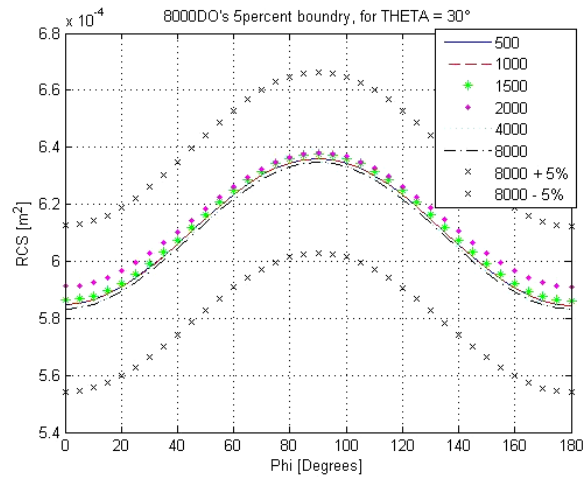


Figure 25 Average RCS as a function of the number of dipoles in as set, data plot for bistatic angle $\theta = 30^\circ$

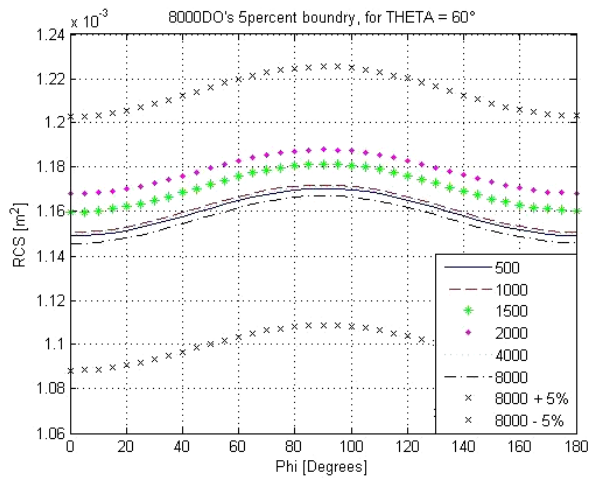


Figure 26 Average RCS as a function of the number of dipoles in as set, data plot for bistatic angle $\theta = 60^\circ$

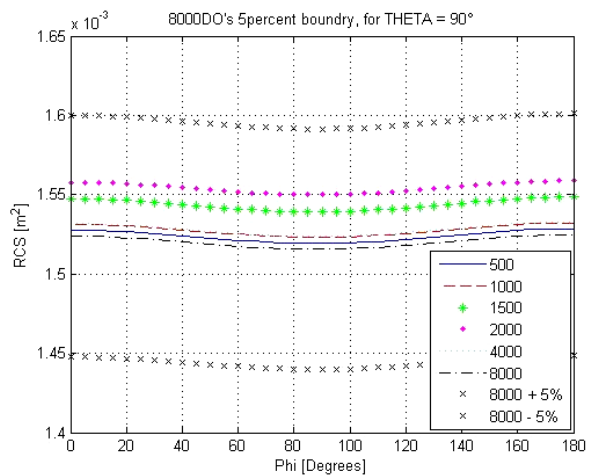


Figure 27 Average RCS as a function of the number of dipoles in as set, data plot for bistatic angle $\theta = 90^\circ$

As can be seen, the results fall well within the 5% limit of variance from the RCS plot for 8000 orientations. The number of orientations that has been chosen for further simulations is 1000. This lower number of orientations greatly helps in reducing simulation time, but still produces results within 1% of the 8000 DO results.

3.4.5.2 Determining the number of farfield points

The number of FF points computed for each dipole orientation has an influence mainly on the volume of data being stored, but also has a simulation time factor. For the case of gathering bistatic data the FF points had to be densely enough distributed not to miss sharp changes in RCS sidelobes over a wideband, especially at frequencies much higher than that of the dipole resonance.

Through continuous evaluation of data size and simulation time, the number of FF points was determined and 61 points in each of the θ and ϕ phi angles was decided on. This results in a matrix of 61^2 data points and gives an angle spacing of 3° between the FF points.

The number of FF points, along with other factors determining the data storage size required, resulted in data size of 18KB for a single frequency point over all orientations.

3.4.5.3 Determining the number of frequency points

The number of frequency points directly influences the simulation time, which must thus be traded off against missing RCS peaks.

Frequency Band

The initial dipole length or resonant frequency had to be specified. 1GHz was chosen as a practical specification for a resonant dipole. The frequency band was chosen a factor 20 above and below the 1GHz first resonant length, resulting in a frequency band from 0.05GHz to 20GHz.

Simulation Setup

The dipole length was taken at half a wavelength at 1GHz, and the segment lengths were taken at $\lambda/60$ to ensure that segmentation rules (specified by FEKO) were met at the highest frequency.

It was decided to divide the frequency band of interest into 3 divisions:

- Below initial resonance: 0.05 to 1 GHz
- Above initial resonance: 1.00 to 10 GHz
- Far above initial resonance: 10.0 to 20 GHz

Results

Figure 28 is the simulated result for an upright dipole over the complete frequency band chosen to give an overview of the RCS behaviour over the wide frequency band. The non-normalised RCS result in Figure 28 shows that the fluctuating behaviour becomes scarcely noticeable at 14GHz and strives toward a straight line.

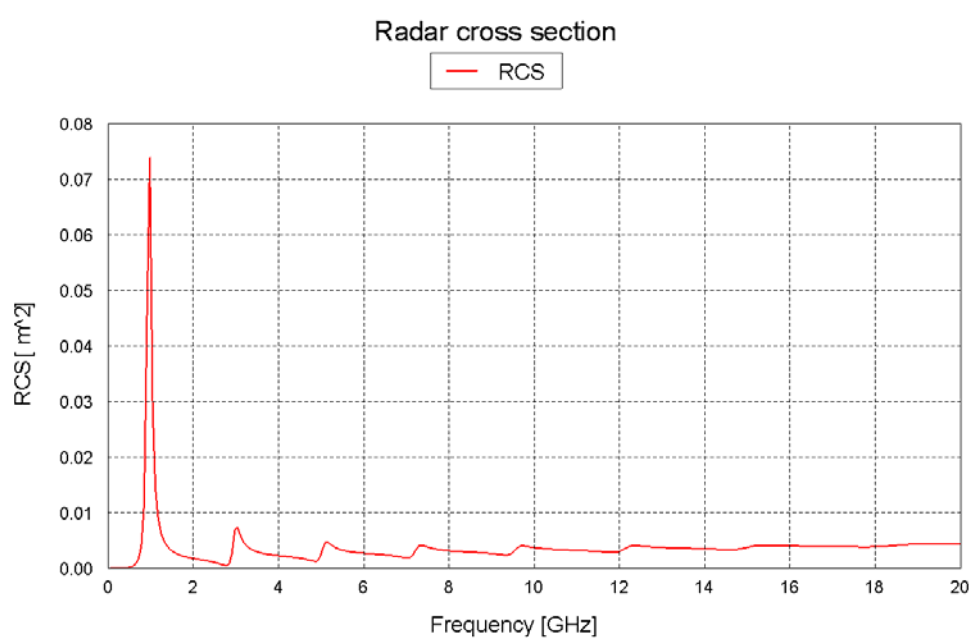


Figure 28 RCS for an upright dipole over a wideband

The FEKO simulation results for an upright simulated dipole will now be presented over the three frequency bands for various numbers of frequency points.

In Figure 29 to Figure 31 the RCS in three frequency band divisions is presented. From these figures it can be seen that there is little difference between the simulations for 51, 101 and 201 frequency points. The simulation with 201 frequency points was chosen in order to give the most accurate results for modelling the spatial average RCS over a

wideband. The greater number of frequency points would result in more data points and better data manipulation for the GUI tool (Appendix B).

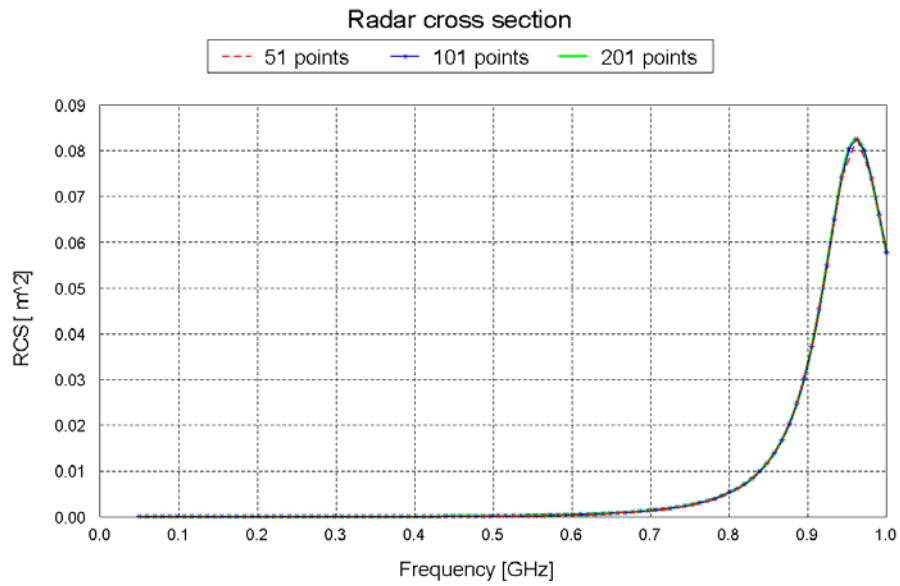


Figure 29 RCS of a 150mm half wave dipole sampled over a 0.05 to 1 GHz frequency band

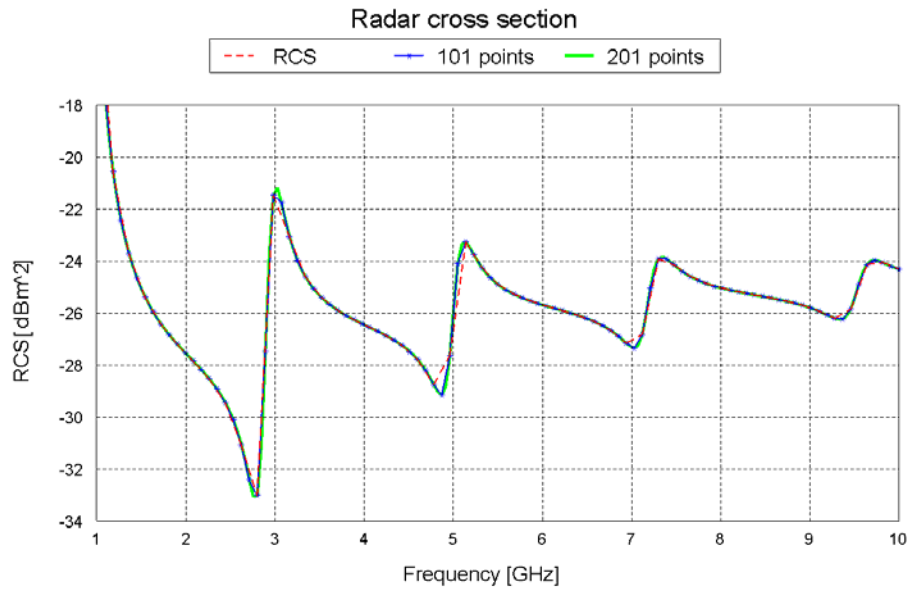


Figure 30 RCS of a 150mm half wave dipole, zoomed in view, sampled over a 10 to 20 GHz frequency band

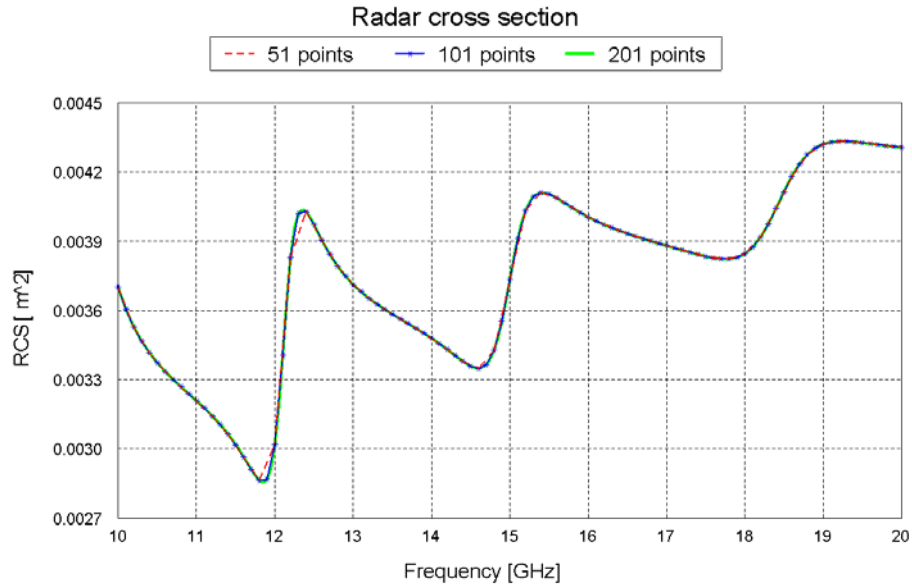


Figure 31 RCS of a 150mm half wave dipole, sampled over a 10 to 20 GHz frequency band

3.4.6 Wideband spatial average RCS simulation

Simulating the dipole spatial average RCS over a wideband not only allows one to see how the RCS changes, but also allows the scaling of data for various lengths of dipoles without necessitating re-simulation of the band. From this data the RCS of a chaff cloud comprising various dipole lengths can be calculated.

Before results are presented, the parameter specifications of the simulation will be discussed.

Simulation Parameters

As discussed in the previous section the frequency band of interest lies between 0.05GHz and 20GHz. The dipole to be simulated was chosen to resonate at 1GHz.

For scaling purposes the simulation with the 1GHz resonant dipole will provide the most accurate data with the correct length and diameter. When this data is scaled, however, the result will be less accurate since only the length of the dipole was scaled and not the diameter. To reduce this inaccuracy it was decided to scale the diameter for the simulation five times higher ($25\mu\text{m} \times 5$), to $125\mu\text{m}$. The data will now be most accurate when the frequency is scaled 5 times higher, thus scaled from a resonant frequency at

1GHz to a frequency of 5GHz. The concept is illustrated in the Figure 32. Simulation parameters can be summarized as presented in Table 8.

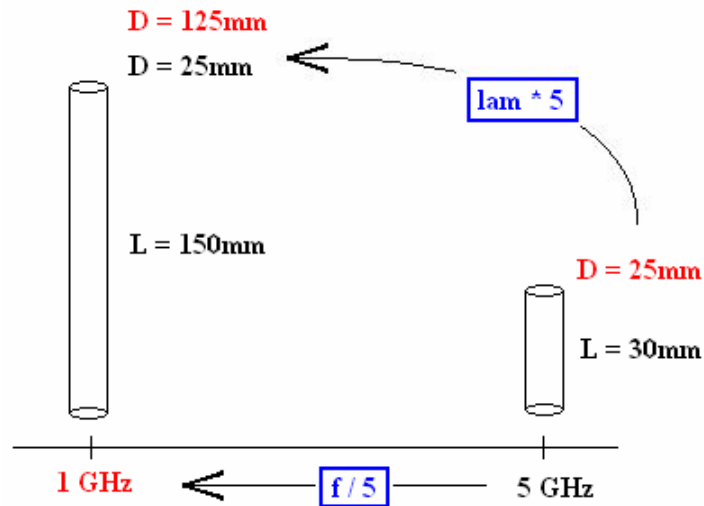


Figure 32 Illustration of frequency and dimension scaling

Table 8 Simulation specifications

Parameter	Value	Effect on simulation time/accuracy/data size
Resonant Frequency	1GHz	None
Segmentation	$\lambda/13$	Time, accuracy
Length	$0.488\lambda_0$	None
Number of DOs	1000	Time, accuracy
Number of FF points	61 in θ direction 61 in ϕ direction	Time, data size
Frequency bands	0.05GHz - 1GHz 1.00GHz - 10GHz 10.0GHz - 20GHz	Time, data size
Number of Frequency points per band	201 per band	Accuracy, data size

3.5 Wideband Dipole RCS Results

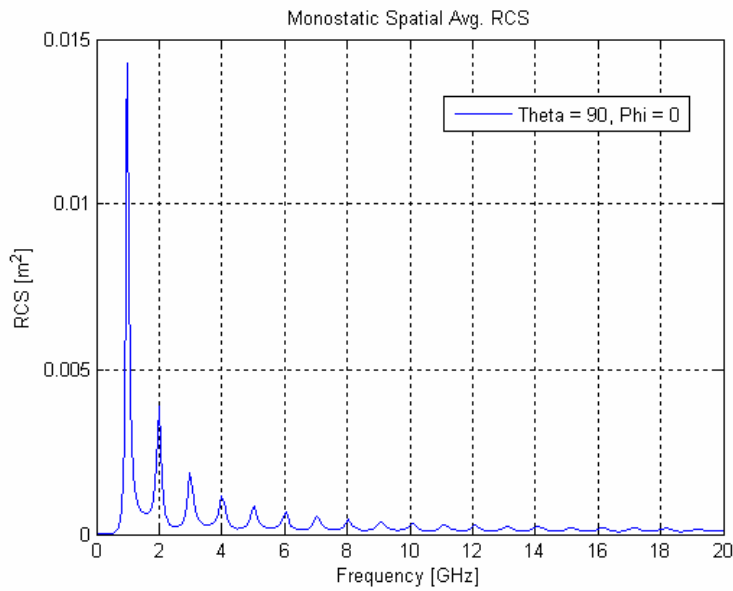


Figure 33 Monostatic spatial average RCS (m²) of a dipole

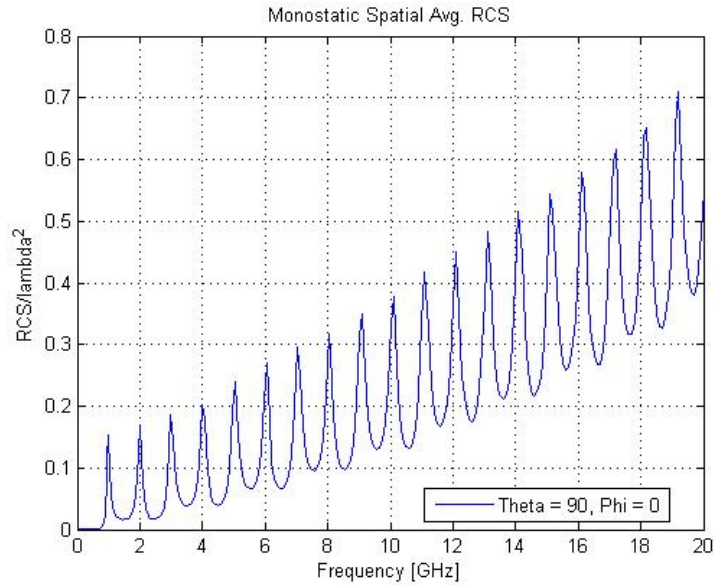


Figure 34 Monostatic spatial average RCS of a dipole, normalized to wavelength (m²/λ²)

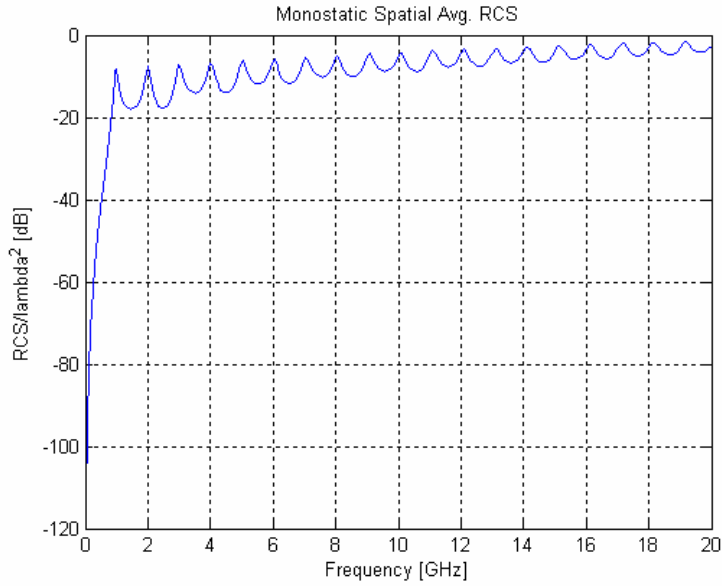


Figure 35 Normalized spatial average RCS on dB scale

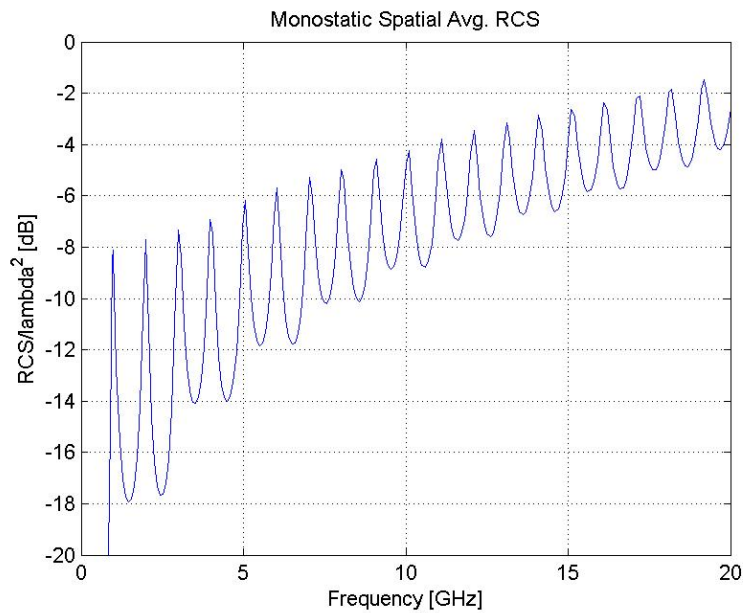


Figure 36 Zoomed in view between 0 and -20dB over the frequency band

The low dB RCS value below 1GHz in Figure 35 indicates the low average RCS below resonance. It is interesting to note that the RCS for spatial average modelling and that of a single vertical dipole show the same oscillating behaviour.

3.6 Verifying results with the literature

To validate the monostatic spatial average RCS of a dipole over a wideband, results were compared to those of [13]. Since only the total scattering cross section was presented in the literature, the SCS results of the simulation were used for validation. This is acceptable, as the RCS component is calculated from the SCS results and will behave in the same manner. The theoretical and simulated results are shown in Figure 37 and Figure 38.

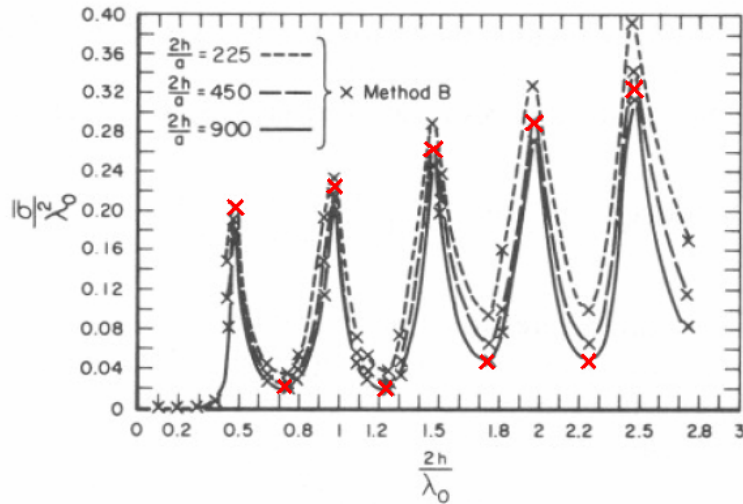


Figure 37 Spatial Average SCS [after Van Vleck *et al*]

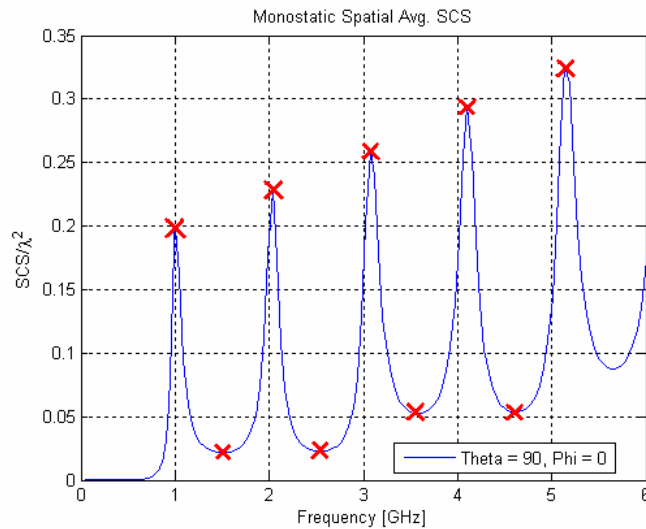


Figure 38 Spatial Average SCS simulated

Chaff is very thin and Figure 38 should be compared to the $2h/a = 900$ solid line plot in Figure 37 ($2h$ is the dipole length and a is the dipole diameter). Though it may seem that the horizontal axes differ, they are relative to each other, $f = c0/\lambda$.

The first peaks in both graphs clearly agree, peaking just below $0.20\lambda^2$, as do the last peaks, peaking at about $0.32\lambda^2$. By investing the graphs closely one can see that the peaks and valleys agree well, as marked by the red crosses.

3.7 Verifying wideband results with a chaff cloud simulation

To investigate the reliability of the spatial average RCS model, a chaff cloud was simulated in FEKO and compared with a calculation applying the wideband results. 1488 Dipole elements were simulated in a chaff cloud. These elements were of various lengths and were simulated far enough apart to ensure that coupling would be negligible.

The chaff cloud RCS was calculated from a GUI tool (see Appendix B) implementing the dipole spatial average RCS model. In Figure 39 GUI refers to the calculated chaff cloud value and FEKO to the simulated chaff cloud value.

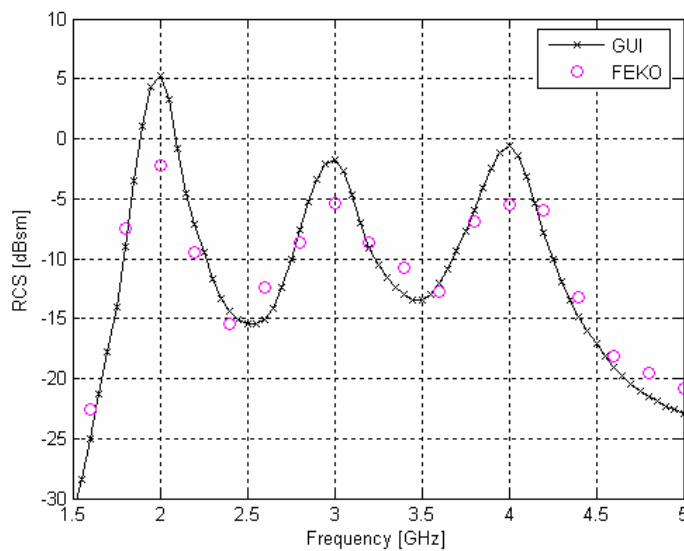


Figure 39 Dipole spatial average RCS Model vs. FEKO Simulation of a Chaff Cloud (see Figure 60)

The calculated and simulated dipole RCS values seem to differ by up to 7.2dB at 2GHz. Though this is a big difference, it can be seen in Figure 42 that the RCS of a chaff cloud deviates by up to 7dB from the average RCS in the upper limit and up to 34dB in the lower limit.

The RCS peaks seem to agree at frequency but the valleys differ, being either higher or lower in frequency. This can be ascribed to a number of factors, namely the high variance of chaff cloud RCS, the dipole diameter scaling and the simulation meshing. Further investigation will be needed to determine the exact influence of each of these factors, if any, on the RCS.

3.8 Conclusion

The computational model for calculating the spatial average RCS at resonance has been determined and expanded to calculate spatial average over a wideband. All the necessary parameters for making a practical wideband simulation were investigated and determined. It is therefore possible to make an effective simulation, acquiring spatial average data, over a wide frequency band.

The necessary changes in dimension were made for frequency scaling for dipole lengths between 1GHz and 10 GHz. Simulation data were obtained over the 0.05GHz to 20GHz band. In comparing the results of dipole spatial average RCS data and a chaff cloud simulation it was found that data differed by up 7.2dB. This can be explained by the variance in chaff cloud RCS as illustrated in Figure 42. From these results it is concluded that the RCS model over a wide frequency band is acceptable and can be applied in the theoretical calculation of chaff cloud RCS.

Chapter 4

Chaff cloud RCS & dipole density

4.1 Introduction

The modelling discussed in the previous chapter can be divided into three parts. The first is the meshing of simulations and convergence of results (computational parameters), the second is the determining of the spatial average RCS at resonance and last is the extension of the spatial average RCS over a wide frequency band (modelling parameters).

The next step is the modelling of chaff cloud RCS. Simple linear equations exist to address this problem analytically [10], [14] and [18]. With these linear equations and the results from the previous chapter, it is possible to calculate the RCS of a chaff cloud over a wide frequency band. The linear equations are, however, limited to low dipole densities for which coupling between dipole elements is negligible.

It is the purpose of this chapter to determine for which dipole density regions these linear equations are applicable and what the effect of coupling is on the RCS of a chaff cloud.

No simple analytical models incorporating coupling exist, therefore the chaff cloud modelling will be investigated computationally. As previously stated, a chaff cloud consists of up to several million dipoles. In the simulating environment this can result in 5 to 10 times this number of wire segments, depending on the meshing specifications of the simulation. A simulation of this magnitude would require very powerful computing capabilities; therefore modelling is done on a much smaller scale. The analytical and computational approach applied to the small scale modelling is the same as would be applied to a full scale model, making it of practical use.

4.2 Backscatter RCS for N dipoles

From the literature [5], [8], [10] and [14] the following simple relationship exists for calculating the backscatter RCS of a chaff cloud:

$$\sigma = \sigma_{\text{avg}} N \lambda^2 \quad (4.1)$$

For a sparsely spaced chaff cloud, with negligible inter-dipole coupling, the RCS is equal to the dipole spatial average RCS, times the number of dipoles. The average dipole RCS is usually normalized to the wavelength, hence the $\sigma_{\text{avg}} \lambda^2$ expression. This formulation is well known and will not be discussed. The simulation results will be presented in sections 4.5 and 4.6.

4.3 Hypothesis of Forward Scatter RCS

The forward scattering of a chaff cloud is not usually considered, as it is never observed by monostatic radar. However, as will be shown, the σ_{forward} of a chaff cloud can be found more accurately than the σ_{back} as it has a comparably small variance. This makes it a better measure for detecting the chaff density where coupling between dipoles become evident.

This section presents the following hypothesis:

A relationship exists between the forward scatter RCS (being coherent) and the number of dipoles, such that the forward scatter RCS is directly proportional to N^2 :

$$\sigma_{\text{forward}} = k N^2 \lambda^2 \quad (4.2)$$

When investigating the E-fields propagating through a spherical chaff cloud, as will be shown in Figure 47 and Figure 48 in Chapter 5, one finds that the back scattered near

fields fluctuate around 1 V/m, the incident field strength. The total E-field initially drops just behind the chaff cloud to form a shadow region. Moving further behind the chaff cloud the E-field strength starts rising asymptotically to the incident E-field strength value. This is due to the scattered E-fields dropping by $1/R^2$ while the incident field strength remains 1V/m everywhere, due to the plane wave excitation.

The drop in E-field behind the cloud can be seen as a scattering effect. This scattering phenomenon seen from the simulation results can also be described in terms of coherent and incoherent field behaviour. In [27] these fields are described as follows:

“The average field $\langle u \rangle$ is also called the coherent field and the fluctuating u_f is called the incoherent field”

The fluctuating behaviour of the backscattering RCS is referred to as incoherent and that of the forward scattering RCS, approaching a constant value, as coherent.

For the chaff cloud consisting of “random media”, the back scattered E-field and incident E-field adds in and out of phase and the RCS calculation is therefore a power relationship proportional to N.

For the forward scatter the E-fields add in phase, so that the RCS calculation is a field strength relationship proportional to N^2 . The N^2 relationship for coherent intensities is also mentioned in the literature [4]. This leads to the hypothesis that a $N^2\lambda^2$ relationship exists, with a proportionality constant k. The proportionality will be determined from simulation results, which will be presented in the following sections.

4.4 Chaff Cloud Simulation – Approach & Parameters

4.4.1 Simulation Using Matlab and FEKO

The method of calling FEKO to determine the RCS of a chaff cloud was much the same as the code for calculating the spatial average RCS:

- The number of dipoles and the cloud size was specified in Matlab before simulation.
- The dipole orientations were first generated by using FEKO to divide a sphere into the same number of triangular segments as the number of dipoles. The centre coordinates of the triangular segments were used to achieve a spatial average distribution.
- The dipole coordinates were generated for a cube and then filtered to achieve a spherical cloud shape.
- FEKO was then called to do the necessary calculations and export the data to the *.out-file.
- This file could then be loaded by Matlab for processing and interpretation.

4.4.2 Chaff Cloud Shape and Dipole Distribution

Even though the spherical chaff clouds used here are not necessary a true reflection of the shape of a real chaff cloud, the shape was chosen as a good platform from which the chaff cloud model and application could be investigated and developed for further investigation as discussed in Chapter 1.

Generating a uniform distribution of spherical coordinates appeared to be a deceptively simple task, but the results of simple solutions were not truly uniformly distributed.

The solution adopted was to generate the chaff cloud in the shape of a cube and to take all the element coordinates that fell within the specified radius. To achieve the same dipole density as before it was necessary to generate a cubical density greater than the specified number of dipoles to ensure that enough dipole element coordinates fell within the specified radius. This is illustrated in Figure 40.

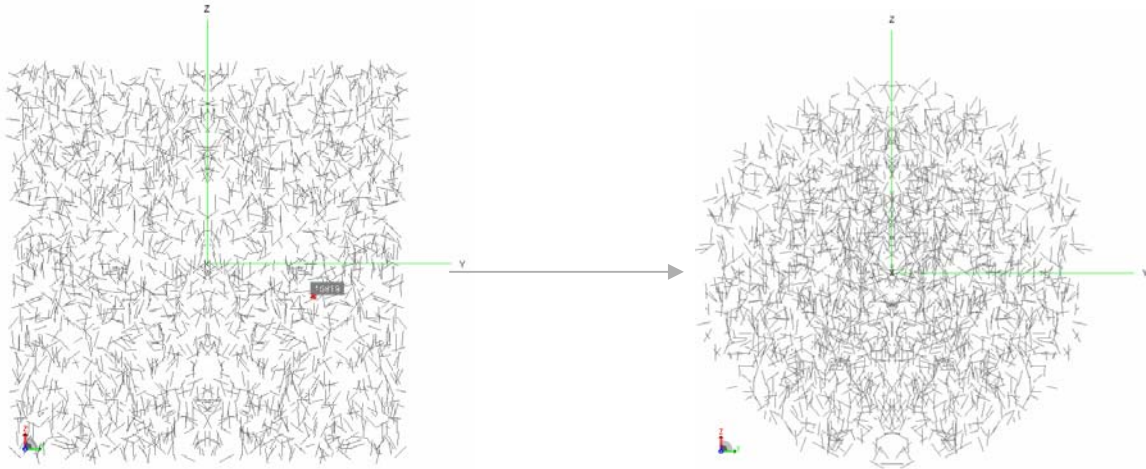


Figure 40 Generating a Spherical Chaff Cloud from a Cube

4.4.3 Simulation Results

The simulation was run for a chaff cloud with a volume of 1m^3 with dipoles resonant at a frequency of 3GHz. Results were averaged over 50 simulations for an increasing number of elements of up to $N \approx 4500$. This was to achieve a statistical average. Two further single data points were added for $N \approx 10000$ (30 hours simulation time) and $N \approx 15000$ (180 hours simulation time). The sparse cloud results in section 4.5 are expressed as a function of dipole density, while the dense cloud results in section 4.6 are expressed as a function of the number of dipoles N .

4.5 Results for Sparse Cloud Simulation

4.5.1 Back Scatter RCS results

In Figure 41 the simulation results from FEKO are compared with the literature. The solid blue line represents equation 4.1 and the dashed magenta line represents simulation results.

The simulation plot follows the calculated plot within 0.1m^2 below $N \approx 450$ dipoles. It then starts deviating below the calculated plot, due to dipole coupling as a result of the denser spacing.

The random distribution of the dipole coordinates and orientations, along with incident and scattered E-fields adding in and out of phase, are among the factors contributing to the fluctuating back scatter RCS average, over the 50 simulations. This is illustrated in Figure 42.

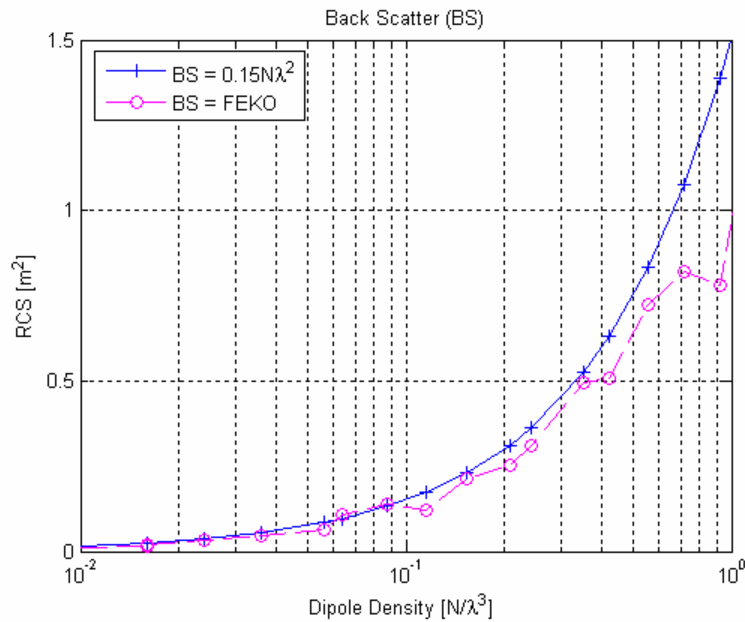


Figure 41 Back scatter RCS plot for a 1m^3 chaff cloud with up to 1000 dipoles resonant at 3GHz

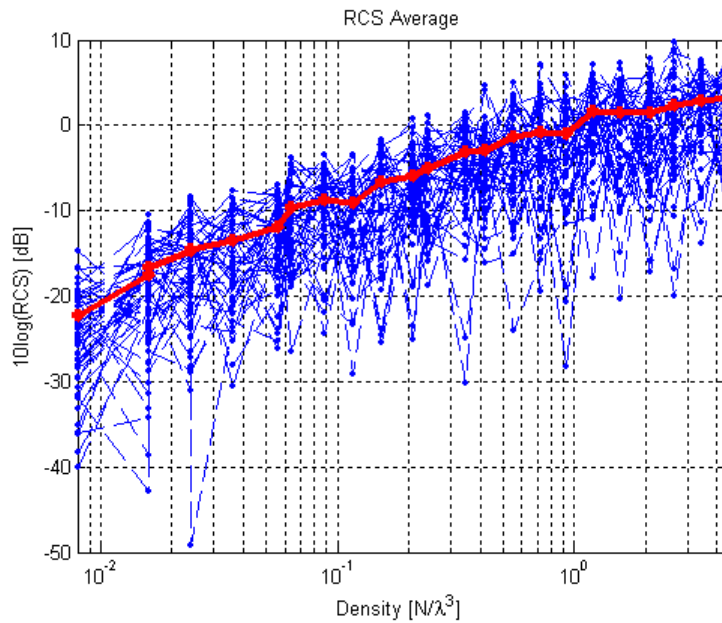


Figure 42 Average RCS plot along with the 50 simulations over which average RCS was calculated

4.5.2 Forward Scatter RCS Results

From equation 4.2, the forward scattering constant k can be written as:

$$k = \sigma_{\text{forward}} / N^2 \lambda^2 \quad (4.3)$$

From simulation results the proportionality constant k is approximated as 0.07. This allows the calculation of the forward scattering RCS as:

$$\sigma_{\text{forward}} = 0.07 N^2 \lambda^2 \quad (4.4)$$

The result is plotted in Figure 43 along with simulation results and it delivered coupling results in accordance with that of the back scatter RCS results in the previous section at $N \approx 450$ dipoles or density, $\rho \approx 0.46$.

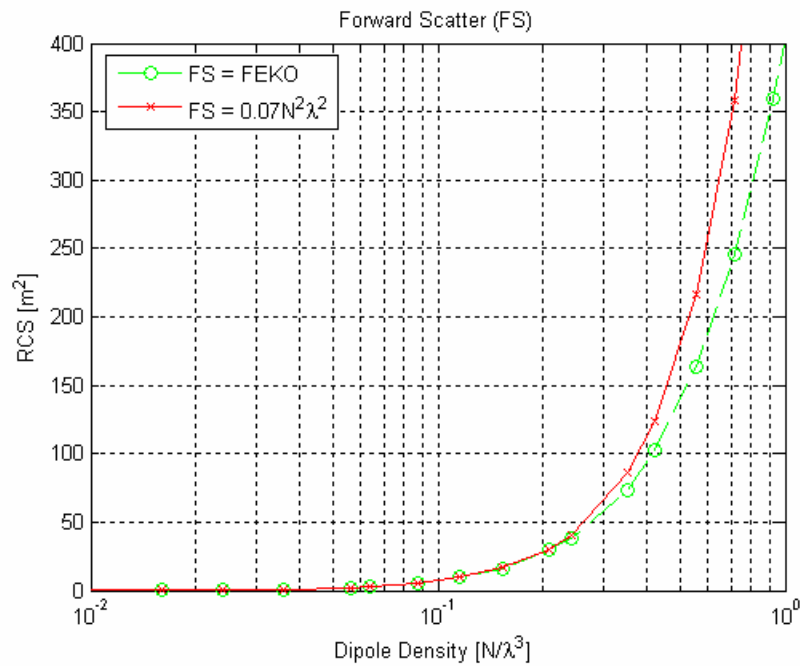


Figure 43 Forward scatter RCS plot for a 1m³ chaff cloud with up to 1000 dipoles

4.5.3 Back Scatter & Forward Scatter RCS Results on dB scale

In Figure 44 the RCS vs. density results are plotted on a dB scale. From this the accuracy of the estimated constant k is clearly visible. Both the back scatter and forward scattering RCS can be approximated to within 2dB accuracy for the region of no coupling.

It is also interesting to note how smooth the forward scattering is compared to the back scattering. This makes an accurate forward scatter average RCS estimation possible, after only one tenth of the number of simulations needed for the back scatter average RCS.

It should be noted that, for one dipole, the forward scatter and back scatter RCS are equal, as was seen from the average radiation pattern in Chapter 3. From equations 4.1 and 4.2 this is, however, not the case since $k \neq 0.15$ and this makes equation 4.4 inaccurate for a low number of dipoles.

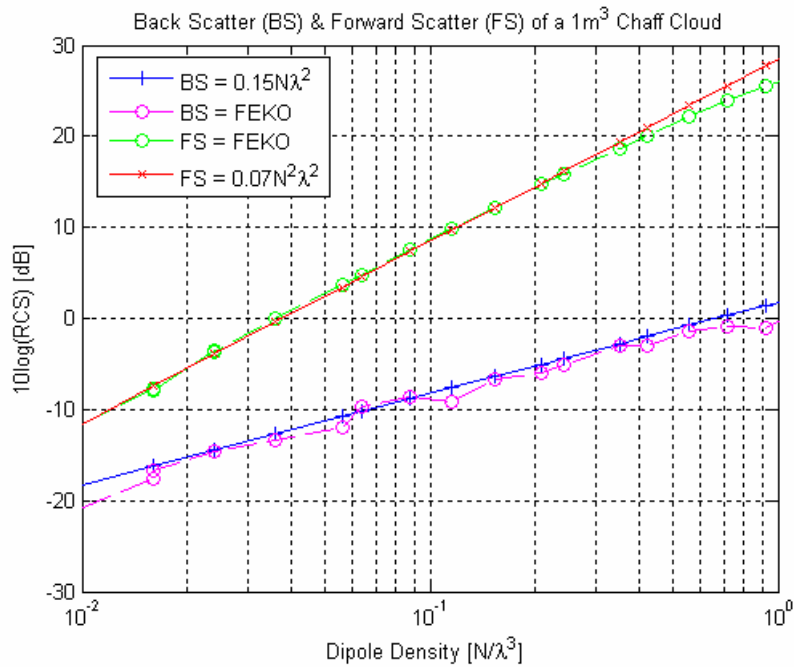


Figure 44 Back scatter and Forward scatter RCS results on dB scale

From the results the hypothesis has been validated and can be applied for further chaff RCS modelling and investigation.

4.6 Results for Dense Cloud Simulation

The purpose of this chapter is to investigate the dipole density region for which coupling is negligible. This will determine the dipole density region to which the chaff modelling results obtained thus far will be applicable. In this section coupling is discussed and results are presented from the simulation.

The RCS of chaff has until now been modelled for sparse clouds. Sparse clouds have been defined as clouds with dipole elements being far enough apart so that no, or very little, inter-dipole coupling takes place. Thus coupling is negligible and can be ignored in calculation and or simulation. Having defined the model for sparse clouds, a boundary density has not yet been set for this definition.

Coupling within chaff clouds is a complex phenomenon. A few papers exist on complex calculation through iterative calculation, making use of mutual coupling matrixes [9] and approaching dense clouds as a continuum [28].

From the literature [5], [9] the general approximation is that for a dipole spacing of at least 2λ apart (density = 0.125 dipoles/ λ^3) almost no coupling takes place and for dipole spacing down to 0.4λ apart (density = 15.625 dipoles/ λ^3) a loss of up to 3dB could be expected.

To investigate these approximations, a spherical chaff cloud of 1m^3 was simulated for an increasing number of dipoles of up to 4500 in a 1m^3 spherical volume at a resonant frequency of 3GHz. This relates to a maximum density of 4.5 dipoles/ λ^3 . The RCS was calculated and averaged over 50 simulations and the results are presented in Figure 45.

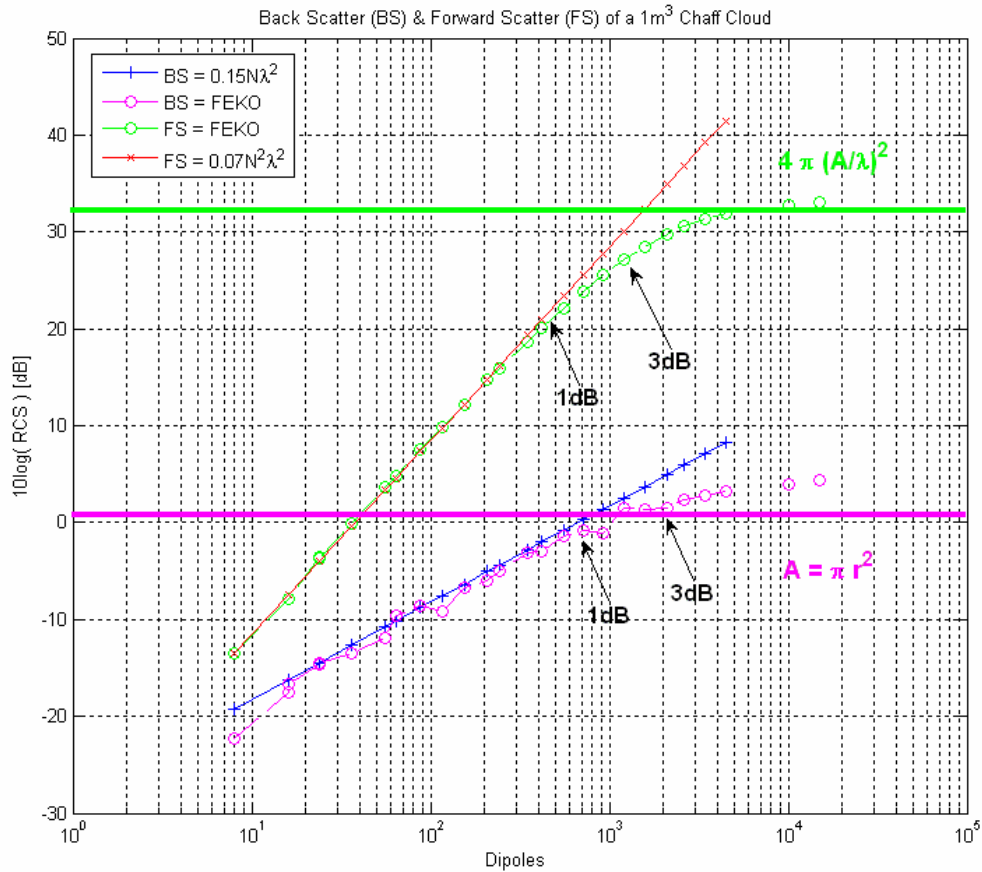


Figure 45 RCS back and forward scatter results averaged over 50 simulations for a cloud of volume = of 1m^3

It can be seen that the 1dB and 3dB compression points for the back scatter and forward scatter RCS differ as the number of dipoles increases. This can be explained by the back scatter RCS being incoherent, visibly varying in the figure even after being averaged over 50 simulations, while the forward scatter RCS being coherent, adds in-phase which results in a smooth average curve. The forward scatter is taken as the more accurate indication of coupling, as it does not display the incoherent variance in the results.

With very large numbers of dipoles (10000 – 15000) the forward scatter strives towards a value of $4\pi A^2/\lambda^2$, where A is the cross sectional area of the spherical cloud. This value is in line with forward scatter literature for a solid body [10], which is an indication of the accuracy of the modelling results. Deviation of the forward scatter far from the $4\pi A^2/\lambda^2$ value would have indicated an inaccurate approach.

For the back scatter RCS, applying the same theoretical principles as for a solid sphere, an RCS value equal to the cross sectional area of a sphere was expected in the limit [12]. The RCS was, however, found to be 3dB above the cross sectional area. A RCS value below that of the cross sectional area could have been explained by the screening within the chaff, but the reason for 3dB above the expected RCS value is not clear and poses a possible question for future investigation.

The results are summarized in Table 9. Taking the 3dB compression point as guideline, it can be seen from the forward scatter results that dipole coupling should be taken into consideration for dipole densities above approximately $1.2\text{dipoles}/\lambda^3$. This value is well below the value given in reference [5]. The reason for this is not clear, although a possibility is that the meshing is not fine enough ($\lambda/13$). Due to the long simulation time that finer meshing would require, this will not be further investigated, but it poses a question for future investigation.

The FEKO results can be perceived as conservative relative to the literature, but will serve as guidelines for the application of modelling results presented this thesis.

Table 9 Coupling results expressed as density

	1dB compression density (N/λ^3)	3dB compression density (N/λ^3)
Literature	0.125	15
Back Scatter (FEKO)	0.60	2.0
Forward Scatter (FEKO)	0.45	1.2
Variance (rel. to BS)	25%	40%
Variance (rel. to FS)	33%	66%

4.7 Conclusion

In this chapter the linear equations for calculating the RCS of a chaff cloud were presented. A hypothesis for forward scattering was included and the proportionality constant approximated. The results obtained from applying these equations were compared with simulation results to determine the dipole density for which coupling is negligible and the linear equation applicable.

From simulation results it was found that coupling started influencing chaff cloud RCS at a dipole density of $1.2 \text{dipoles}/\lambda^3$. This value is lower than the dipole density stated in the literature [5], but will be the “conservative” guideline applicable to the modelling results presented in this thesis.

Chapter 5

Screening Effect of Sparse Clouds

5.1 Introduction

The primary application of chaff is as a military defence mechanism to avoid detection or attack by the defence systems of adversaries. In reference [29] it is stated that a chaff cloud forms the EM equivalent of a visual smoke screen that can temporarily hide the target from radar. According to another reference [15] this method of applying chaff is outdated and is now seldom used, due to modern radar capabilities

It is the purpose of this chapter to investigate the screening effect of chaff and to determine whether it is possible or practical to hide a target behind a chaff cloud.

Available literature [10] and [27] focuses on E-field scattering in the far field (back and forward scatter) and little is said regarding the screening effect of sparse clouds in the near field region. Here the screening effect also known as “shadowing”, will be investigated by computing the E-field propagation through the chaff cloud.

A hypothesis will be presented and investigated to predict the screening properties behind the cloud, including the E-field drop and screening effectiveness.

5.2 Screening Hypothesis

This section discusses the following hypothesis:

If the forward scattering cross section of a cloud is known, the E-field behind the cloud can be estimated from the following relationship:

$$\sigma_{fs} \propto 4\pi \frac{A^2}{\lambda^2} |E_{drop}^2| \quad (5.1)$$

The hypothesis will be tested computationally, but first the rationale of its formulation will be discussed.

In the previous chapter it was shown that, unlike for σ_{bs} , the σ_{fs} can be computed quickly because its deviation from the expected value is small for different cloud distributions and thus only limited averaging is needed. With σ_{fs} known this hypothetical formulation allows the field behind the cloud to be estimated. The rationale behind the formulation can be explained with reference to Figure 46. The figure shows the near field magnitude, E_{AA} , on the A-A plane behind a scattering object for four cases:

- case a) With no object present the E-field on plane AA is equal to the incident field, $E_{AA} = E_{inc} = 1\text{V/m}$.
- case b) A black body radiator is present (absorbing all incident energy). E_{AA} is 1V/m everywhere except directly behind the body, where it is zero.
- case c) A black body radiator is present. E_{AA} is the difference between case a) and case b) and will be called the scattering near field. This field arises due to energy absorbed and reradiated by the black body and is important as the scattered far field can be found from it.

- case d) A chaff cloud is present. In this case the scattering near field magnitude is less than 1 V/m because the chaff is partially penetrable by the incident field.

The hypothesis, using $\sigma_{fs} \propto \text{Area}^2$, assumes that the scattering near field behind the chaff is in phase over the surface. This coherent property produces the σ_{fs} proportional to Area^2 relationship

In summary:

- If σ_{fs} of a chaff cloud is known, the hypothesis can be used to estimate the drop in field strength behind the chaff cloud.
- This drop in field strength represents the screening effect of the chaff.

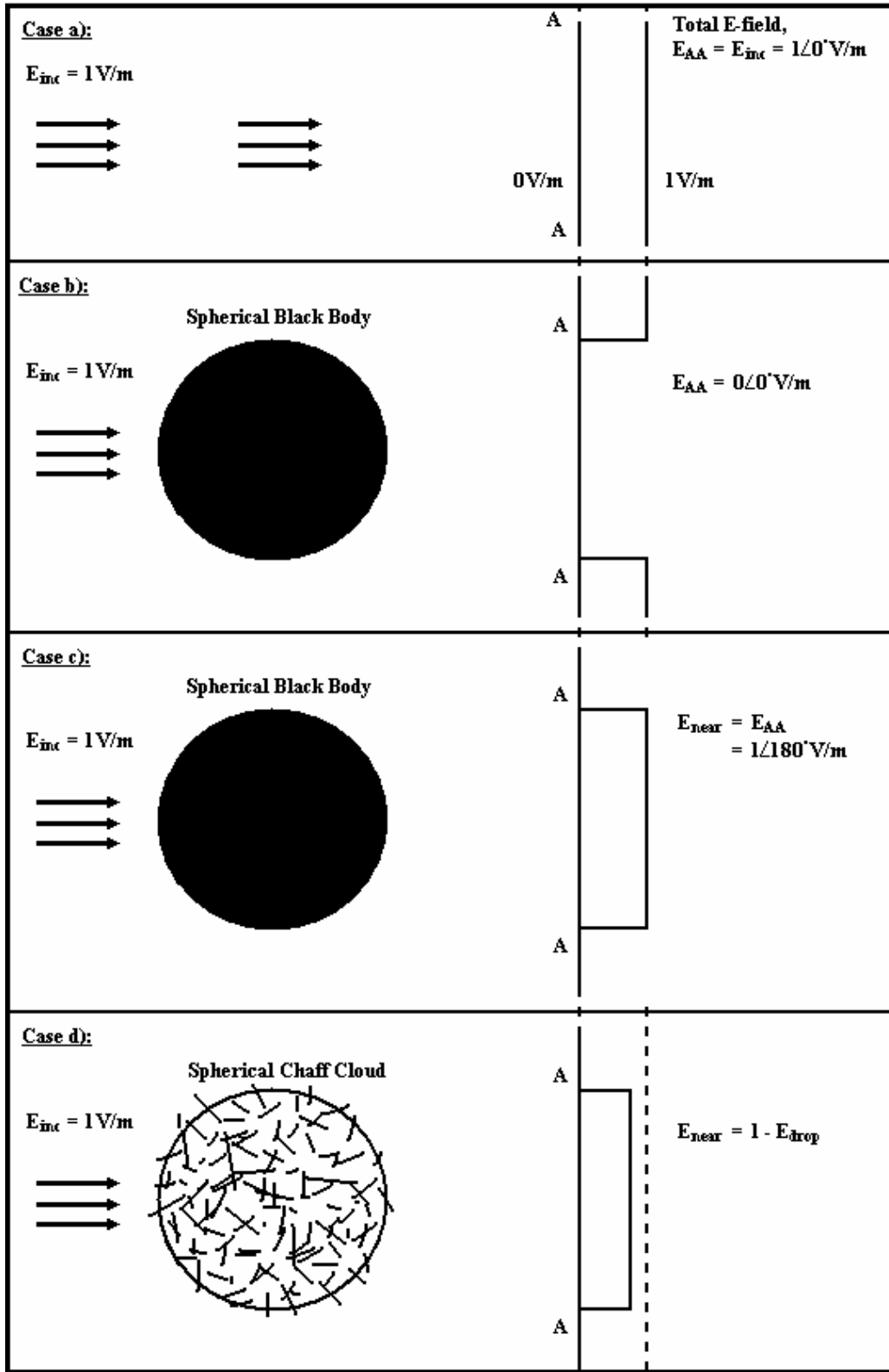


Figure 46 E-field magnitude on a plane A-A for a plane wave incident on (a) a plane A-A (b, c) a spherical black body and (d) a chaff cloud.

5.3 Chaff Cloud Simulation investigating Hypothesis

In this section the E-fields in and around a chaff cloud will be discussed and the hypothesis tested.

An initial simulation was set up to investigate the E-field characteristics through a chaff cloud. To investigate the behaviour of the E-fields in and around a spherical chaff cloud; the near fields were calculated along a line through a 1m^3 cloud as illustrated in Figure 47.

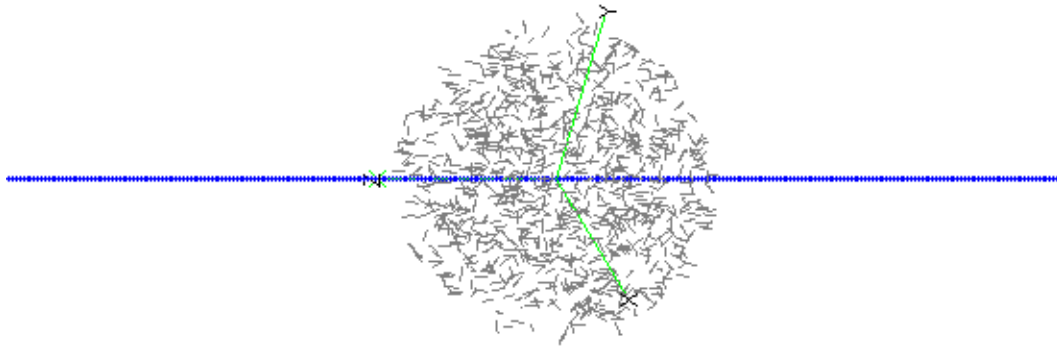


Figure 47 Near field points for calculating E-fields in 1m^3 a chaff cloud with the incident source on the left of the cloud

The simulation results for the near field point are shown in Figure 48. The plane wave incident on the chaff cloud has a field strength of 1V/m . It can be seen that in front of the chaff cloud the incident and reflected wave oscillates around the 1V/m field strength as these fields add in and out of phase. Within the chaff cloud itself the E-field is complex, due to the random nature of coupling and scattering between the dipoles, which are randomly positioned and orientated.

Behind the cloud the E-field drops to below 0.5V/m before increasing again with distance. This is known as the shadow region [10].

Although not illustrated, the fields far behind the cloud increase to the incident E-field value due to incident E-fields passing the chaff cloud and “filling” the shadow region.

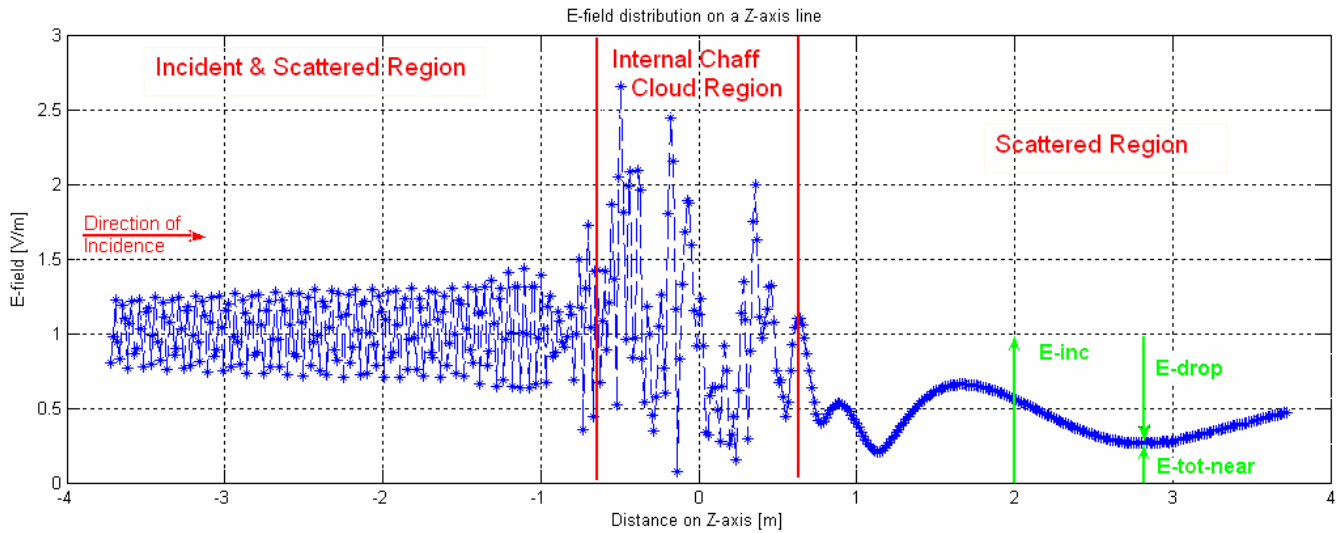


Figure 48 E-fields through a chaff cloud of 1m^3 radiated at 3GHz

Two simulations were set up to further investigate the near field characteristics of the chaff cloud:

- The first was for an increasing number of dipoles in a spherical volume of constant dipole density. This implies an increasing volume with increasing number of dipoles. This was the main simulation and results were analyzed to test the hypothesis of section 5.2 and find the proportionality constant.
- The second was for an increasing number of dipoles in a sphere of constant volume, implying an increasing dipole density. The results of this set of simulations confirmed the proportionality parameters of the hypothesis.

5.4 Near field Results

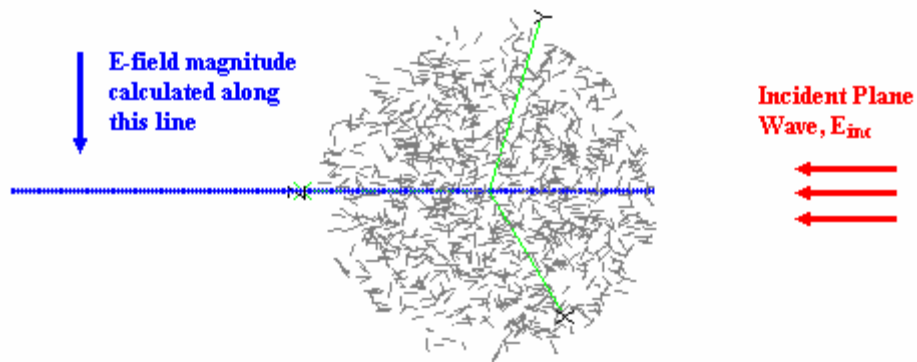


Figure 49 Near field points for calculating E-fields in a 1m³ chaff cloud, with the incident source on the right of the cloud

Figure 49 illustrates the simulation setup for investigating the near fields behind the chaff cloud and Figure 50 shows results of the E-field magnitude behind the chaff cloud. Two points are noted:

- The distance between the E-field minimum and chaff cloud increases as the number of chaff elements and cloud volume increases.
- A linear relationship appears to exist between the near field minimum (E_{drop}) and the logarithmic increase of dipoles.

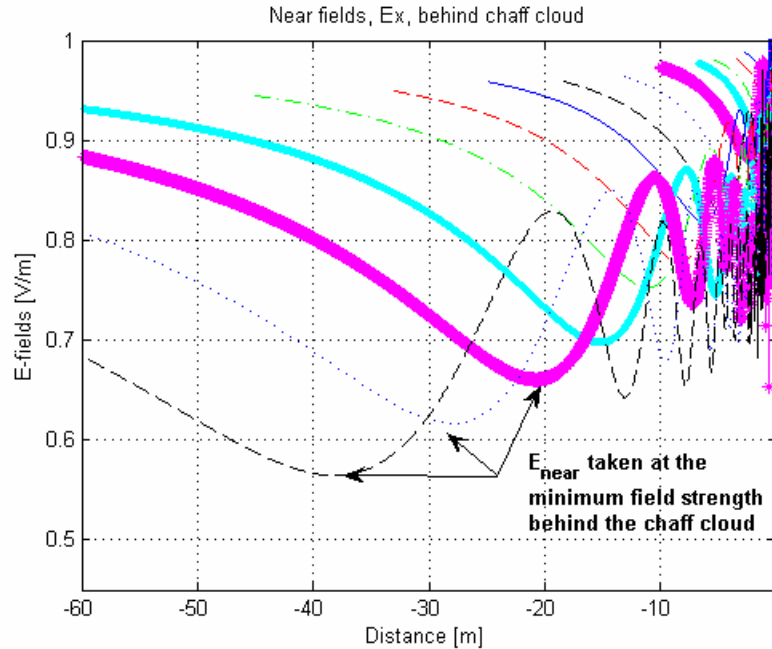


Figure 50 E-field magnitude behind a chaff cloud for an increasing number of dipoles and increasing spherical volume, (constant density)

Simulations were run over 3 densities for 2 different numbers of chaff elements within the cloud. The data was averaged over 15 simulations and the simulated data is presented in Table 10. The maximum dipole density that was investigated was at 0.125 dipoles/ λ^3 . This is equivalent to a dipole spacing of 2λ between dipoles as given by literature (Chapter 4). The coupling is therefore negligible.

Table 10 Spherical dimensions for screening simulations

Number of dipoles (N)	1678			4045		
Dipole density	0.07	0.1	0.125	0.07	0.1	0.125
Forward Scatter (dB)	33	33	33	40.6	40.6	40.6
Sphere Radius (m)	1.76	1.56	1.45	2.38	2.12	1.96
Sphere CSA (m ²)	9.74	7.67	6.61	17.79	14.12	12.07
Sphere Volume (m ³)	22.84	15.90	12.77	56.47	39.91	31.54
Simulated E_{near} (V/m)	0.725	0.607	0.56	0.659	0.645	0.50

Inspection of the results shows that for the equation postulated in 5.1 a proportionality constant of 0.5^2 is valid:

$$\sigma_{fs} \approx 4\pi \frac{A^2}{\lambda^2} |(0.5E_{drop})^2| \quad (5.2)$$

$$\sigma_{fs_dB} \approx (4\pi \frac{A^2}{\lambda^2})_{dB} + 20\log(0.5E_{drop}) \quad (5.3)$$

Analytical results are compared with numerical results in Table 11.

Table 11 Scattered E-field minimum and distance relationship behind cloud

Number of dipoles (N)	1678			4045		
	0.07	0.1	0.125	0.07	0.1	0.125
Dipole density	0.07	0.1	0.125	0.07	0.1	0.125
Simulated E_{near} (V/m) (FEKO)	0.725	0.607	0.56	0.659	0.645	0.50
Calculated E_{near} (V/m) $E_{near} = 1 - E_{drop}$	0.74	0.62	0.58	0.68	0.66	0.50
Distance to E_{scat_Min} to spherical radius ratio $D_{E_{scat}} / A_{Spere}$	2.67	2.62	2.66	2.66	2.67	2.64

In Table 11 it can be seen that the approximated E-field minima relate quite closely to those of the FEKO simulation. The analytical and numerical values differ on average by 2.25%.

The relationship between the distance of the minimum E-field behind the chaff cloud and of the spherical radius is also approximately constant. The average value for this ratio is 2.65 and the variance is less than 1% from the average.

The hypothesis presented has been confirmed by simulation with a proportionality constant of 0.5². Thus, if the number of dipoles and the size of the spherical chaff cloud are known, it is possible to approximate the E-field minimum behind the cloud. Furthermore, the distance behind the cloud at which this minimum can be expected, can be approximated with the ratio:

$$\begin{aligned} D_{\text{Escat}} &\approx 2.65A_{\text{Sphere}} \\ &\approx 2.65\pi R_{\text{Sphere}}^2 \end{aligned} \quad (5.4)$$

To confirm the accuracy and application of the above derived approximations, a second set of simulations were run for a 1m³ chaff cloud, resonant at 3GHz. This for a constant sphere volume with an increasing number of dipoles. Results are presented in Figure 51 and Figure 52.

It can be seen in Figure 51 that the position of the E-field minimum stays approximately constant (for a constant cloud volume) while the magnitude of the E_{drop} increases as the dipole density increases.

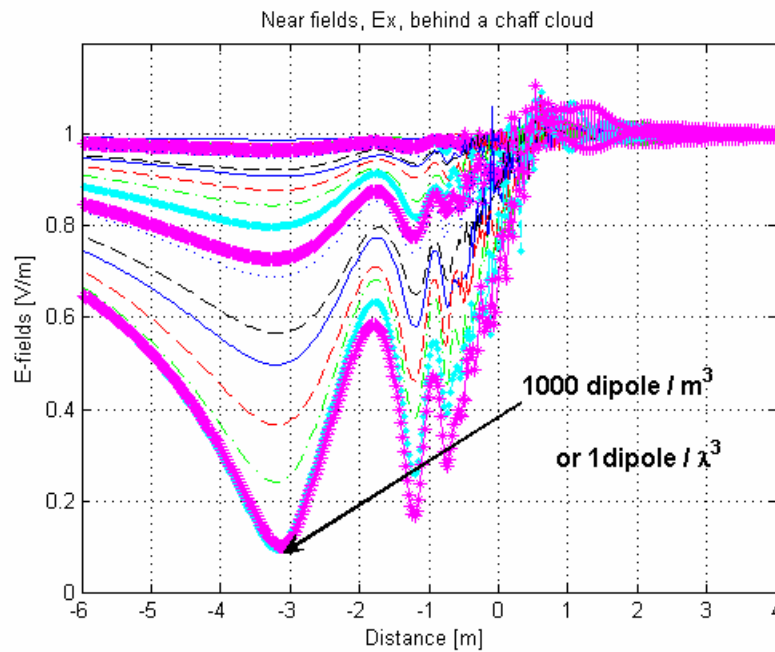


Figure 51 Drop in E-field behind a 1m³ spherical chaff cloud for an increasing number of dipoles

As the chaff cloud becomes denser, coupling starts taking effect to the point where the position of the E-field minimum shifts closer to the cloud in Figure 52, as if for a solid sphere. Such dense clouds have complex coupling characteristics and will not be further investigated.

The accuracy of the approximate drop in E-field and distance to E-field minimum is illustrated in Figure 53 to Figure 55. Figure 53 illustrates the approximation of the E-field minimum. Even for a small number of dipoles the approximation renders accurate results. At high densities (10 000 – 15 000 dipoles/m³), far surpassing the limit of density (125 dipoles/m³) at which no coupling occurs, the graph shows simulation values deviating from the calculated approximation.

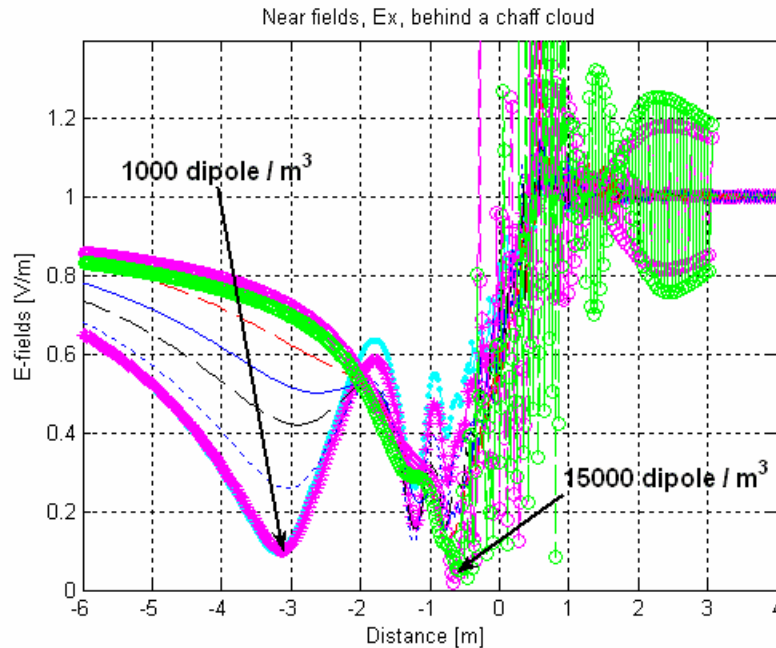


Figure 52 Drop in E-field behind a 1m³ spherical chaff cloud for an increasing number of dipoles

For high density clouds the magnitude of the hypothetical approximated E-field drops to below 0V/m, which is non physical and confirms that the hypothesis is only valid for sparse clouds.

Figure 54 and Figure 55 shows the accuracy with which the distance to the E-field minimum behind the chaff cloud can be approximated.

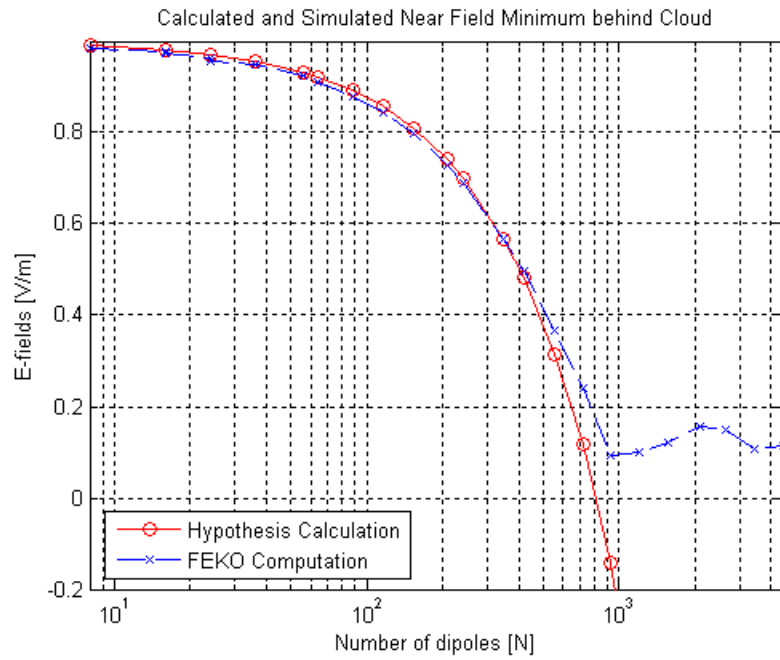


Figure 53 Validating the accuracy of derived hypothetical parameters for approximating the E-field minimum

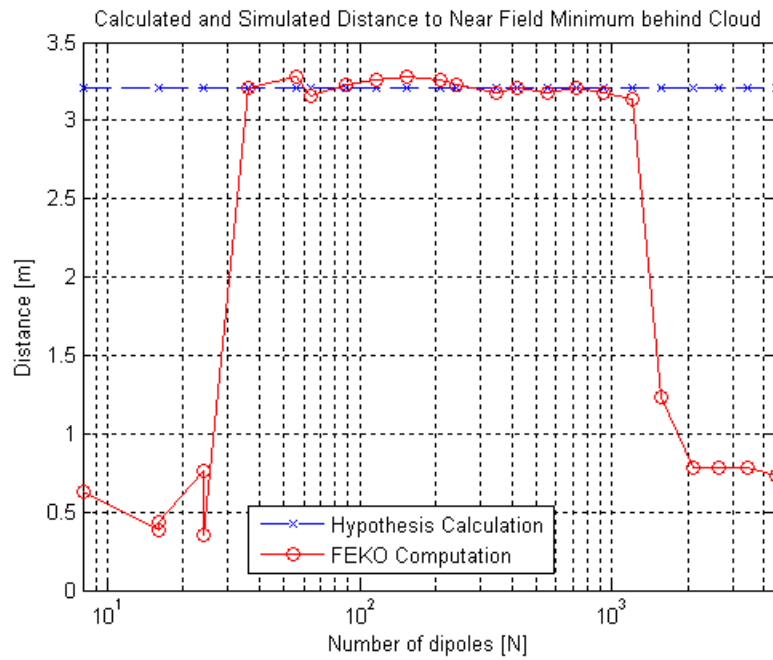


Figure 54 Validating the accuracy of derived hypothetical parameters for approximating the distance to the E-field minimum

In Figure 55 it can be seen that for a dipole density as low as 40 dipoles/m³ (explained in Chapter 3) to as high as 1000 dipoles/m³, the FEKO results fall within 2.5% of the hypothetical approximation. This confirms the accuracy of the approximation.

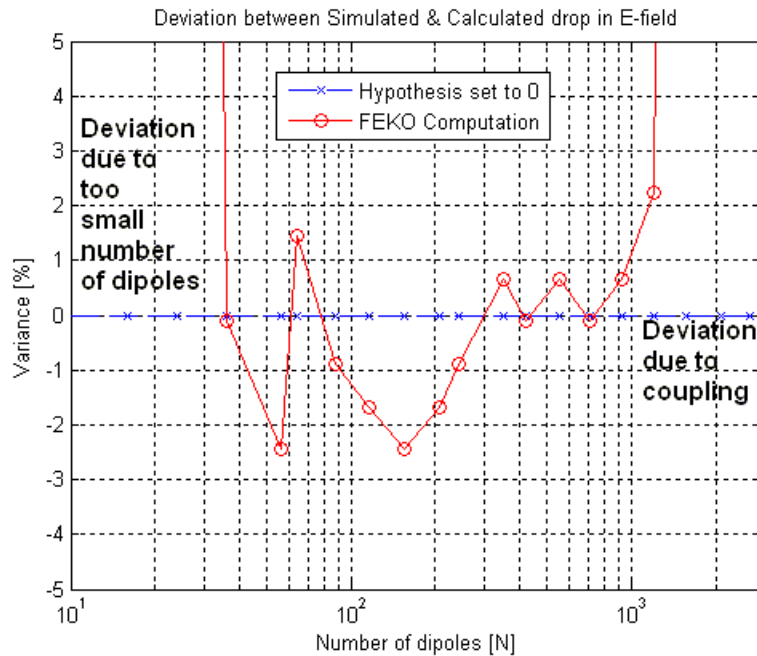


Figure 55 The accuracy of approximating the distance to the E-field minimum expressed as a percentage.

5.5 Conclusion

This chapter investigated the screening effect of chaff clouds based on a postulated result which was validated by FEKO simulation.

It is concluded that although coupling starts showing noticeable effects at 450 dipoles/m³, the drop in E-field can be modelled for densities as high as 1000 dipoles/m³ for the range in which parameters were investigated. This relates to a density of 1 dipole/λ³.

From computational results a model has been developed for estimating the position and drop in E-field behind the chaff. This model has been validated against a second set of simulation results.

From the results presented in this chapter the question of whether it is possible or practical to hide a target behind a chaff cloud can be answered. In Figure 52 it is clear that it would be possible to achieve a very low E-field behind a chaff cloud for a high dipole density ($1 \text{ dipole}/\lambda^3$). From the figure and results leading to equation 5.4 it is clear that the drop in E-field is cloud size dependant and effective at a specific distance behind the chaff cloud. It is concluded that, although it is possible to hide close behind a high density chaff cloud, it would not be practical to do so given modern chaff applications.

Chapter 6

Conclusion

6.1 Conclusion

This thesis aimed at the following goals: Development of a tool for determining chaff parameters and calculating theoretical RCS of a typical chaff cartridge when deployed. Determination of the dipole density region for which the tool developed is valid and investigation of the influence of inter-dipole coupling on chaff cloud RCS. Lastly, the screening effect of chaff was investigated to determine whether it is possible or practical to hide a target behind a chaff cloud.

Initially the dipole resonant properties were presented relative to its physical dimensions. Chaff materials were discussed and results presented on the dipole resonant length as a function dipole diameter. It was concluded that the general resonant length of a dipole, 0.47λ , is acceptable and is still applicable.

The investigation was then broadened to include dipole scattering properties as a function of orientation and frequency. The dipole spatial average RCS was modelled over a wide frequency band and results were compared with those of a chaff cloud. The results differed by up to 7.2dB, but this is ascribed to the variance in chaff cloud RCS, as illustrated in Figure 42.

An integral part of the research was determining the dipole density region for which the modelled results were applicable. Chaff cloud RCS was investigated computationally for an increasing number of dipoles. From simulation results, coupling was found to be negligible for dipole densities below $1.2\text{dipoles}/\lambda^3$. The results differed from those reported in the literature ($15\text{dipoles}/\lambda^3$), the reason for which is unclear, but they serve as conservative guidelines for the chaff modelling results presented in this thesis. From

these results it was also concluded that for a high density chaff cloud the back scatter RCS strives towards a value close to the cross sectional area of the cloud shape (within 3dB for the spherical cloud simulated).

To answer the last research question, chaff cloud screening was investigated by computing the E-field scattering through a spherical cloud. From the results obtained, a model was developed to predict the drop in the E-field behind a chaff cloud. This was, however, limited as to chaff cloud size and dipole density. Finally, from the results it was concluded that it is indeed possible to hide a target behind a chaff cloud, but that this is not practical. This is due to the requirements that the chaff cloud should exhibit a large drop in E-field and also to the fact that the positional requirements of the target were impractical.

6.2 Recommendations

The following recommendations are made for further work:

- The RCS of a resonant dipole for any orientation is available analytically, with the addition of a correction factor. An investigation is recommended as to whether this result can be expanded for a non-resonant dipole. It is unlikely that a direct analytical result be found, but techniques such as numerical integration could prove practical. This would allow the computation of σ_{cloud} for dipoles of specified orientation over a wide frequency band.
- The difference between the results obtained from dipole modelling and chaff cloud simulation results as shown in Figure 39 has been attributed to the RCS variance of a chaff cloud. Another possible contributing factor that could be investigated in future work is screening within a low density chaff cloud.
- Dense clouds have only been investigated computationally. A body of literature exists for managing the dense cloud problem analytically, incorporating dipole coupling, and this is a potentially rich field for further work.
- The reason for the difference in dipole density for the 3dB compression points taken from literature and those shown in the results of computation have not been resolved, and this needs further investigation.

- In general: The modelling results presented in this thesis have been based largely on theory from literature and on computational results in ideal conditions. For future chaff modelling to be of practical value, it is recommended that modelling development be based on a specific chaff application, along with the applicable chaff measurements.

Bibliography

- [1] W.P. Arnott, A. Huggins, J. Gilles, D. Kingsmill, J. Walker, *Determination of radar chaff diameter distribution function, fall speed and concentration in the atmosphere by use of NEXRAD radar*, Desert Research Institute, Reno, NV 89512.
- [2] J. Paul, H. Anthony, B. Kochtubajda, G. Kutznetsov, Study of airflow in Alberta hailstorm using chaff and polarization radar, Proc. 1997 28th Conference on Radar Meteorology, Austin, TX, pp 549 – 550.
- [3] B.E. Martner, J.D. Marwitz, R.A. Kropfli, Radar observations of transport and diffusion in clouds and precipitation using TRACIR, Journal of Atmospheric and Oceanic Technology, Vol. 9, No 3, Jun 1992, pp 226 – 241.
- [4] S.W. Marcus, Electromagnetic Wave Propagation through Chaff Clouds, IEEE Transactions on Antennas and Propagation, Vol. 55, No. 7, July 2007, pp 2032 – 2042.
- [5] P.Z. Peebles JR., Bistatic Radar Cross Section of Chaff, *IEEE Transactions on Aerospace and Electronic Systems*, Vol. AES-20, No. 2, March 1984, pp 128 - 140.
- [6] P. Pouligen, O. Bechu, J.L. Pinchot, Simulation of chaff cloud Radar Cross Section, *IEEE Antennas and Propagation Society International Symposium*, Vol. 3A, pp. 80-83, 2005.
- [7] G.S. Smith, Teaching Antenna Radiation from a Time-Domain Perspective, *American Journal of Physics*, Vol. 70, No. 8, August 2002, pp 829 – 241.

- [8] B. Butters, Chaff, *Proceedings of the IEE*, Vol. 129, No 3, pp. 197-201, June 1982.
- [9] Z.D. Zaharis, On the Electromagnetic Scattering of Chaff Clouds, *Electrical Engineering (Archiv fur Elektrotechnik)*, Springer Berlin/Heidelberg publishers, Vol.85, Number 3 / July 2003, pp129-135.
- [10] V.S. Chernyak, *Fundamentals of Multisite Radar System*. CRC Press, 1998.
- [11] Y. Guo, H. Überall, Bistatic Radar Scattering by a Chaff Cloud, *IEEE transactions on Antennas and Propagation*, Vol. 40, No. 7, July 1992, pp 837 – 841.
- [12] M.I. Scolnick, *Introduction to Radar Systems*, 3rd edition, McGraw Hill, 2001.
- [13] G.T. Ruck, D.E. Barrick, W.D. Stuart, C.K. Krichbaum, *Radar Cross Section Handbook*, Plenum Press, 1970.
- [14] G.R. Curry, *Radar System Performance Modeling*, Artech House, 2001.
- [15] Filippo Nero, *Introduction to Electronic Defence Systems*, Sci Tech Publishing, 2005.
- [16] C.A. Balanis, *Antenna Theory – Analysis and Design*, 3rd edition, Wiley, 2005.
- [17] Z. Yinan, J. Ming, Q. Xiaolin, Z. Zhiquan, Study on scattering characteristics on Chaff for Radar, *International Conference on Microwave and Millimetre Wave Technology Proceedings*, 2004, pp 673 – 676.
- [18] N.J. Willis, *Bistatic Radar*, 2rd edition, Sci Tech Publishing, 2005

- [19] J.H. Van Vleck, Theory of Radar Reflection from Wires or Thin Metallic Strips, *Journal of Applied Physics*, 18, 1947.
- [20] C.T. Tai, Electromagnetic back-scattering from cylindrical wires, *Journal of Applied Physics*, Augustus 1952, pp 909 – 916.
- [21] P.Y. Umfitsev, Diffraction of plane electromagnetic waves by a thin cylindrical conductor, *Radio Eng. Elecron. Phys.*, Vol 7, 1962, pp 241 – 249.
- [22] A. Nagl, D. Ashrafi, H. Überall, Radar Cross Section of Thin Wires, *IEEE transactions on Antennas and Propagation*, Vol. 39, No. 1, January 1991, pp 105 – 108.
- [23] O. Einarsson, Electromagnetic Scattering by a thin finite wire, *Acta Polytechnica Scandinavica*, Electrical Engineering Series 23, UDC, 538.566, 621.396.67, Stockholm, May 1969.
- [24] O. Einarsson, “The Wire” in *Electromagnetic and Acoustic Scattering by Simple Shapes*, J.J. Bowman, T.B.A. Senior and P.L.E. Uslenghi, Eds. New York: Hemisphere, 1987, pp 472 – 502.
- [25] C. Cloete, *CSIR Memo: Chaff Modeling Requirements*, August 2007.
- [26] D. L. Mott, On the Radar Cross Section of a Dipole, *Proceeding Letters*, May 1970, pp793 – 794.
- [27] A. Ishamaru, *Wave Propagation and Scattering in Random Media*, IEEE Press, 1997.

- [28] S.W. Marcus, RCS of Large Dense Chaff Clouds, *IEEE Antennas and Propagation Society International Symposium*, 2006, pp 3251 – 3254.
- [29] www.globalsecurity.org/military/systems/aircraft/systems/chaff.htm
- [30] G.S. Smith, *An Introduction to classical EM radiation*, Cambridge University Press, 1997

Appendix A

Deriving equations for equal spherical division

From Figure 56 it can be seen that to calculate the area of a sphere one needs to integrate over θ and ϕ since the radius r (ρ in the figure) is constant for area. The mathematical approach is derived as follows.

$$\begin{aligned}\Delta Area &= \iint r^2 \sin \theta d\theta d\phi \\ &= r^2 \Delta\phi \int_{\theta_1}^{\theta_2} \sin \theta d\theta \\ &= r^2 \Delta\phi \cdot -\cos \theta \Big|_{\theta_1}^{\theta_2} \\ &= r^2 \Delta\phi [\cos \theta_1 - \cos \theta_2]\end{aligned}\tag{A 1}$$

Thus

$$\begin{aligned}\cos \theta_1 - \cos \theta_2 &= \frac{\Delta Area}{r^2 \Delta\phi} \\ \cos \theta_2 &= \cos \theta_1 - \frac{\Delta Area}{r^2 \Delta\phi} \\ \theta_2 &= \arccos\left[\cos \theta_1 - \frac{\Delta Area}{r^2 \Delta\phi}\right]\end{aligned}\tag{A 2}$$

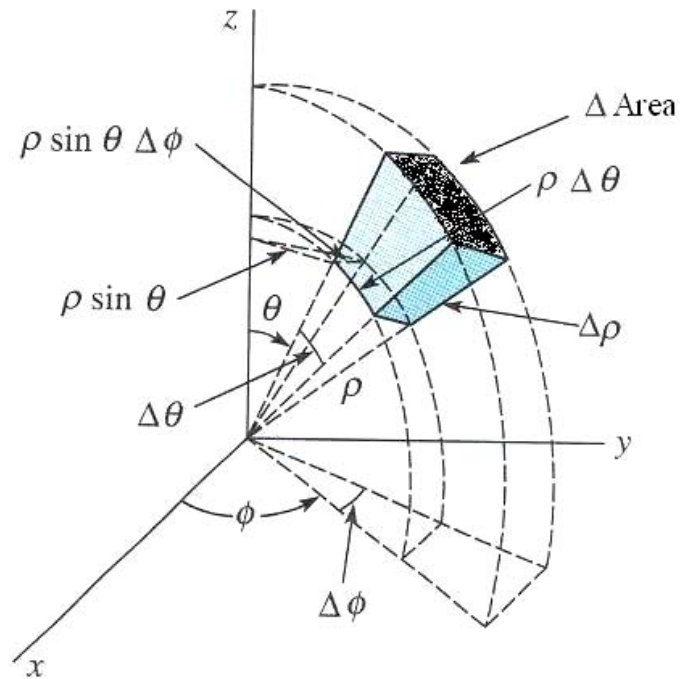


Figure 56 Integration in spherical coordinates, from [Advanced Engineering Mathematics, Z. Cullen]

Assume dipole orientation for θ and ϕ from 0° to 180° , thus half a sphere. $\Delta Area$ can be calculated by dividing the area of half a sphere into the total number of angle divisions in θ and ϕ .

$$Area_{Sphere} = 4\pi r^2$$

$$\frac{1}{2} Area_{Sphere} = 2\pi r^2$$

$$Division_{Sphere} = Division_{\theta} \times Divisions_{\phi}$$

$$\Delta\phi = \frac{180^\circ}{Division_{\phi}} = \frac{\pi}{Division_{\phi}}$$

$$\Delta Area = \frac{\frac{1}{2} Area_{Sphere}}{Division_{Sphere}} = \frac{\frac{1}{2} Area_{Sphere}}{Division_{\theta} \times Divisions_{\phi}}$$

From equation A 2

$$\begin{aligned}
 \theta_2 &= \arccos\left[\cos \theta_1 - \frac{\Delta Area}{r^2 \Delta \phi}\right] \\
 &= \arccos\left[\cos \theta_1 - \Delta Area \cdot \frac{1}{r^2} \cdot \frac{1}{\Delta \phi}\right] \\
 &= \arccos\left[\cos \theta_1 - \frac{2\pi r^2}{Division\theta \times Divisions\phi} \cdot \frac{1}{r^2} \cdot \frac{Division\phi}{\pi}\right] \\
 &= \arccos\left[\cos \theta_1 - \frac{2}{Division\theta}\right]
 \end{aligned} \tag{A 3}$$

By setting θ_1 initially to 0° and running the loop simulation for the number of divisions, the dipole will be orientated from 0° to 180° in the θ angle.

To test the result, the same derivation was done for a quarter sphere with $\theta = 0^\circ$ to 90° , the change in θ and sum of θ angles are shown in the figure below.

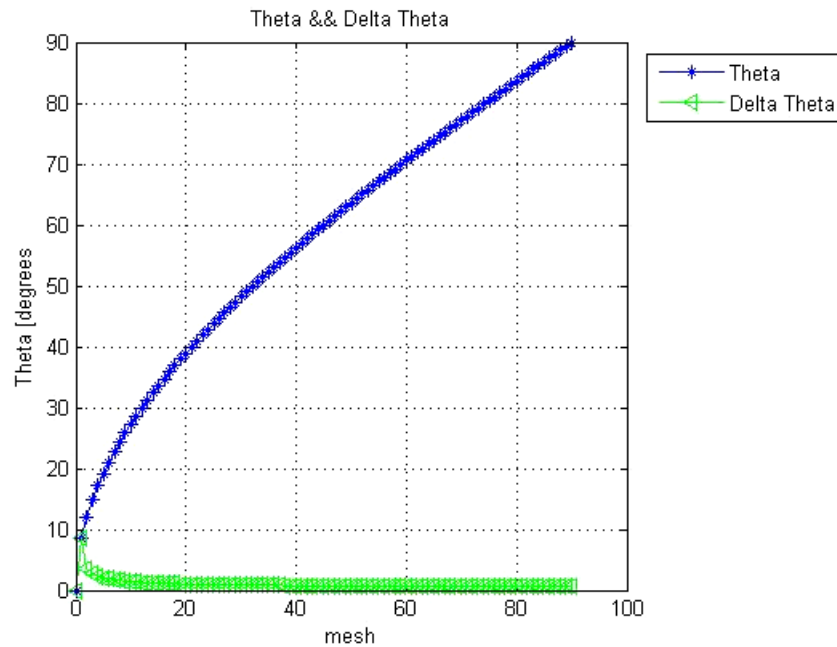


Figure 57 Change in theta angle and sum of theta angles

Appendix B

Graphical User Interface

B.1 Introduction

One of the outcomes of this project is to present a Graphical User Interface (GUI) tool for investigating back scatter RCS and E-field properties through a chaff cloud. Matlab was the program of choice for developing the GUI Tool, since this has been the software used for all previous data analysis and presentation.

The GUI tool consists of a RCS component and an E-field component, as shown in Figure 58. The components will be discussed separately.

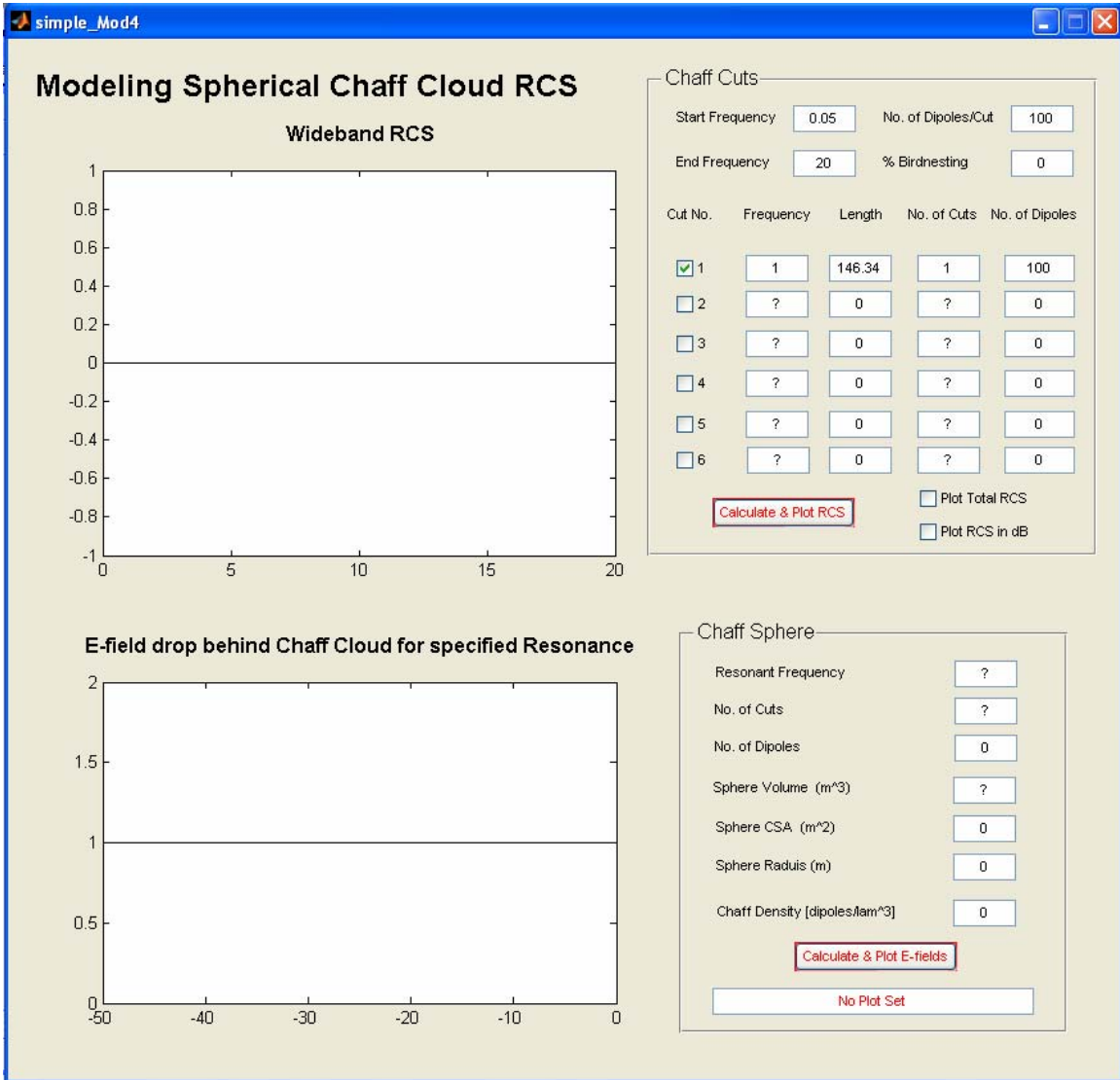


Figure 58 GUI tool for Investigating Chaff Cloud RCS and E-field Properties

B.2 Chaff Cloud Wideband RCS Tool

The chaff elements found in a chaff dispenser comprise a number of dipole lengths or chaff cuts. This tool allows the modelling of multiple dipole cuts in a chaff cloud over a wide frequency band. Provision is also made for the phenomena of dipoles clustering or “birdnesting”, which renders the scattering of the dipoles in the cluster ineffective.

The default display is shown in Figure 59, it has been set to calculate and plot the default RCS (shown in Figure 58) for this display.

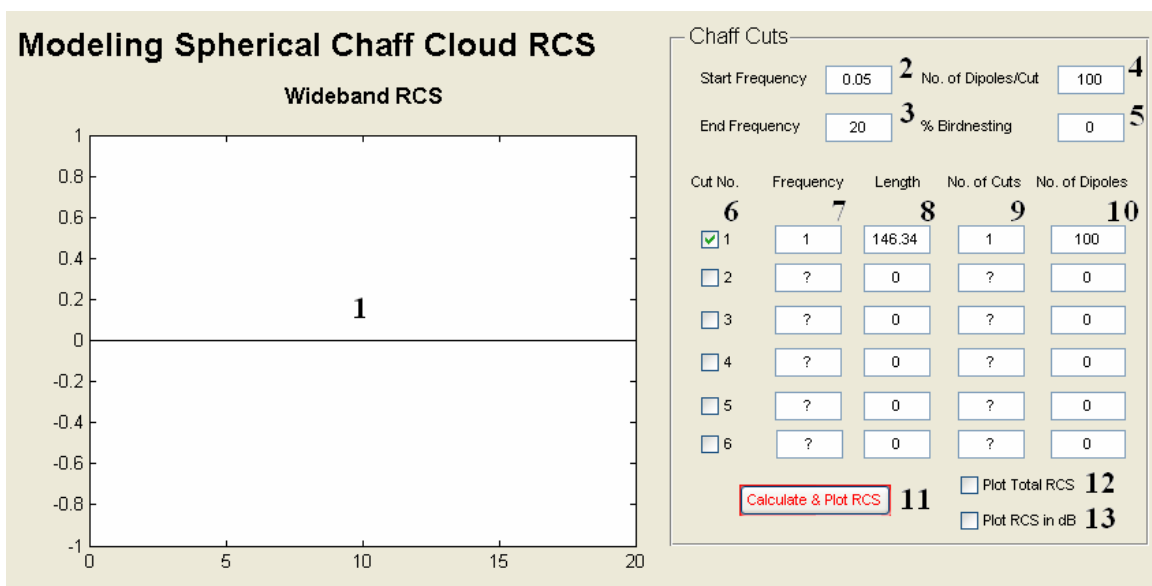


Figure 59 Default Wideband RCS Tool

The following features and settings are implemented:

1. RCS display

Displays the RCS as specified by the user.

2. Starting frequency of display

Starts the RCS display at this frequency, default value can be changed by user.

3. End frequency of display

Ends the RCS display at this frequency, default value can be changed by user.

4. Number of dipoles per cut

Default value should be changed by user.

5. Percentage birdnesting

Value set by user lowers the effective number of resonant dipoles and RCS

6. Tick chaff cut to include in display

Tick to include or exclude chaff cuts into calculation and display

7. Dipole resonant frequency

Resonant frequency of chaff cut as specified by user

8. Dipole resonant length

Resonant length is set to 0.4878λ and displays automatically when frequency is entered.

9. Number of cuts

Number of cuts as specified by user

10. Number of dipoles

Number of dipoles calculated as $N_{cuts} * (N_{dipoles}/cut)$ and displayed automatically.

11. Calculate and Plot RCS button

Calculates and display RCS as specified by previous settings and parameters, illustrated in Figure 60

12. Tick to plot total RCS

Can plot total RCS with or without (see Figure 61) RCS of specified cuts. By unticking the previous chaff cuts and only ticking the Plot-Total-RCS button only the total RCS will display. Keep the chaff cuts ticked to include chaff cuts and total RCS in display.

13. Tick to plot on dB scale

Tick to plot chaff cuts and or total RCS on dB scale, total RCS in dB scale illustrated in Figure 62.

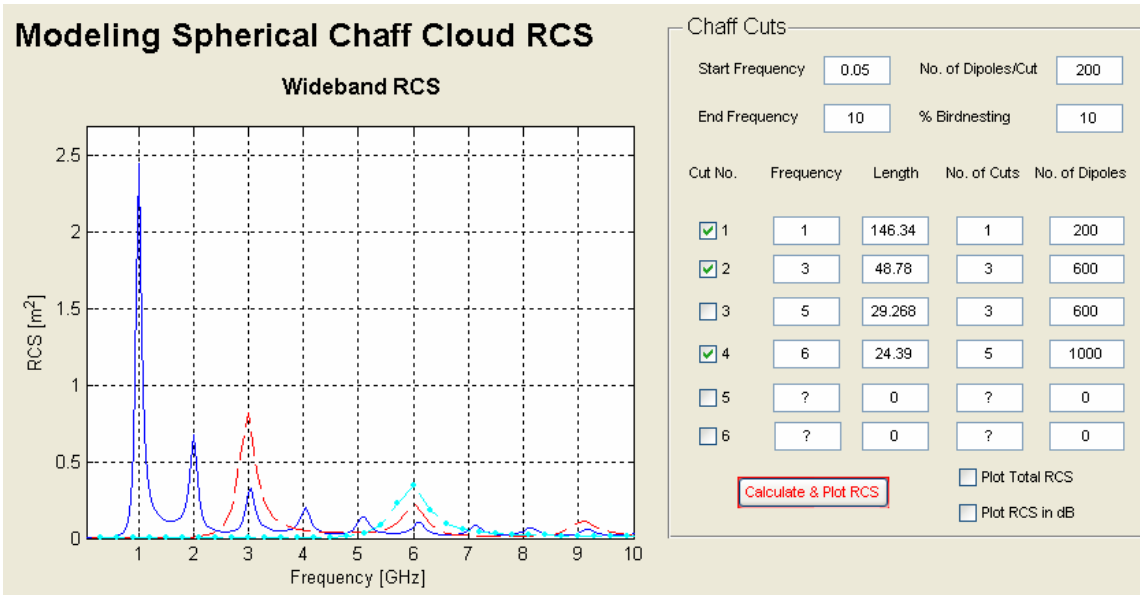


Figure 60 Plotting Multiple Chaff Cuts over a wide frequency band

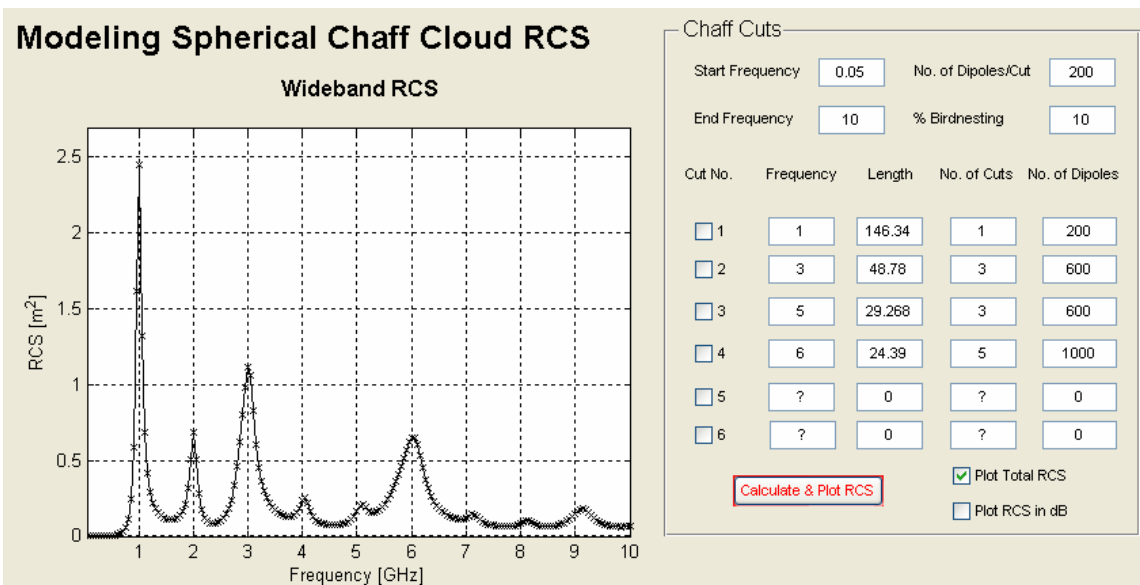


Figure 61 Plotting the Total RCS only, for the specifications set in the previous figure.

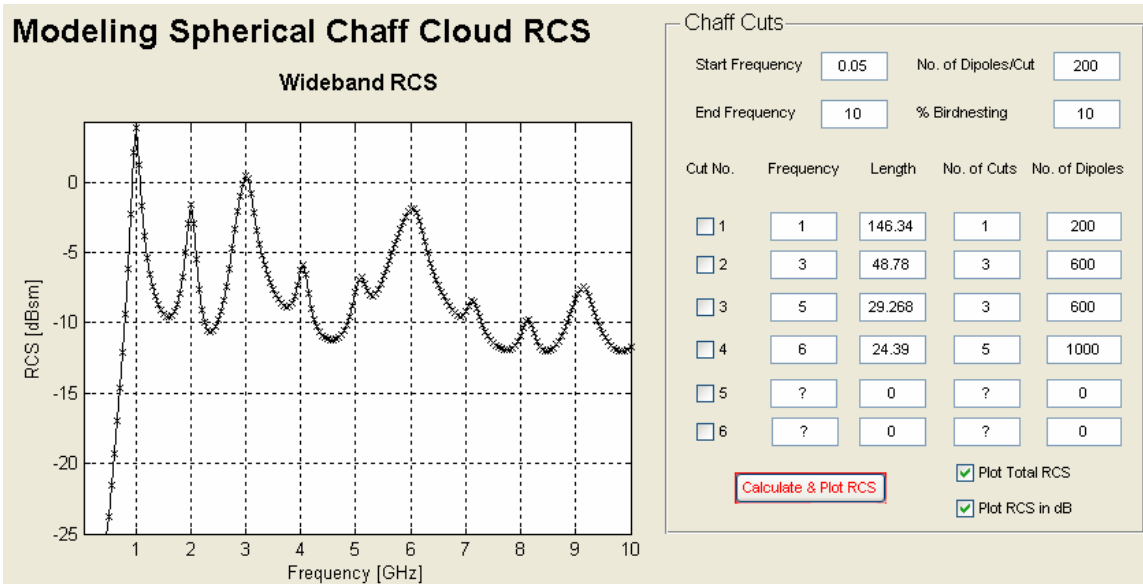


Figure 62 Plot total RCS on dB scale

The validity of the GUI was investigated for a small scale simulation. Results are shown in Figure 63. The variance in results can be ascribed to the statistical nature and deviation of chaff back scatter, and the small scale of the simulation, 1488 dipole elements.

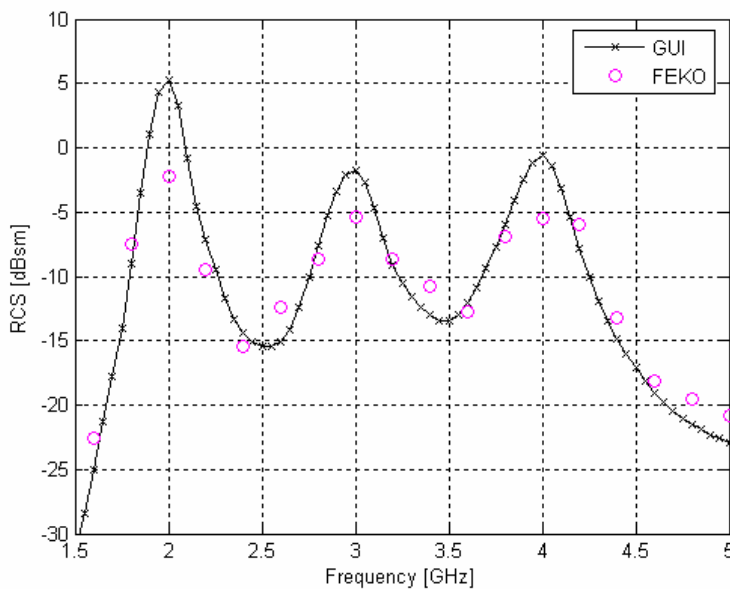


Figure 63 GUI estimation vs. FEKO simulation

B.3 E-field characteristics Tool

This tool allows the investigation of E-field propagation properties through and behind a chaff cloud. The application is only on small scale but gives a good illustration of E-field behaviour behind the cloud. Plot application and accuracy is limited to the number of dipoles and dipole density due to modelling scale limitations. The default display before any calculated plots is shown in Figure 64.

The following features and settings are implemented:

14. E-field propagation behavior display

Displays the E-field propagation behaviour through and behind the cloud.

15. Resonant frequency

Resonant frequency set by user

16. Number of cuts

Number of dipole cuts set by user

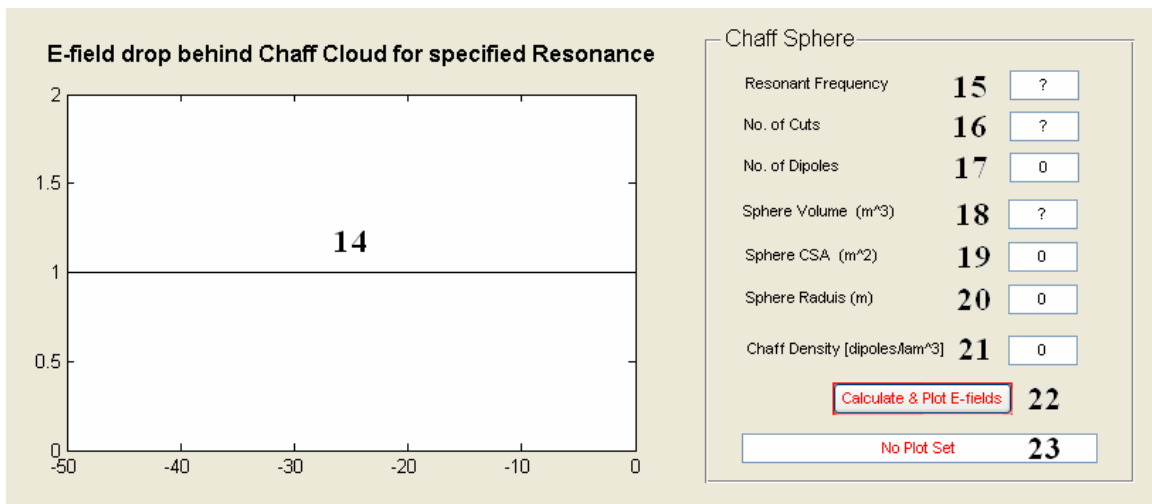


Figure 64 Default E-field characteristics Tool

17. Total number of dipoles

Number of dipoles calculated as $N_{cuts} * (N_{dipoles}/cut)$ and displayed automatically. The number of dipoles per cut is taken from the value specified in the Chaff Cuts Panel and can be changed there for application in the Chaff Sphere Panel

18. Sphere Volume

Specify one of the following: sphere volume, cross section area or radius to calculate sphere size.

19. Sphere Cross Sectional Area (CSA)

See 18, above.

20. Sphere Radius

See 18, above.

21. Chaff density in dipoles/ λ^3

The dipole density is calculated and displayed along with E-field when the Calculate-&-Plot-E-field button is entered.

22. Calculate and Plot E-fields button

Calculates and displays the E-field propagation through and behind the chaff cloud, as illustrated in Figure 65 and Figure 66. The chaff density is calculated from the set parameters and displayed.

23. Warning display

Information is displayed on the accuracy of the displayed results. A warning is given if the near field drops below 0.45 V/m as this value is below the accurate modelling range

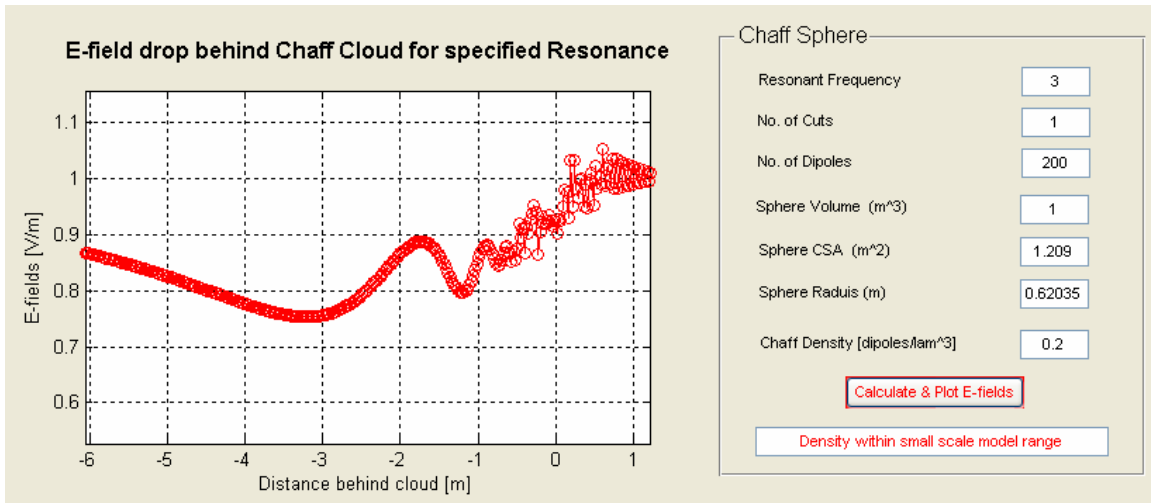


Figure 65 E-field behaviour display for specified settings at reasonable dipole density

It should be noted that the *number-of-dipoles-per-cut* parameter, set in the Chaff Cuts Panel, is the only parameter that affects the parameters set in the Chaff Sphere Panel. The *percentage birdnesting* parameter for example has no mathematical effect on the E-field propagation calculations!

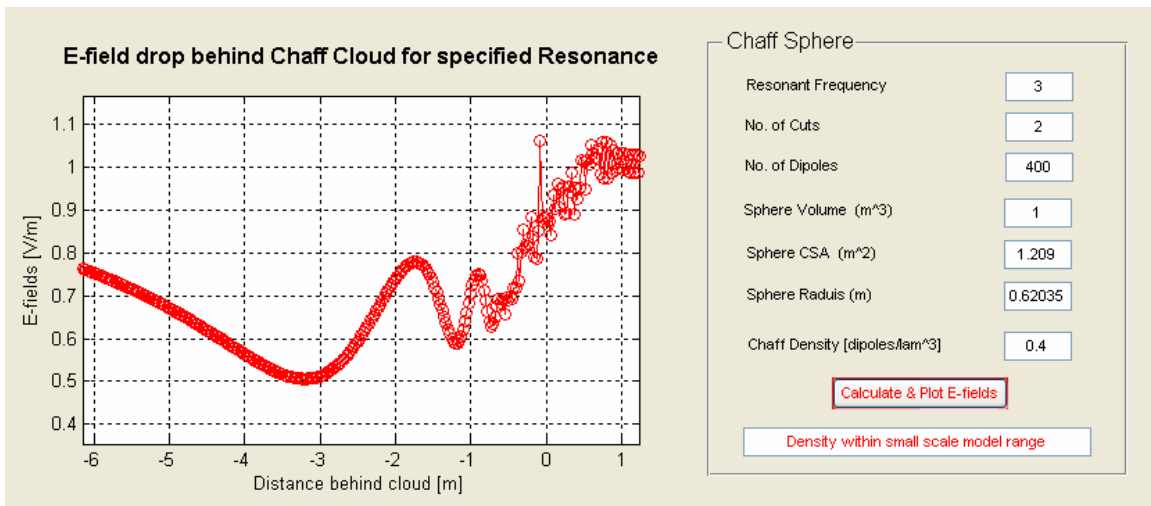


Figure 66 E-field behaviour display for specified settings at 1dB compression point density

From experimenting with the GUI data it was realized that the application of the E-field propagation tool is limited. Modelling was only done for sparsely spaced chaff clouds

and the E-field properties can be investigated with confidence on a small scale. However, even for low density clouds, the application is limited to the number of dipoles, as illustrated for the low density chaff cloud (density = 0.1 dipoles/ λ^3) in Figure 67.

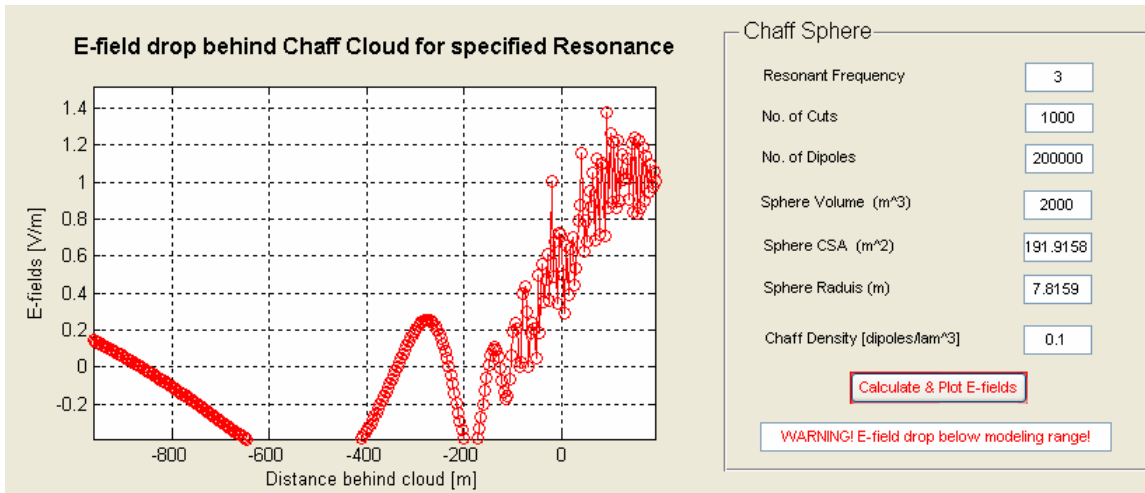


Figure 67 Error display for specified settings beyond model limitations

From the results in Chapter 4 the following guidelines are set to assure accurate and acceptable results:

- From Figure 53 it can be seen that for chaff densities of up to 0.4 dipoles/ λ^3 the modelling parameters are quite accurate on the small scale at which it was modelled
- The accuracy of the drop in E-field deteriorates to a density of 1 dipoles/ λ^3 where it reaches a point of almost constant compression with increasing density. The E-field drops further (though very little) for higher densities, as illustrated in Figure 52. In Figure 53 the 1 dipoles/ λ^3 density relates to 1000 dipoles for the 1 m³ sphere modelled at a resonance of 3GHz.
- Since compression of the drop in E-field starts taking place from E-field values below 0.35 V/m, this is the limit value to be taken as trust worthy, even for low density clouds with high numbers of dipoles.

The limitations on the application of the E-field tool cannot be verified, due to the limited number of dipoles that can be used in simulations and to time restrictions. The accuracy

of the near field estimation was investigated for a 1m^3 spherical chaff cloud at 3GHz. The change in the accuracy of the results as the number of dipoles increases is illustrated in the following figures.

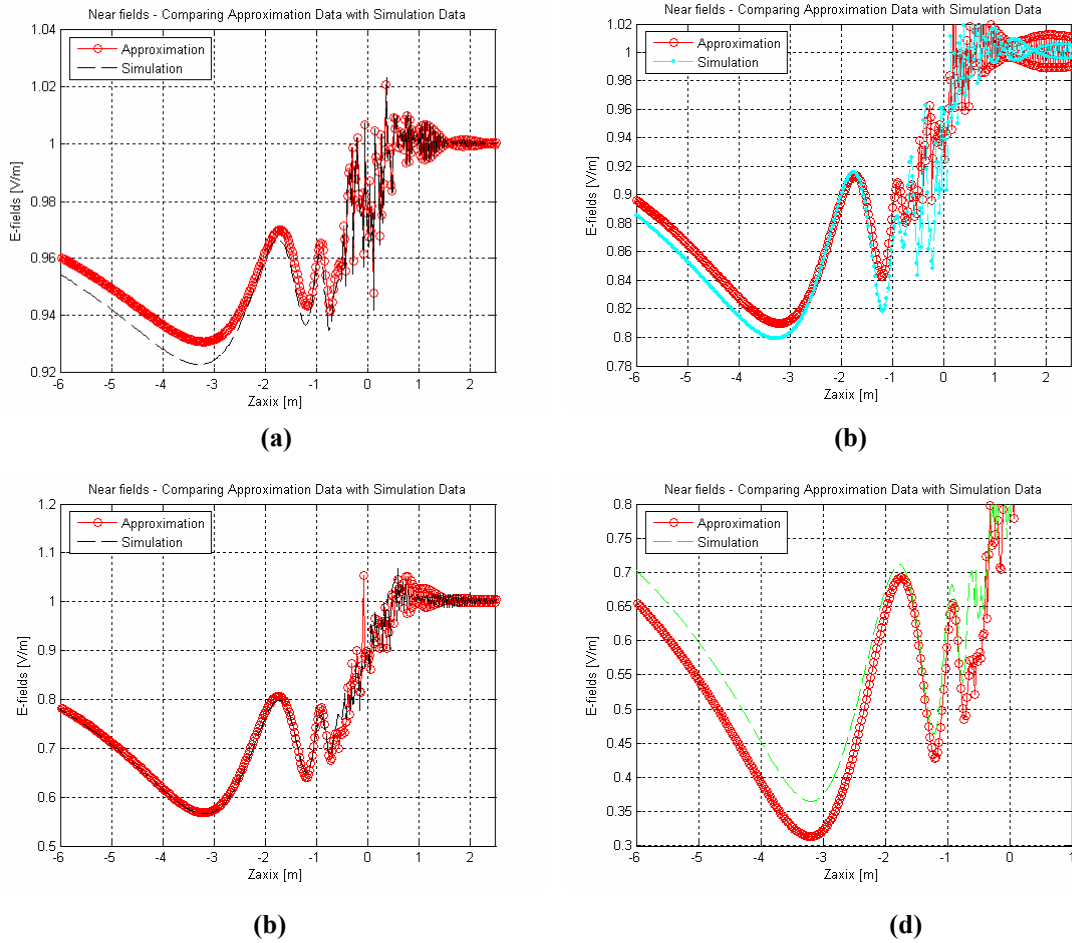


Figure 68 Deterioration of Estimated results as dipole density increases for (a) 56 dipoles/m³, (b) 154 dipoles/m³, (c) 350 dipoles/m³, (d) 556 dipoles/m³,

Appendix C

Matlab Simulation Functions

Matlab and FEKO simulation functions can be found on the accompanying CD.